POLITECNICO DI TORINO

Master of Science in Mechanical Engineering

Master's Degree Thesis

USE OF METALLIC FOAM IN AUTOMOTIVE APPLICATIONS

Supervisor

Prof. Graziano Ubertalli (DISAT)

Co-supervisor

Prof. Sara Ferraris (DISAT)

Candidate

Muhammad Umer Aziz
s289663

Academic year 2022/2023

Abstract

There is a growing demand for high-quality, energy-absorbing structural elements in numerous industry sectors, including automotive, aerospace, building, and biomedical. With growing automobile speeds and possible impact energy, the desire for improved crash-worthiness of the vehicle is a critical concern. This involves the development of innovative materials capable of effectively absorbing and dissipating impact forces, assuring increased safety. Aluminum foam sandwiches (AFSs) with closed cells are among these materials, and because of their lightweight nature, high strength, and excellent energy absorption properties, they can be used as shock absorber structures, such as bumpers, door pillars, and so on, by converting impact energy into plastic deformation energy and keeping the peak force acting on the protected objects below the level that could cause damage. However, understanding the mechanical behavior of these aluminum foam sandwiches (AFSs) is crucial for a wide range of possible applications. In this regard, this research demonstrates the mechanical characterization of aluminum foam sandwiches (AFSs) which are created by brazing and consisting of Alporas-made aluminum foam core and aluminum alloy as face-sheet material subjected to fatigue (compression-compression) loading conditions. Three-point bending fatigue tests are performed on all the samples of aluminum foam sandwiches (AFSs). The optical and scanning electron microscopy (SEM) along with energy dispersive x-ray spectroscopy (EDS) are utilized for surface characterization and analyzing foam's microstructure, chemical composition, and bonding interfaces.

Acknowledgement

I would like to express my deepest gratitude and appreciation to all those who have contributed to the completion of this master's thesis.

First and foremost, I am immensely thankful to Professor GRAZIANO UBERTALLI, Department of Applied Science and Technology (DISAT), Politecnico di Torino, for providing me with the opportunity to conduct my research and access the necessary resources. His assistance and cooperation have been essential to the successful completion of this study.

Besides my advisor, I would like to thanks Professor SARA FERRARIS, Department of Applied Science and Technology (DISAT), Politecnico di Torino, for continuous support during the research, for her patience, motivation, enthusiasm, and immense knowledge. Her guidance helped me in all the time of research and writing of this thesis.

I am also grateful to Professor RAFFAELLA SESANA, Department of Mechanical and Aerospace Engineering (DIMEAS) for her valuable time and thoughtful suggestions.

Lastly, I am forever grateful to my family for their unwavering love, understanding, and encouragement. Their constant support and belief in my abilities have been a source of inspiration, motivation, and strength.

Table of Contents

List of Tables

List of Figures

1. Introduction to Metallic Foam

Metallic foams are a unique family of materials having innovative physical, mechanical, thermal, electrical, and acoustic properties that are yet not fully understood. At the moment, there is some variability in the properties of metallic foams due to their incomplete characterization and imperfect process control. However, the control over processing is rapidly improving, and even the current generation of metallic foams have property profiles with attractive potential. Metallic foams significantly improve the performance for a variety of applications including stiff structures, efficient absorption of energy, thermal management, acoustic control, and other more specialized applications. Moreover, they are recyclable, non-toxic and have low densities [1].

Porous metals and metallic foams exhibit combinations of properties that cannot be produced with dense polymers, metals and ceramics, or polymer and ceramic foams. For instance, metallic foams have higher mechanical strength, stiffness, and energy absorption than polymer foams. Since they are thermally and electrically conductive, they can withstand significantly higher temperatures than polymers while still maintaining their mechanical properties. Also, compared to polymer foams, they are typically more stable in extreme environments. In contrast to ceramics, they can absorb energy and deform plastically. They can have extremely high specific surface areas if they have open porosity, which is a quality needed for flow-through applications or when chances of surface exchanges are involved [2].

1.1 Open and Closed Cell Metallic Foam

The production of open cell and closed cell foam structures is connected to the kind of foaming agent, as well as the amount of foaming agent and the foaming process itself. The cell structure is intimately tied to the kind and quantity of the foaming agent as well as its dispersion and solubility. The open and closed cell morphologies are shown in figure 1, and figure 2 illustrates the various production pathways based on the type of cell.

1.1.1 Open Cell Metallic Foam

The open cell foam material's cells are linked to one another or entirely interconnected, one or three dimensional, and may flow gas or liquid. Its pores are between 0.3 and 5 mm in size, its porosity ranges from 70 to 90%, and through porosity is between 55 and 65%. Because of its unique structure, the open cell foam possesses properties like superior compressibility, thermal insulation, and sound absorption. The applications for open cell metal foams include the following areas: filter and catalyst carrier, thermal management, biomaterials, mechanical and plant engineering.

1.1.2 Closed Cell Metallic Foam

The closed cell foam has an independent structure, and the internal cells are separated by a wall membrane, and they are not connected to each other. The size of pores or cells is usually between 1 to 8 mm. The closed cell foam material has extremely excellent impact resistance,

resilience, flexibility, sound insulation, heat insulation, water resistance, vapor resistance and floating properties. The applications for closed metal foams include automotive industry, aerospace industry, space, and machine industries. It can be utilized as a reinforcing element, for mechanical damping, and for vibration control in the machine industry [3].

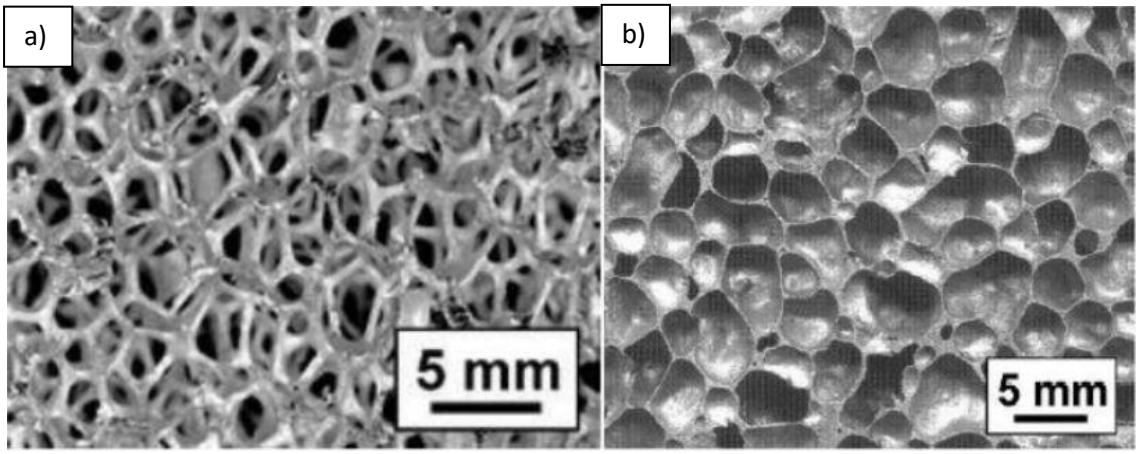

Figure 1 a) open cell b) closed cell aluminum foam [4]

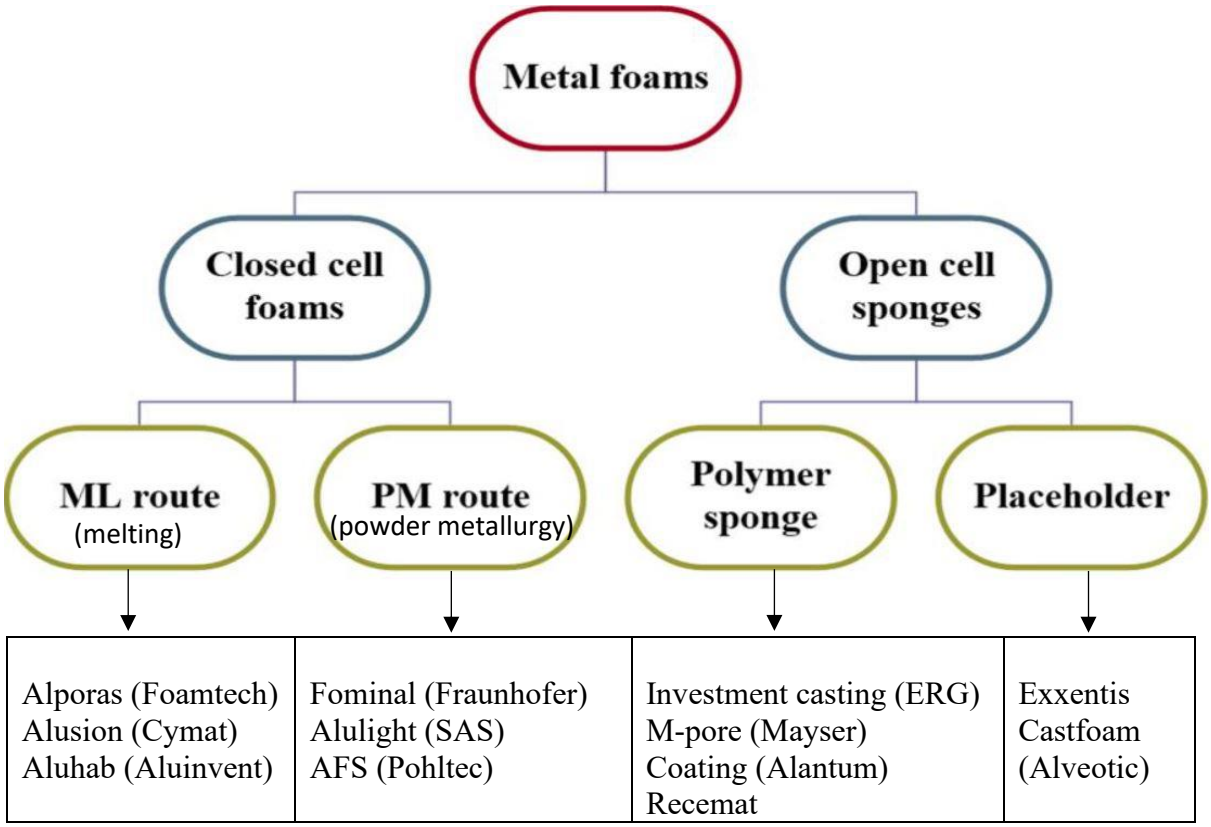

Figure 2 Production routes of metallic foam depending on type of cell [5]

1.2 Production Methods For Aluminum foam

There seems to be lot of ways to make aluminum foams, and they can be divided into two main categories: direct foaming methods and indirect foaming methods. Direct foaming techniques begin with a molten metal that contains uniformly dispersed ceramic particles. Gas bubbles are

then either directly injected into the melt, chemically produced by the breakdown of a blowing agent (such as titanium hydride) or precipitated by regulating temperature and pressure. Indirect foaming methods need the synthesis of foamable precursors, which are then heated to foam.

1.2.1 Direct Foaming Methods

Under certain conditions, the direct foaming of metallic melts is possible by injecting gases into the liquid. Due to the strong buoyant forces in the high-density liquid, the gas bubbles that are subsequently generated in the metallic melt usually tend to rise to the surface fast. Nevertheless, this rise can be slowed down by increasing the viscosity of the molten metal usually by adding fine ceramic powders or other alloying elements. There are two methods available at the moment for directly foaming metallic melts.

1. **Foaming Melts by Gas Injection (ALCAN)**

In this process metallic foam is produced by introducing gases into the liquid metal. To improve the viscosity of melting, reinforcing particles such as Al_2O_3 or SiC (5-20%) are added to it. Then injection of gas (air, nitrogen, or argon) into the melt takes place through the use of rotating impeller. The floating foam is then pulled off from the surface of melt. It requires a lot of care not to damage the foam structure by shearing the semi solid foam. From this method, foam slabs up to (0.1 x 1 x 10 m) in size can be produced. The end result of this technology results in a porous sheet material with porosities between 80% and 97%. The production process is shown in figure 3.

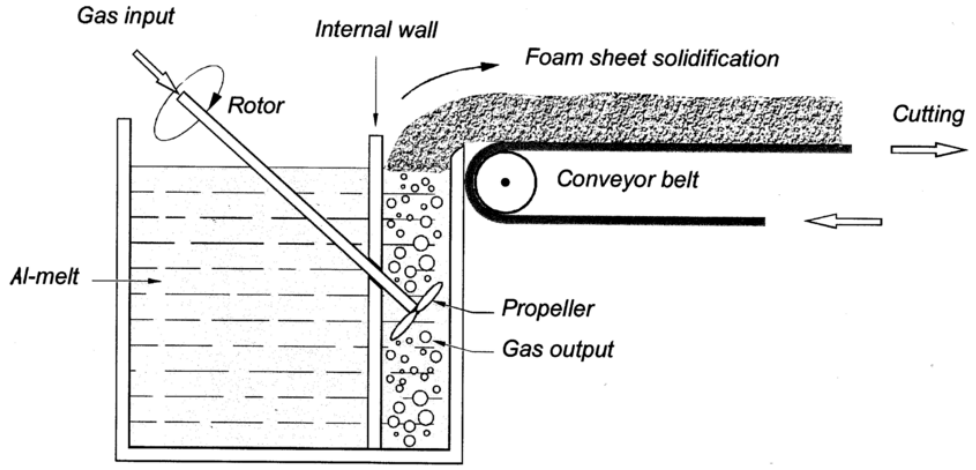

Figure 3 Foaming melts by direct gas injection process [6]

2. **Foaming Melts with Blowing Agents (ALPORAS)**

This method involves the addition of foaming agent into the aluminum melt rather than blowing gas. Calcium up to 1.5% is introduced to the molten aluminum (for thickening the melt) at 680°C and then it undergoes stirring for almost 6 minutes in ambient atmosphere. This thick melt is then poured into a casting mold and further stirred after adding foaming agent (powered TiH_2) by using a rotating impeller. By guaranteeing the right amount of foaming agent (usually 1.6%), it decomposes under the influence of heat and releases hydrogen gas. As a result, the

foam expands and fills the mold in about 15 minutes. With a porosity of between 89% and 93%, it solidifies as a block after being cooled down by fans inside the mold. The different process stages are shown in figure 4.

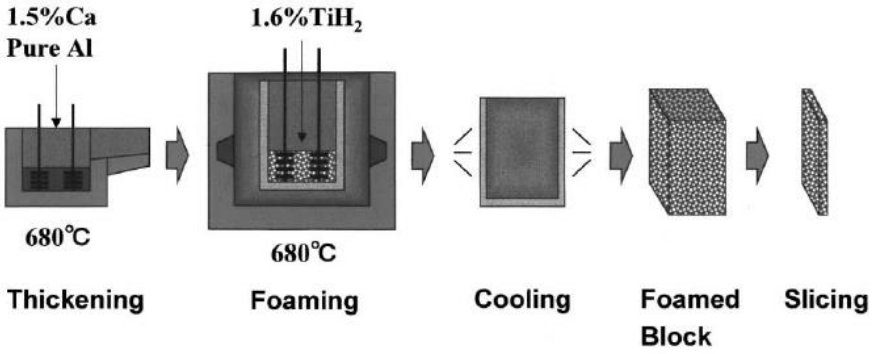

Figure 4 Foaming melts by adding gas releasing powder [7]

1.2.2 Other Processes

1. Foaming Melts by the Gasar process

The Gasar method is based on hydrogen's variable solubility as a function of pressure. After melting the metal in an autoclave, it is brought under high pressure for solving large amount of hydrogen. The solubility of hydrogen gas depends upon pressure, alloy composition etc. Into a mold inside the autoclave, this saturated melt is poured. The melt then undergoes a directional solidification under decreased pressure, which results in the precipitation of hydrogen gas at the solidification front. The maximum porosities cannot be achieved by this process and lie in the range between 5% and 75%. However, metals with high and medium melting points such as copper and nickel can be foamed. Since liquid can be solidified directionally, there is a possibility of creating foams with elongated pores [8].

2. Metallic Foams By Investment Casting Process

There is also a possibility to create the metallic foams without first foaming the metals. This process starts with the polymeric foam and is transformed into a structure with open pores by utilizing the foaming process or reticulation treatment. A slurry of heat resistance substance is then poured into the foam. The molten metal is cast into the resulting open voids/mold left by the removal of polymer after it has dried. The mold material is then removed (by pressurized water) and the metallic foam is obtained which resembles polymer foam. This process can induce porosities ranging from 80% to 97% [8]. The process flow diagram is depicted in figure 5.

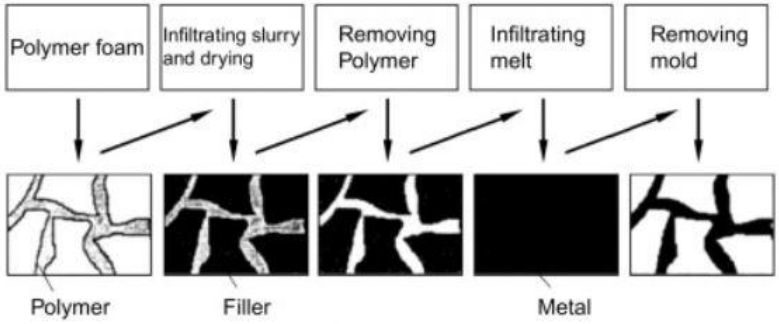

Figure 5 Indirect metal foaming by investment casting process [8]

1.2.3 Foams Made From Metal Powders

A powder metallurgical technique developed and patented at Fraunhofer-institute in Bremen, Germany, ma be used to create foamed metals [9], [10]. This process, which is based on the use of foaming agent begins with the mixing of metal powders (powder blend, pure metal, or an alloy) with a foaming agent (for aluminum and its alloys usually 0.4 - 0.6 wt. % of TiH_2). Wrought and cast alloys are the most common alloys to be used as a foaming agent e.g., $AlSi_7$ and $AlSi_{12}$. To create a dense and semi-finished product, the compaction of mixture then takes place. There are various compaction methods available such as uniaxial compression, extrusion, or powder rolling. The only thing is that the adopted compaction method would have to ensure that the foaming agent is embedded into the metal matrix without any residual open porosity. Moreover, the selection of compaction method also relies on the required shape of precursor material. At the moment extrusion seems to be the most economical compaction method and is therefore preferred. The following stage is the heat treatment at temperature close to the matrix material's melting point. The blowing agent which is uniformly dispersed throughout the thick metallic matrix, decomposes, and the resulting gas causes melting precursor material to expand, thus resulting in a very porous structure. The length of time required for complete expansion varies from a few seconds to several minutes depending on the temperature and size of the precursor. With the right blowing agents and process parameters, other metals and alloys may also be foamed, in addition to aluminum and its alloys, such as tin, zinc, gold and others. The process flow by this approach is displayed in figure 6.

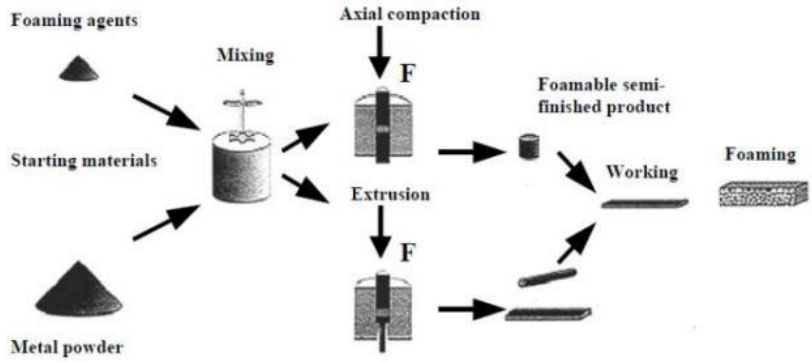

Figure 6 Foaming from powder compaction process [7]

1.3 Aluminum Foam Sandwich (AFS)

A wide range of uses for sandwich materials are made possible by the challenge of making products and structures lighter. A particularly creative material combination for use in lightweight constructions is aluminum foam sandwich (AFS), which is illustrated in figure 7. Stainless steel or other materials, such as aluminum alloy sheets, titanium, steel, wood, ceramic, may also be utilized for the external layers (solid panels) of AFS. Aluminum-based porous foam makes up the sandwich's middle portion [11]. Despite the poor mechanical performance of the porous aluminum foam core, the external solid panels of the AFS can support the bulk of the load to shield the core from being destroyed in a crash (impact). The

aluminum foam core lengthens the gap between the two solid plates at the same time, increasing the second-moment area of the AFS. As a result, the structural rigidity and strength rise. Additionally, plastic deformation of the porous aluminum foam core has the potential to absorb the external deformation energy. The low-density aluminum foam core significantly reduces the mass of the AFS from the standpoint of lightweight structures, resulting in high specific strength and specific stiffness [12].

Since powder metallurgy is well suited for industrial applications, it has emerged as one of the most popular manufacturing methods for AFS with aluminum face sheets among the many other processes that could be used [13]. The face sheets and foam core are joined together through this manufacturing process by a metallic bond that does not need adhesives and is highly recyclable [14]. The aluminum foam sandwich offers a wide variety of potential applications because of additional benefits including a high bending stiffness at a low density and good energy absorption properties.

Despite the material being suitable for mass production and having numerous benefits, there are not as many industrial uses for aluminum foam sandwich as it could have [13], [14]. In an industrial environment survey, the reasons for the obstacles to the use of AFS were looked at [15]. Excessive cost, a lack of design expertise, and lack of reference applications were the primary causes of non-use. Although the price will decrease as the material is used more frequently, the lack of design knowledge and the absence of reference applications point to the need for additional research.

Figure 7 Aluminum foam sandwich

1.3.1 Joining of Aluminum Foam Sandwiches

The aluminum foam sandwich is composed of external solid panels and an internal aluminum foam core. Titanium, steel, zinc, ceramic, carbon fiber and some other materials can be used to create solid panels, depending on the service conditions and the production process. Some of the techniques to join an aluminum foam core to the skin or the solid panels are as follows:

1. **Adhesive Bonding Method**

The most direct and efficient way to join the solid panels to aluminum foam core is by using adhesive bonding which also serves the benefits of being both highly effective and inexpensive. The prescribed process involves the following phases. In order to ensure superficial roughness, the bonding surfaces of solid panels and aluminum foam core surfaces are first polished with sandpaper. Then ethanol or acetone cleaning to remove oil and impurities is considered on the preprocessed panels and aluminum foam core. In the end, the parts are combined by utilizing adhesive to the preprocessed surface under certain temperature and pressure [16]. Low thermal

stability, an incompatible expansion coefficient, and potential for the development of a thermal and an electrical insolation barrier are some of the disadvantages of using this process [1].

A porous structure creates a rough bonding surface from the standpoint of bonding surfaces, meaning that only a skeleton area can contact a solid panel at an adequate pressure, and hence an effective bonding surface is insufficient. Cutting fluid, grease and debris stick to the inside surface of concave pores make them harder to clean and thus reduce the bonding strength. To boost the bonding strength of AFS, numerous researchers have used various modifications methods to modify both the panel and aluminum foam core surfaces, as well as an elevated temperature adhesive approach. For instance, aluminum foam and aluminum plates have been pretreated with nitrogen plasma to improve the surface hydrophilicity of aluminum and the adhesive [17]. Aluminum foam and fiber metal laminates have been joined using surface modification techniques including silane treatment and silane treatment coupled with the inclusion of polypropylene base layer. An AFS made of aluminum alloy sheets and bonded with an epoxy adhesive demonstrated high bonding strength, and the entire AFS exhibited superior compression and energy absorption properties [18]. The high temperature mechanical properties of AFS can be enhanced by using elevated temperature adhesives in place of conventional ones [19]. Similarly certain bonding strengths are also present in AFSs manufactured directly with carbon fiber/epoxy composite laminates as upper and bottom panels.

In summary, the bonding region serves as an intermediate layer transmitted load, the external solid panels carry the primary loading, and an inside aluminum foam core adds to the functional properties. Several researchers have explored ways to improve adhesive technology in order to increase the bonding strength. Epoxy resin, polycarbonate resin and AB adhesives are the most often used adhesives. However, the adhesive's working conditions are limited by melting and metamorphism because of the characteristics of the polymer itself. Despite the fact that some high temperature adhesives may adapt to short term high temperature settings, the aging problem worsens over long term usage, which limits their applicability [20].

2. Welding Method

The main welding methods for joining aluminum foam sandwiches include brazing, diffusion welding and friction stir welding.

- **Brazing**

For braze welding, molten solders that fill the welding region are required [21]. The primary production approach is similar to that of adhesive bonding. Initially, the core and the solid panels are cleaned to get rid of oxide layers and grease. Then flux aqueous solution is sprayed when solders are inlaid on one side of the panel. The final step is to place the combined foam core and solid panels in a brazing furnace filled with nitrogen.

The joint quality is mostly dependent on the holding temperature and time during the brazing process. Experiments have revealed that many intermetallic compounds (Al/Fe) are induced in the joint if the brazing time is too lengthy which further reduces the shear strength of the joint and the mechanical properties of aluminum foam sandwich are also affected [22]. The bonding strength between the aluminum foam core and the solid panels can be enhanced by improving

solder's wetting and diffusion behavior, thus resulting in joints with high bending strength [23]. An aluminum foam sandwich produced with the zinc-based solder has demonstrated good bending characteristics [24].

The Metallurgical combination is produced when a suitable solder is applied during high temperature brazing to fabricate an AFS. If the brazing temperature is too high, then several defects emerge in the brazing joint at the same time. The primary reason is the formation of oxide layers on the bonding surfaces under high temperature, together with the altered wettability caused by a covered oxide layer. Consequently, the reduction in joints oxidation would result in improved brazing process. In accordance with the experimental findings, the aluminum foam core and panel generate metallurgical bonding without stratification. Despite the fact that the welded AFS possess good quality at the brazing joints but an incomplete melting of the solder layer and over burning of both the panels and core material can readily occur during high temperature brazing.

Overall, the temperature, time, solder, cleaning, and heating methods are the primary control parameters for brazing AFSs, and many researchers have worked hard to increase the bonding strength between the panel and aluminum foam core. The brazing process for the AFS fabrication provides a possible industrial use due to the joint quality and low cost. Brazing is widely accepted in the industry and is ideal for welding precise, complex, and multi-material components.

- **Diffusion Welding**

This process involves the diffusion of atoms at the interface under certain temperature and pressure and resulting in a strong joint. A vacuum or protective environment is an essential requirement for this process. Atomic diffusion is facilitated by microplastic deformation (solid phase diffusion) or the micro liquid of the welding surface (liquid phase diffusion). Aluminum foam sandwich is made by diffusing atoms between the solid panels and core, thus creating metallurgical connections [25]. The contact area gets expanded as a result of microplastic deformation that first takes place at the interface under pressure during the process. A bonding region is created by atomic interdiffusion at the enlarged contact area. Increased holding time causes atomic diffusion to proceed gradually to deep layer, producing intermetallic compounds and resulting in acceptable joints.

Transient liquid diffusion welding, as opposed to solid phase diffusion, is more appropriate for creating an AFS because of the necessary requirements of high-quality surface and a lengthy holding time in the latter process [26]. According to the experimental data, fatigue life of an AFS generated by ultrasound assisted liquid diffusion welding is longer than that of adhesive bonding approach [27]. The vibration assisted liquid bonding technique has been used to successfully build open cell AFS; shear testing revealed that vibration may greatly enhance the bonding quality. Despite all this, there are benefits of using solid phase diffusion welding process to create an AFS, such as good boding strength and the fact that metal is not melted.

- **Friction Stir Welding**

Friction stir welding, known as solid state bonding technique, has been extensively employed to join materials with different properties (dissimilar). In this process, after starting the high-speed rotating stirring head, the cylindrical stirring needle is squeezed into the combined plates until the shaft shoulder has contact with the panel [28]. Mechanical energy from the stirring needle is transferred into the material's thermal energy, and powder in the combined plate induces plastic rheology and mixing. Contrarily, friction stir welding simultaneously implements the core's foaming process as well as the joining of panel and the core.

Aluminum foam complex shaped parts with a consistent porosity structure were found when the weld spacing, speed, and rotating speed were 3 mm, 50 mm/min, and 2000 r/min, respectively. An AFS created by this process demonstrated good bending strength, impact protection performance, sound absorption, and reduction performance [29]. Using friction stir welding, Hangai created an aluminum foam/dense steel composite in which the bonding of aluminum precursor and steel, and the mixing of foaming agent and aluminum powder were accomplished concurrently [30]. Despite the fact that the precursors created an intermetallic compound layer at the interface that was brittle but had a greater strength than the aluminum foam core. The high bending strength of AFS produced by the prescribed process is typically due to two factors [31]. Firstly, the connection between panel and core is made through plasticized metal flow without the use of additional materials. Secondly friction stir welding makes improvement in the panel by refining the panel's grain.

Friction stir welding may also be utilized to connect AFSs from the standpoint of joining technique. An AFS that was successfully created by utilizing friction stir welding is depicted in figure 8. Several small pores were produced at the core and panel mixing region as a result of the stirring head's rapid rotation and movement. The average cell wall thickness for the bonding sections was thicker than the core material for internal pore structures, and a clear welding interface could be seen. After the agglomeration of foamable particles during the mixing phase, a few large pores developed as a result of random foaming process. On the exterior of panels, the welding marks can be seen.

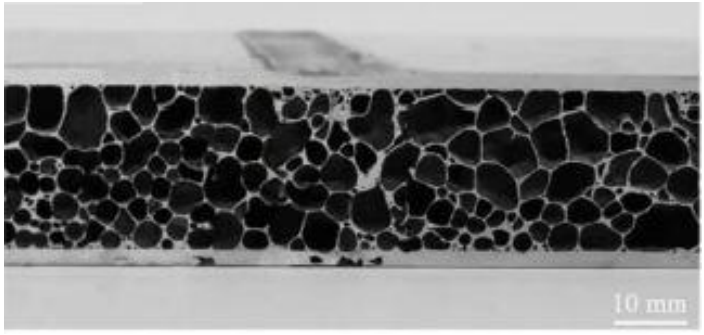

Figure 8 Cross-section of a friction-stir-welded AFS [32]

1.4 Potential Applications of Aluminum Foam Sandwich

An AFS with lightweight and porous structure has a wide range of applications in the various industries such as an automotive, railway industry and infrastructure, the protection against explosions, fire and ballistics, aerospace engineering, shipbuilding, wind energy, mechanical engineering, construction industry and energy technologies.

1.4.1 AFS Current Trends and Future Perspectives in Automotive Sector

The Aluminum is a lighter weight material as compared to steel and works well in circular economy approach since it can be easily recovered and reused in new goods. The North American Light Vehicle Aluminum Content and Outlook report shows that the aluminum usage in the automotive industry has grown from 154 kg (340 lbs) per vehicle in 2010 to 208 kg (459 lbs) per vehicle in 2020 [33]. European data shows that the amount of aluminum increased from 50 kg per vehicle in 1990 to 151 kg currently, with a projection of 196 kg per vehicle by 2025 [34]. But aluminum's uses are still mostly restricted to the engine, gearbox, wheels, heat exchangers, chassis, and suspension. At present, cost is seen to be the greatest obstacle to further usage of aluminum.

The history of aluminum sheet development for the automotive sector includes the 2000, 5000 and 6000 series of Al-Mg, Al-Cu, and Al-Mg-Si [35]. A focus on the dissimilar materials joining technology for aluminum and high strength steel has recently drawn attention to heat treated 6000 series alloys for skin panels because 5000 series is prone to stretch strain marks. These alloys also have the advantage of becoming stronger after being processed through a paint-curing cycle, increasing the exterior dent resistance [36], [37]. The car industry is striving for higher strength aluminum materials needed for strength drive safety critical parts, and experimental 7000 alloys are being produced for these purposes [38]. Aluminum use may be expanded further by using sheets for automotive hoods, trunk lids, outside panels such as doors, and protective coverings.

1.4.2 AFS in Battery Housing for Electric Vehicles

In conventional combustion engine driven automobiles, the body in white (BIW) has mostly remained the same for decades and was designed primarily from the perspective of the usage of steels or aluminum alloys. Therefore, it is quite challenging to incorporate AFS or even any other metal foam into this highly optimized system. AFS has tremendous potential for weight saving of up to 70% while maintaining a consistent bending stiffness. The thinnest AFS is made up of 6.5 mm of foam and two face sheets that are each 0.75 mm thick for a total thickness of 8 mm, making it a new and complicated material only by virtue of its size. Until now, metal sheets with a thickness of 1-3 mm have often been used in basic BIWs. Therefore, a straight replacement of conventional sheet-based structures by AFS would result in an overdesign and would not be practical from an economic standpoint [39], [40].

Although there are several potential conceptual ideas for lightweight construction but design for electric cars is still not obvious. The lack of a powerful engine at the front or rear of the vehicle and the requirement to transfer the power to the wheels from there allows for a flat underbody structure, which is the first factor permitting a sensible use of AFS. Then, it is possible to mount electric engines directly on the axes. Contrarily, the batteries account for a significant portion of the vehicle's weight and must be accommodated. Skateboard design is a basic yet exciting concept that might set a standard for most electric vehicles. The batteries in this "skateboard" configuration accept the area between the underbody sheet, the passenger compartment floor, and the wheels. The center of gravity is maintained low in this manner,

which further improves the driving dynamics. The conventional design, which is still utilized for the majority of the battery compartment modules, consists of a layered structure made of different Al or steel plates that serve a variety of objectives such as impact protection, cooling, bracing, etc. Although it is a reasonable approach, it adds significant weight to the vehicle. Therefore, an alternative solution based on AFS was developed in accordance with the principles of light weighting while keeping mechanical properties at the required level. The battery compartment in the AFS idea is made up of an underfloor and a floor panel (shown in figure 9). Both were manufactured by AFS and were held together with punch rivets and automotive glue to extended aluminum alloy surfaces. Some of the AFS sections underwent partial densification in order to seal the elements and join them to the substructure using common connection methods such as riveting and gluing. The majority of the AFS, however, was not densified. This method resulted in greater stiffness and impact protection while decreasing mass [39], [40].

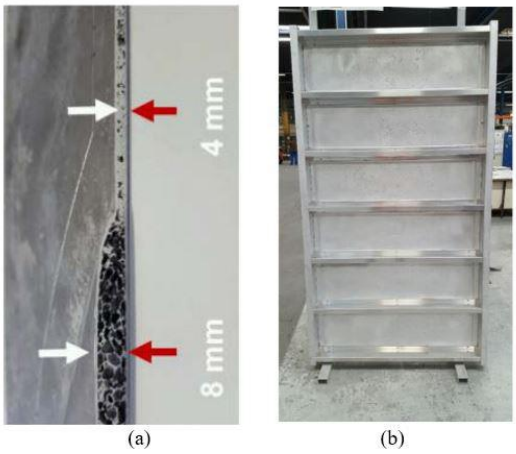

Figure 9 Concept of an electric vehicle's underbody and battery compartment. (a) a compressed AFS panel with sealed edges; (b) a module with a battery compartment on the back and an underbody on the front [39], [40]

The following increased structural and functional qualities, in addition to stiffness, make AFS appear to be a viable substitute for steel or aluminum alloy sheets:

- Protection of battery from external impacts particularly from being punctured by the sharp objects.
- Increased safety in the event of battery failure.
- Improved sound and vibration damping
- Increased safety of electromagnetic damping
- Improved crashworthiness

1.4.3 Crash Absorbers

The need for innovative ideas and materials for lightweight construction is growing as a result of new trends and advancements in the automobile industry, particularly in the electric car market. In addition, new car designs are required due to the component rearrangement, allowing cellular materials to be considered from the start. Another crucial consideration is passenger safety. Since there is no longer a conventional front engine, there is a greater demand for a

light, small and highly effective crash protection system. An example is reported in figure 10. A recent advancement was achieved by the European Project "Evolution", which resulted in the creation of a prototype for an ultra-light electric car, most likely using metal foam components [41].

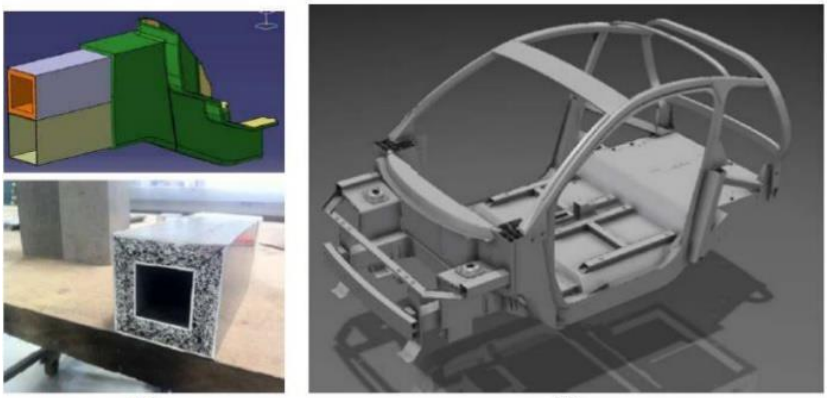

Figure 10 (a) crash absorber box made in the European project Evolution. (b) BIW's CAD design [41]

2. Mechanical Characterization of Metallic Foams

The characterization of cellular metals begins with a comprehensive understanding of the basic criteria required to define the architecture and hierarchy. Firstly, a cellular metal can be considered a heterogeneous composite material made of a metal and a gas. The microstructure of the metal which is made up of grains, precipitates, dendrites, or other phases, can be seen if the metal matrix alone is examined, but the architecture of the cellular metal is not revealed. This level of hierarchy is frequently referred to as the metal's microstructure. The volume fraction of metal and gas affects the density of the cellular metal. As a result, cellular metals are distinguished by their relative density. There is a wide range of relative densities for porous metals, including different metal foams and sponges, based on their unique structures and production methods. The relative densities of commercial metallic foams are 0.02-0.2 for Cymat, 0.1-0.35 for Alulight, 0.08-0.1 for Alporas, 0.05-0.1 for ERG and 0.03-0.04 for Inco. One of the key characteristics of cellular metals is their density, either in absolute or relative terms. This characterization can be termed as 'macro' level. The second most important attribute is cellular architecture. The local density distribution can more clearly characterize a cellular metal because changes in cellular architecture frequently result in inhomogeneity in density. This way of characterizing cellular structures pertains to the 'meso' level. The terms 'meso', 'macro' and 'micro' are not yet standardized. However, figure 11 shows the list of variables useful for characterizing the structure of metallic foams.

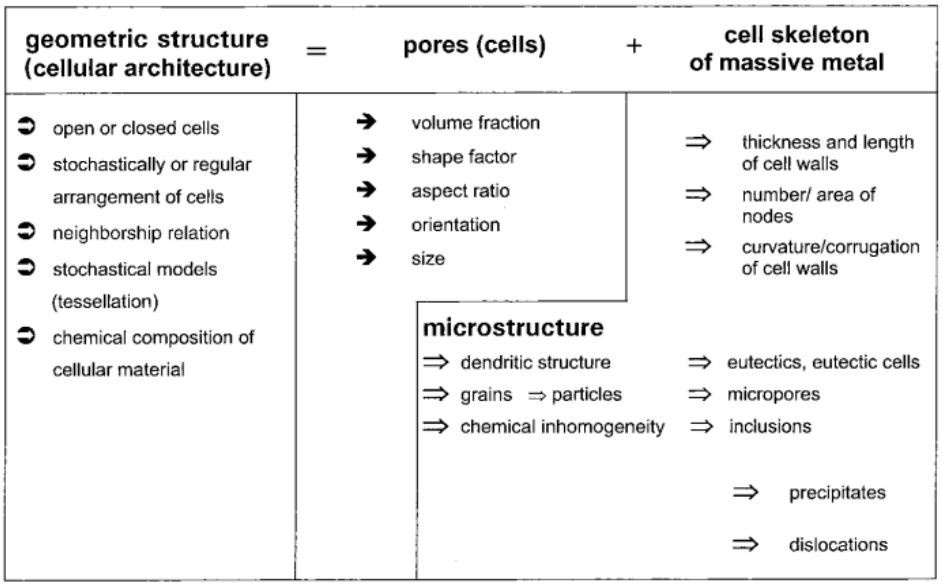

Figure 11 List of parameters for describing the structure of metallic foam [42]

2.1 Methods for Characterizing Metallic Foam

The metallic foams are characterized using a variety of approaches to get information about their microstructure, density, morphology, mechanical properties, etc. According to whether the foam is permanently deformed or otherwise modified, or whether it stays the same or is only slightly altered during characterization, one can generally distinguish between non-destructive and destructive approaches.

2.1.1 Non-destructive Testing

There are numerous non-destructive techniques for describing materials and components. Some of these techniques which have been used for investigating metallic foams are listed below.

1. **Density Measurements**

A porous material's overall density can be calculated by weighing it and estimating its volume using the Archimedes' principle i.e., measuring its buoyancy in a liquid of known density. If the sample to be characterized lacks a closed outer skin, then liquid entering into the pores must be stopped by coating the surface, such as with a polymer film [7].

2. **Dye Penetration Measurements**

Imperfections typically develop during the foam making process, for instance, during the cooling phase after foaming. Small holes or cracks in the cell walls or the outer skin are examples of such defects. These imperfections are best found using penetrant techniques [43]. For doing this, the foam under investigation is first treated with a liquid chemical. The chemical gets absorbed by the cracks and holes. After the surface has dried, a coloring developer is used to add color to the areas where the penetrant chemical has been retained. Maps of the defects can thus be generated in a simple visual method [44].

3. **X-ray Radiography**

Transmission radiography, a simple X-ray absorption technique, can be used to map porous metals. The attenuation of an X-ray beam is measured after it is directed through a sample. By averaging across a specific lateral area and doing two dimensional scans, a foam's 2D absorption map can be produced. The process results in an integrated signal in the beam's direction and the attenuation is correlated to the total mass in a material column. It is possible to distinguish between individual pores and map the true pore morphology if thin slices of foam are examined with a thickness equal to the average pore diameter. However, single pores cannot be further distinguished if the slices are substantially thicker. In certain scenarios, attributes like large pores or holes that are one fourth of the thickness of the foam cannot be resolved adequately [44]. Figure 12 shows the transmission of an inhomogeneous lead foam where it is possible to see large pores, but small pores are difficult to distinguish since several pore images are stacked on the top of each other.

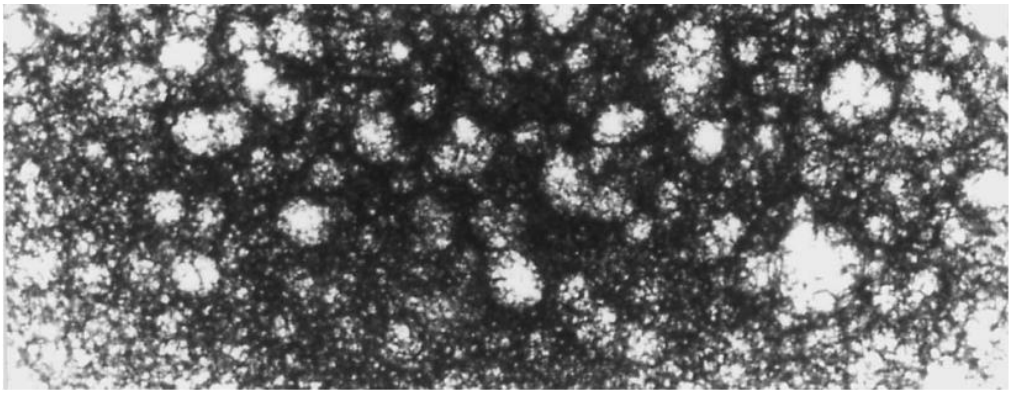

Figure 12 Transmission of an inhomogeneous lead foam [7]

4. **Optical Microscopy**

Optical microscopy is useful for analyzing cell morphology and microstructure. Sample preparation is necessary for optical microscopy and involves cutting, polishing, and etching of samples. By utilizing optical microscopy, one can determine the size and distribution of pores.

5. **Scanning Electron Microscopy (SEM)**

Scanning electron microscopy (SEM) is used to analyze surface and grain structures that are not immediately observable by optical microscopy with a large depth of field. SEM is capable of identifying surface variations. Because of SEM broad working distance and excellent depth of focus, three-dimensional graphs of rough samples can be acquired at all magnifications.

6. **Electrical and Thermal Conductivity Measurements**

Since metallic materials have a low electrical resistivity, the measurements of this property are simple, and a small cross-section is preferred. The restricted cell size, however, puts a minimum on the cross-section. It is important to establish a suitable contact between the leads and the foam. Rectangular specimens having a cross-section of 200 mm^2 and a length of 200 mm have been employed for aluminum foams with a typical pore diameter of roughly 2 mm. Using copper contact plates clamped on the foam, measurements have been taken in the four point-mode [45]. On samples of aluminum foam with 20 mm cross-section, thermal conductivities have also been measured using a modified standard approach.

2.1.2 Destructive Testing

Destructive testing methods involve the physical change or full destruction of the metallic foam sample during the testing procedure. The mechanical properties and behavior of the metallic foams are more precisely and thoroughly described by these techniques.

1. **Mechanical testing**

The mechanical characteristics of metallic foams are mostly determined through mechanical testing. It offers useful information regarding load bearing capability, deformation behavior, and energy absorption properties of metallic foams. The features listed below can be used to categorize many different mechanical tests.

- **Applied Stress**

Uniaxial, biaxial, multiaxial, and hydrostatic stresses can all be applied to the metallic foams. Until now, the majority of experimental studies on the mechanical characteristics of metallic foams have used uniaxial testing as a standard practice. Multi-axial testing has only recently been conducted, with two perpendicular compression axis [46], and one compression axis paired with hydrostatic compression [47].

- **Mode of Loading**

Different loadings, including compression, tension, shear, bending, and torsion, can be employed. The most common tests are compression tests since they may be performed on simple cuboid specimens without the need for clamping. Both dogbone and cuboid specimens

have been used in tension tests. In order to conduct shear testing, one or two flat sheets of cellular metal must be fastened to two or three steel panels. It is possible to conduct bending tests using a three-point or four-point arrangement. The supporting and force transmitting rollers must be carefully chosen since local indentations might invalidate the test findings. When testing foams with closed outer skins, it is important to consider that they have a considerable impact on test results [7].

- **Time Dependance of Load**

The loading can be dynamic, cyclic, or steadily rising (quasi-static). The majority of the research was carried out in almost quasi-static conditions. High strain rates can be achieved in drop weight tests using a split Hopkinson pressure or in ballistic testing [48]. For the same reasons that apply to quasi-static testing, fatigue tests are most conveniently conducted in a compression-compression mode, although compression-tension, tension-tension, and cyclic bending tests have also been carried out by creating suitable samples. If we identify the failure in compression, then the next challenge is to determine the point of failure. A critical strain might be defined as a failure criterion or the knee of the strain versus cycle curves [49]. Similarly, creep tests are performed under predetermined constant loads.

2.2 Literature Review of AFS's Mechanical Characterization

To characterize aluminum foam sandwiches, a variety of techniques can be used to assess their mechanical properties, structural behavior, failure mode, and other important aspects. Most often used characterization methods for the aluminum foam sandwiches are compression testing (to evaluate energy absorption capacity, stiffness, and compressive strength), flexural testing (to measure panel's resistance to bending loads), shear testing (to assess panel's resistance to shear forces), impact testing (to examine the potential of panel to absorb and discharge energy during impact events), fatigue testing (to determine panel's behavior under dynamic loading conditions), thermal testing (to know about thermal properties) and microstructural analysis (to analyze cell morphology, foam structure and bonding interface between core and face sheet materials). The characterization of AFSs is strongly influenced by a number of factors such as density of core material, face sheet materials and its thickness, boding quality, production methods, loading conditions, environmental factors and panel geometry and size.

2.2.1 Quasi-Static / Static Compressive Behavior of AFS

Testing aluminum foam sandwiches under quasi-static or static conditions involves applying a static force gradually in order to access the sandwich's mechanical performance. In the test setup, the sandwich is mounted on the testing device, and a regulated amount of force is slowly applied to the sandwich structure until a certain load or deformation criteria is met. In order to assess the mechanical behavior of the AFS under the imposed load, data is gathered during the test and examined after. Among the several factors evaluated are the load-deformation curve, compressive or tensile strength, energy absorption, stiffness, and failure analysis. The failed AFS may be visually inspected to recognize failure mode and damage patterns.

Zhang Huiming [50] studied the quasi-static behavior of aluminum foam produced by the ALCAN approach. The analysis was devoted to only aluminum foam as a core material. The material used, production method and test conditions made for the test are presented in table 1 whereas the observations from the test are summarized as follows.

It was noticed that the aluminum foam compression is typical of metallic foam deformation under both quasi-static and dynamic compression. It goes through three stages: elastic deformation, plastic deformation, and densification. A partially reversible cell wall bending occurs during the elastic deformation stage as the load increases and the aluminum foam deforms. After the first maximum, the aluminum foam began to deform plastically, and a long plateau region occurred, where the foam cell walls bend, yield, and fractured. The crushing of the foam took place in the sections (of the specimen) with the lowest density or clusters of defects, and the failure progressed along the defects until the deformation covered the entire specimen and the foam became squeezed together. Under quasi-static compression, the higher plateau stress and large load-carrying capacity for aluminum foam with the same average pore size are correlated with the lower porosity of the foam and thicker cell wall as shown in figure 13. The load that the foam can support, and its yield strength increased as the average pore size decreased.

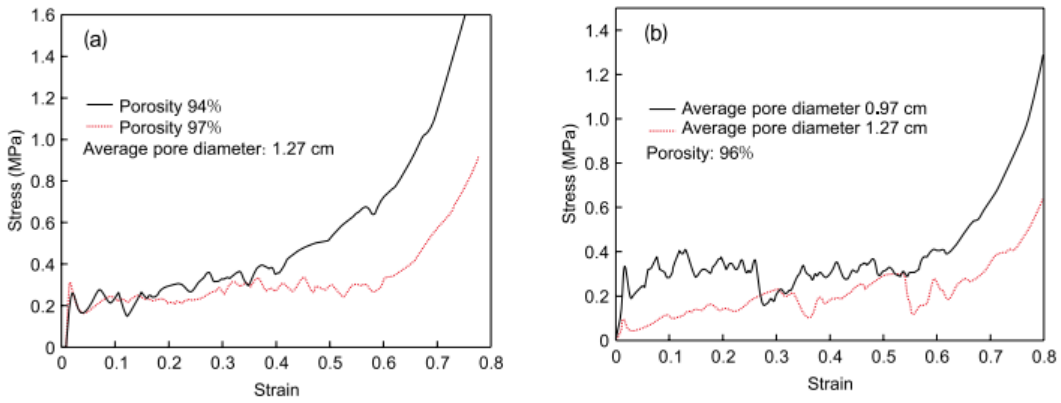

Figure 13 (a) nominal porosities of 94% and 97% at average pore size of 1.27 cm and (b) average pore sizes of 0.97 cm and 1.27 cm at nominal porosity of 96% [50]

Chang Yan [51] examined the mechanical properties of aluminum foam sandwiches when the foam core is sandwiched between different face-sheet materials. The aluminum foam for this study was produced by melt foaming technique and quasi-static three-point bending test was performed for the analysis. The material used and along with joining techniques for AFSs, the production method and the test conditions are reported in table 1 while the important results of the tests are summarized as follows.

Four groups of specimens with varied parameters were examined in order to investigate the mechanical characteristics of AFS structures under a three-point bending. The resulting load-displacement curves are reported in figure 14. It can be observed from the curves that when only the face-sheet materials are different and all other parameters are same, the peak load values of both types of face sheet materials are almost identical and only the plastic stage of the curves is different from one another. When the load increased to its maximum for AFS with

6061 aluminum alloy face sheets depicted in figure 16, it fell swiftly with further displacement increase. The low tensile and yield strengths of the face sheet material made the entire structure break from the bottom face sheet when the load exceeded the yield strength of the AFS beam. The foam core almost crushed at the same time as the face layer failed to absorb sufficient energy. However, in the case of AFS with 304 stainless steel face sheets shown in figure 15, the strength of face sheet material is sufficient to withstand the tensile load without cracking, allowing the load to be transferred to the foam core. As a result, the aluminum foam material, and its unique energy absorption capabilities performed well when reinforced by 304 stainless steels.

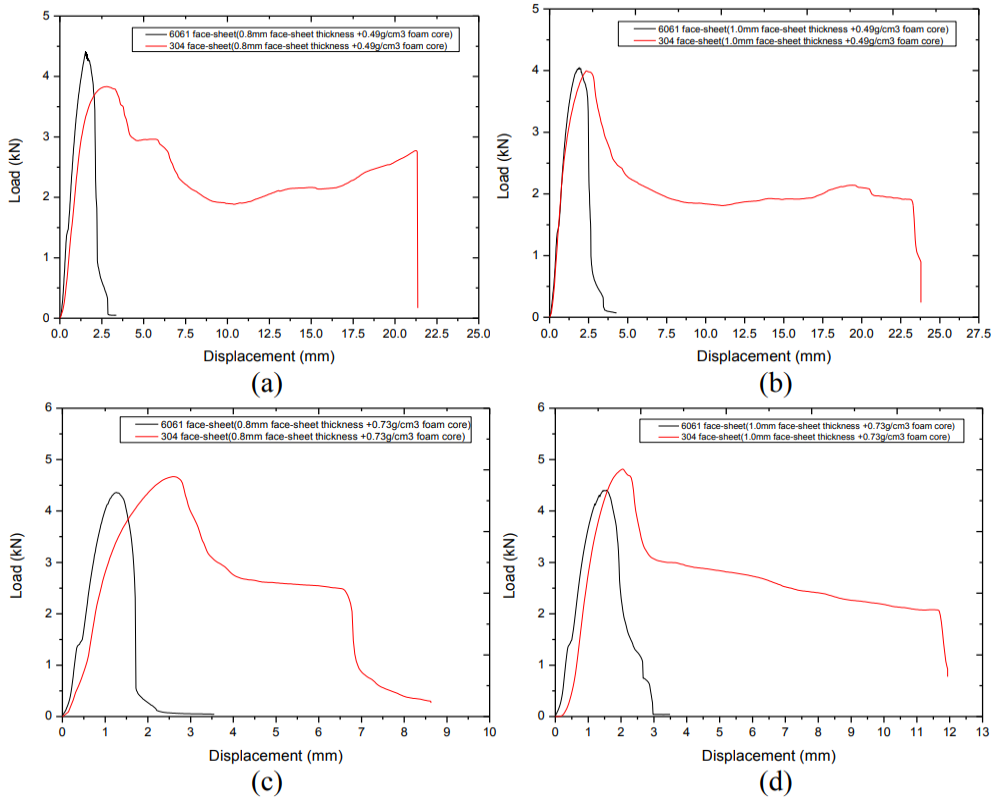

Figure 14 (a) Load-Displacement curves of AFSs with face-sheet thickness of 0.8mm and foam core density of 0.49g/cm3, (b) Load-Displacement curves of AFSs face-sheet thickness of 1.0mm and foam core density of 0.49g/cm3, (c) Load-Displacement curves of AFSs face-sheet thickness of 0.8mm and foam core density of 0.73 g/cm3, (d) Load-Displacement curves of AFSs face-sheet thickness of 1.0mm and foam core density 0.73 g/cm3 [51]

Figure 16 AFS with 6061 face sheets under testing [51]

Figure 15 AFS with 304 face sheets under testing [51]

Guoyin Zu [52] investigated the deformation and failure behavior of AFSs manufactured by

the powder metallurgy method under static three-point bending tests with different span lengths. The typical measured specimens' fracture surface was examined. The material used for AFSs, the production method and the test conditions are reported in table 1 while the important results for the tests are summarized as follows.

Material	Chemical composition (wt.%)					
Aluminum	Al	Cu	Fe	Mn	Si	Zn
1060	~99.60	0.05	0.03	0.03	0.25	0.05

Figure 17 Chemical composition of AA1060 being employed as face-sheet material [52]

Wide (mm)	Length (mm)	Height (mm)	Face thickness (mm)	ρ (g/cm^3)	ρ_{core} (g/cm^3)
10.02	70.01	11.45	1.22	1.01	0.55
10.01	70.01	11.47	0.98	0.93	0.57
10.00	70.01	11.48	0.84	0.86	0.55

Figure 18 Density and dimensions of AFS specimens [52]

The load deflection curve as reported in figure 20 depicts three unique regions; a linear elastic zone at low deflection, a rapid drop region after the load surpassed the yield point (load of 359.05 N and 0.61 mm displacement) and a plateau region with minor load fluctuations aver a large range of deflection. The plateau region's average load seems as high as 368.90 N, which implies that the foam core significantly absorbed energy after AFS passed the yield point. The load deflection curves for various face sheet thicknesses are shown in figure 19, which clearly shows how strongly face sheet thicknesses affects the bending strength. With a thicker face sheet, the ultimate load rises significantly but the ultimate deflection stays relatively constant. This is due to the face sheet's ability to offer significantly flexural strength for the entire AFS [63]. The span's impact on the bending strength is depicted in figure 22. The load deflection curves show that the ultimate load lowers as the span rises. The outcome can be attributed to the foam's core inhomogeneous deformation brought on by the extensive span. Many cracks start in the foam core and propagate along the interface of face sheet and core.

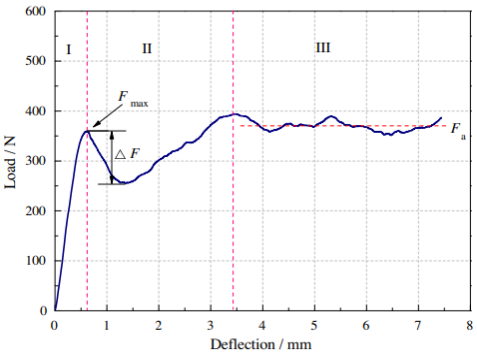

Figure 20 Load–deflection curve of AFS with face sheet thickness of 1.22 mm and span length of 30mm [52]

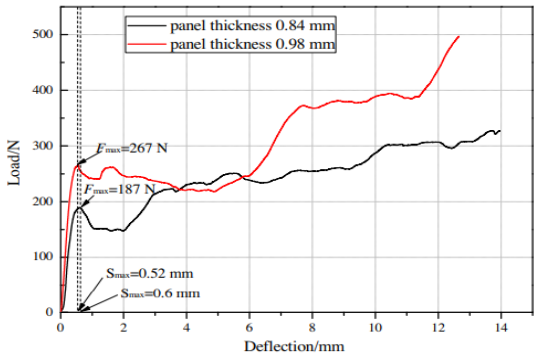

Figure 19 Face sheet thickness's effects on the bending strength of AFS [52]

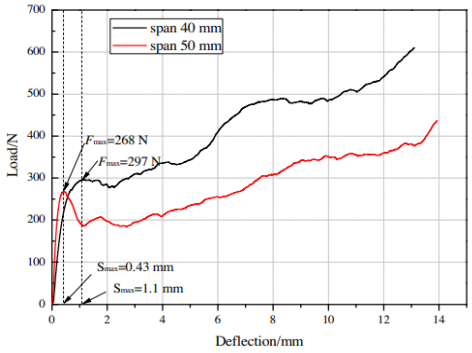

Figure 21 Span's effect on the bending strength of AFS [52]

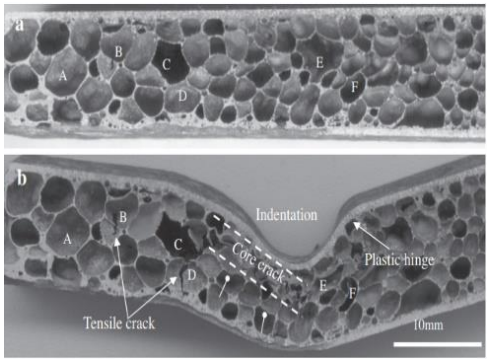

Figure 22 Failure mode of AFS. a) before testing b) after testing [52]

Three obvious failure modes for AFSs including indentation, core shear and plastic hinge can be observed in figure 21. Before testing, six cells, numbered from A to F, were marked. The majority of cells deformed just slightly or not at all such as cell A, but tension stress is introduced into the cell membrane (of cell B and D), which resulted in cracks on the stretched cell face. Most of the cells near to the indentation are displaying significant plastic deformation, whereas cells at the bottom of indentation exhibited little deformation. No delamination is seen between the face sheet and foam core, indicating an excellent bonding on the interface. The damage progression which seems to be steady corresponds to the smooth part of load displacement curve.

Guoyin Zu [53] also researched the deformation and failure behavior of AFSs with different thicknesses of panel and foam core under static three-point bending tests. The melt foaming approach was utilized to produce aluminum foam. The material used along with joining technique for AFSs, the production method and the test conditions are illustrated in table 1 while the important observations from the tests are summarized as follows.

The curves of load vs deflection (figure 24) indicate that the bending strength of AFS increases with the rise of foam core thickness. The mechanical mismatch between foam core and steel panels at the glued interface may be the cause of exception for the 20 mm and 30 mm curves. Figure 25 shows that while the equivalent deflection has a little association with foam core thickness, but the bending load dramatically increases as core thickness rises. This happens because the aluminum foam core effectively absorbs bending loads, delaying the collapse of the entire structure.

For AFSs with thick steel panels, there is a unique adhesive delamination and foam core shear damage (figure 26). Thick panels have good capacity to work against bending loads. For thick panels AFSs, bending load can be diffused through the foam core and translated to the bottom panel. Hence, load between top and bottom panel is different. When the foam core's ability to withstand the bending reaches its maximum, the AFS will be deformed. There is a tensile stress at the bonded interface between top panel and foam core after the crush of foam core under high bending loads. As a result, the bonded interface next to the pressure head delaminates.

Type	Thickness/ mm	*w*(C)/%	*w*(Si)/%	*w*(Mn)/%	*w*(Fe)/%
Q235B	3, 4, 5, 6, 8	0.12−0.2	<0.3	0.3−0.7	Bal.

Figure 23 Thickness and chemical composition of steel panels [53]

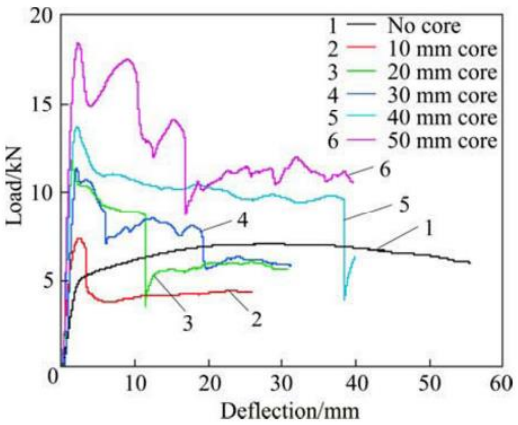

Figure 24 Load vs deflection curves of AFS with different core thicknesses [53]

Core thickness/mm	Maximum bending load/kN	Deflection at maximum bending load/mm
10	7.37	2.39
20	11.91	1.62
30	11.4	2.16
40	13.7	2.34
50	18.52	2.42

Figure 25 Static three-point bending results of AFSS with 3 mm steel panel and different core thicknesses [53]

Figure 26 Bending deformation of AFS with 4 mm panel and 50 mm core thickness [53]

The typical Al-Si (figure 27-a) eutectic microstructure with some microcracks and voids is represented in the SEM image of an aluminum foam wall far from the fracture. The bending deformation is not significantly affected due to small sizes of defects. On the other hand (figure 27-b), a crack of nearly 300 μm in size is propagating along the crack tip. It may be due to the fact that cracks of a particular size experience some stress concentration from external loads. The fracture propagation caused by stress concentration worsens with increased bending load, eventually leading to AFS structural failure.

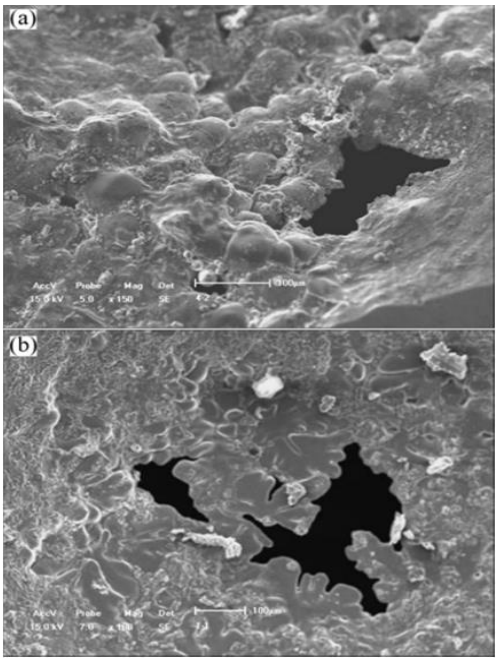

Figure 27 SEM images of foam wall. a) far from the fracture b) near the fracture [53]

No.	Material used and joining technique	Production method	Test conditions	Reference
01	The base material was an aluminum alloy called A356. Only aluminum foam as a core material was studied in this research.	Foaming melts by gas injection method (ALCAN) was employed to produce aluminum foam. The base material was heated by a resistance furnace to 680 °C, where it was melted and maintained. Compressed air was injected into the aluminum melt to produce aluminum foam (closed cell). Al_2O_3 particles (9 μm average size) were added and dispersed by mechanical stirring at 1300 $r \cdot min^{-1}$. Cylindrical specimens (length of 12 cm and diameter of 8 cm) were cut from the collected foams by using electro-discharge machining.	A quasi-static compressive test was carried out (using WDW-100 computer-controlled machine) at room temperature on specimens having porosities ranging from 94% to 97%. 5 $mm \cdot min^{-1}$ was the compressive rate and after data processing, the stress-strain curves were obtained.	50

02	As core materials, two types of aluminum foams (7050 matrix) with densities 0.49 g/cm^3 and 0.73 g/cm^3 were selected. Similarly, two different kinds of face-sheets were used. One of them was 6061 aluminum alloy panel while the other was 304 stainless steels. The thickness of the foam core was 15 mm. For both 304 and 6061 face-sheet panels, the thicknesses were of 0.8 mm and 1.0 mm respectively.	The aluminum foam core was produced by melt foaming method. To create the AFS, E44 and 650 resin firming agents were chosen as the adhesive.	WDW-T100 tensile testing machine was used for three-point bending tests. The diameters of the indenter and two support pins were each 10 mm. The specimens were indented at the center of the top face-sheet material at a rate of 2 mm/min. The span length and overhang distance were 80 mm and 35 mm respectively.	51
03	AlSi9Mg alloy powder (99.0 wt.% purity and 126.8 μm size) was used as a core material for the AFS and AA1060 aluminum shaped tube (length of 130 mm) was employed as the face-sheet material. The chemical composition of AA 1060 is given in figure 17.	The AFS was obtained by means of powder metallurgy process. TiH_2 powder (99.0 wt.% purity and 32.5 μm size) was used as a blowing agent. The alloy AlSi9Mg with 0.6 wt.% was created by properly blending the two types of powders. The densely packed Al shaped tube with alloy powder within was cold rolled by reduction 60-70% and foamed in a resistance furnace for 90 seconds at 700 °C. Foamed sheets were cut by wire electrode into specimens having dimensions of 70 mm long and 10 mm wide, with a consistent thickness of 11.5 mm for face sheet and cell structure.	On the CMT5105 material testing system, the static three-point bending tests of the specimens were carried out for different specimens at a speed of 2 mm/min with varied span lengths of 30, 40 and 50 mm. The density and dimensions of AFS specimens are reported in figure 18.	52

04	The AFS was made of pure aluminum as foam core and the panels were made of steel. The thickness and chemical composition of steel panels are listed in figure 23. The foam and panel were cut to lengths of 240 mm and widths of 80 mm.	The melt foaming method was used to produce aluminum foam core with different thicknesses. The polyamide-epoxy resin was used to bond the aluminum foam core and the steel panels with 1:1 mass ratio and left for 24 hours at ambient temperature.	On a CMT5105 material testing equipment, static three-point bending tests were carried out with five duplicates at a pressure head speed of 5 mm/min. The span's length was 150 mm while the pressure head diameter was 20 mm.	53

Table 1 Quasi static / static behavior of AFSs under various investigations.

2.2.2 Fatigue (dynamic) Behavior of Aluminum Foam Sandwich

To assess the durability and resistance to cyclic loading of AFSs, fatigue testing is done, especially in compression-compression loading mode. The testing machine is equipped with a control system that allows for cyclic loading with controlled magnitude, frequency, and waveform. The required number of cycles or the test duration, as well as the loading amplitude and cycle frequency, are defined as test parameters. The sandwich is put through a loading sequence where it is repeatedly subjected to cyclic compressive loads that follow a waveform. Various parameters are tracked and recorded while the fatigue test is being performed in order to acquire data. The fatigue life evaluation measures the number of cycles or length of the test before failure or a certain degree of damage. The applied stress and number of cycles before failure are related to the S-N curve. The fatigue failure analysis is conducted to identify the failure mode of the failed aluminum foam sandwich.

Zhengfei Hu [27] used scanning electron microscopy, optical microscopy, and energy dispersive spectroscopy to evaluate the microstructure of aluminum foam sandwich joints under fatigue and peel strength tests. The sandwiches considered for the analysis were fabricated by two different manufacturing approaches. The material used along with joining technique for AFSs, the production method and the test conditions are illustrated in table 2 while the important results from the tests are summarized as follows.

The aluminum foam sandwich with different joining interface microstructure is reported in figure 28. A soldering Zn-Al alloy with a eutectic structure makes up the seam of the metallurgical joint (figure 28 - a, b). α-Al dendrites induced on the foam core's and Al sheet's substrate surfaces and spread into the region where Zn-Al fuses. The molten Zn-Al alloy exhibits strong wettability and intimate contacts with substrates, resulting in compact and continuous fusion. The joint interface of adhesive AFS sample (figure 28 - c, d) shows various defects such as holes and uneven inclusions, which may emerge during the gluing process. Since air which cannot be extracted completely from the Al alloy sheets and Al foam may result in air holes when adhesive starts melting. Similarly, the thermoplastic glue film contracts

and form hole defects during melting and remodeling process which lead to a poor strength of adhesive joint

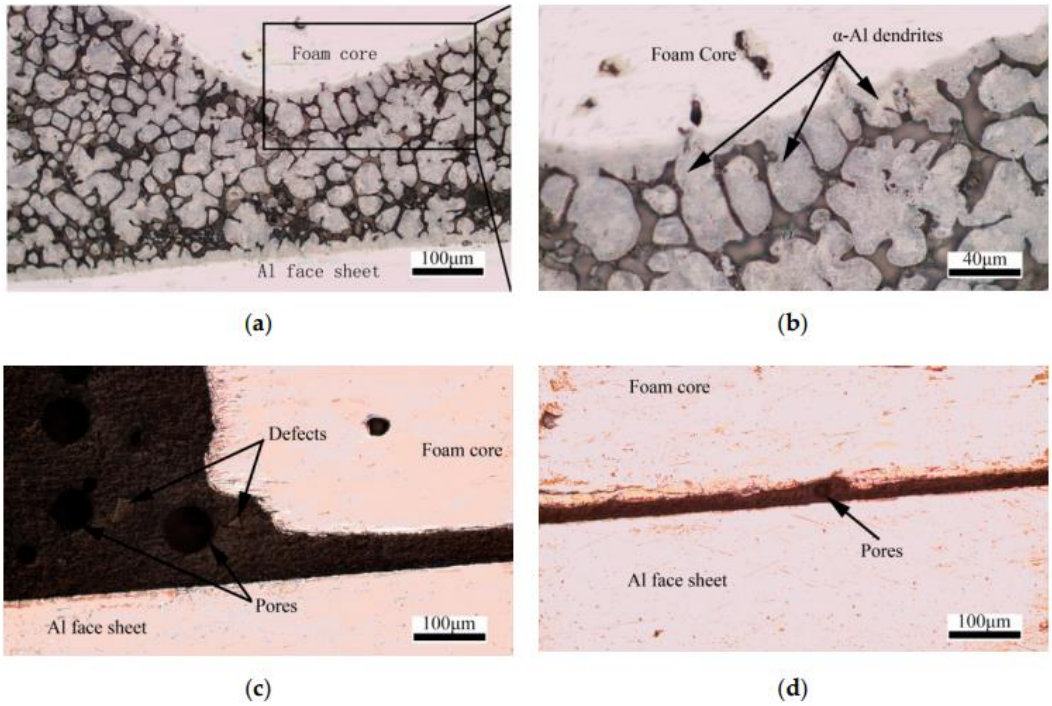

Figure 28 Optical microscopy images of joining interfaces. a, b) metallurgical joining while c, d) adhesive joining [27]

Peel Strength

In order to verify the joining strength of interfaces, three samples each from two different types of AFSs were tested. The reported results in fig 30 indicate that the average strength of metallurgical joining (140 N·mm/mm) is higher than that of adhesive joining samples (27.5 N·mm/mm). Moreover, the fracture morphology of metallurgical joining AFS (figure 29-b) addresses that the destroyed part during the test is the aluminum foam core rather than hot dip coating, resulting in higher joint's strength than core material. In contrast, the glue and sheets look entirely separated in adhesive AFS samples (figure 29-a), indicating that the joints' strength is inferior to both the film and the core. Defects made during the heat press process in the adhesive area may be the possible reason for this failure.

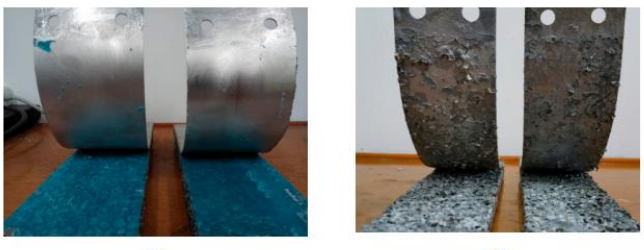

Figure 29 Fracture morphology of AFS samples. a) Adhesive joining b) metallurgical joining [27]

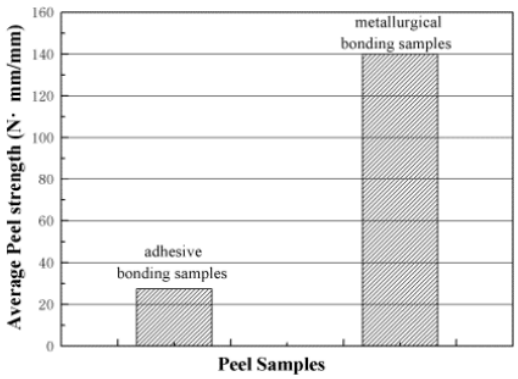

Figure 30 Average peel strength of two types of samples [27]

Fatigue Test

According to S-N curves shown in figure 31, the fatigue life of metallurgical joining AFS is higher than that of adhesive joining AFS under the same load. The experimental relations are obtained by fitting S-N curves with the average fatigue life for every given load. The fatigue limit is defined by considering the force for which the fatigue life is 5 million loading cycles. In this regard, the fatigue limits for metallurgical joining AFS and adhesive joining AFS using equation 1 and 2 are 3058 N and 2829 N respectively.

S=7380-645.2log10 (For metallurgical joining) **1**

S=6162-497.5logN (For adhesive Joining) **2**

By looking at the fracture morphology depicted in figure 32, it is clear that the fracture mode of AFS with adhesive bonding (figure 32-a) is face fatigue and debonding while for metallurgical bonding AFS (figure 32-b) is only face fatigue and no delamination. The failure proceeds in two stages for AFS with adhesive bonding. Initially, debonding takes place between face sheet and core and then the aluminum foam core breaks by the bending force and results in final rupture.

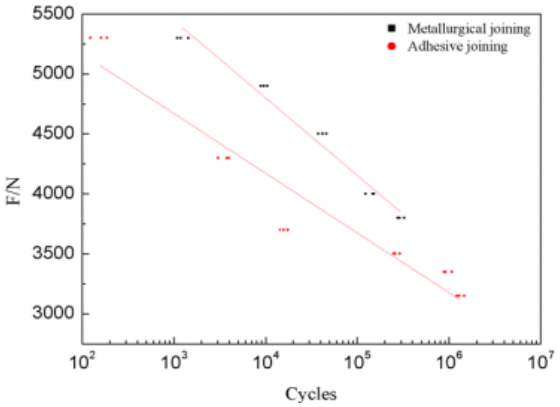

Figure 31 S-N curves of two types of AFSs [27]

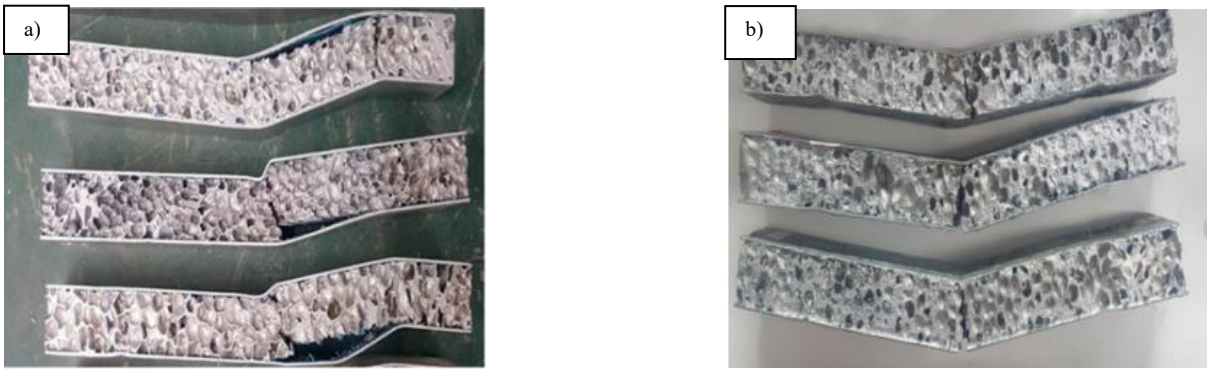

Figure 32 Failure mode of AFSs under fatigue behavior. a) Adhesive joining b) Metallurgical joining [27]

Zhengfei Hu [54] also determined the fatigue strength of adhesively bonded AFSs with different densities of foam core aluminum under three-point bending fatigue tests. The fatigue process of aluminum foam sandwich panels is shown using force cycles curves and deflection curves. The material used, the production method and the test conditions are presented in table 2 while the important details from the tests are summarized as follows.

According to the force-cycle curves shown in figure 33, it can be observed that the AFS with higher density core material shows better fatigue life than AFS with lower density core material. The S-N curves are fitted using non-linear curve fit to develop an experimental relation in order to find out exact fatigue limit of samples.

$$y = a + b \log_{10} X$$

F = 4261 − 262.6 log10 N (AFS with core material having density of 0.3 g/cm^3)

F = 6162 − 497.5 log10 N (AFS with core material having density of 0.4 g/cm^3)

F = 10412.7 − 946.2 log10 N (AFS with core material having density of 0.6 g/cm^3)

The fatigue limit is defined by considering the force for which the fatigue life is 5 million loading cycles. According to this criterion and using above relations, the fatigue limit for 0.3, 0.4 and 0.6 g/cm^3 dense core materials are found to be 2501.8 N, 2829.3 N and 4047.1 N respectively.

Similar patterns can be seen in the deflection curves (figure 34). With increasing cycles, the fatigue response displayed a relatively slow rate of deflection accumulation. The formation of micro-damage caused the defects to grow slowly and progressively during the incubation period. Internal cracks formed quickly and deflection rate sharply increased when micro-damage reached a critical threshold, signaling the end of incubation phase and eventual failure. Considering failure mode shown in figure 35, high density samples failed due to face fatigue whereas, debonding and face fatigue were the causes of low-density samples.

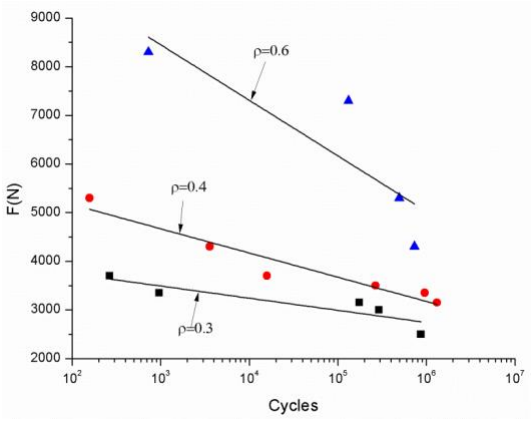

Figure 33 Force-cycle curves of AFSs with different densities of core materials [54]

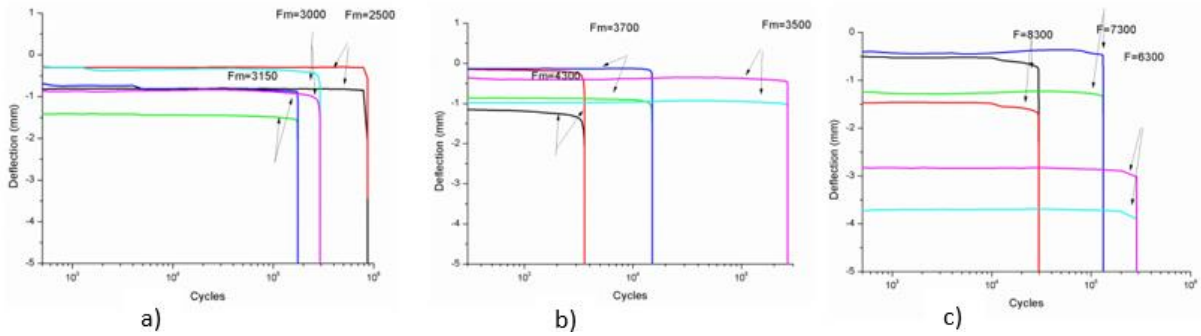

Figure 34 Deflection vs no. of cycles of AFSs. a) 0.3 g/cm3 b) 0.4 g/cm3 c) 0.6 g/cm3 [54]

Figure 35 Failure mode of AFS during fatigue tests. a) 0.3 g/cm3 b) 0.4 g/cm3 c) 0.6 g/cm3 [54]

Guoyin Zu [55] studied the fatigue properties of AFSs prepared by the power metallurgy method. The comparison was made with adhesively bonded AFSs. By examining the fatigue life, deflection curve, and failure mechanism, the fatigue performance was examined. The material used, the production method and the test conditions are presented in table 2 while the important results from the tests are summarized as follows.

AFSs prepared by powder metallurgy and adhesive bonding processes underwent three-point bending fatigue tests. The corresponding results are presented in figure 36. It can be observed that at load level of 95%, the fatigue life of adhesive bonded AFS is 48 cycles while powder metallurgy AFS is 118 cycles. Similarly at a lower load level of 70%, the fatigue lives of adhesive and powder metallurgical AFSs are 615201 and 789508 cycles respectively. At the same load level, the powder metallurgical AFS has higher fatigue life than adhesive AFS. Furthermore, the difference in fatigue life between the two AFSs made using different approaches is not substantial at higher loads. However, it seems that this difference in fatigue lives only becomes important at lower load levels. F_{max} corresponds to maximum load in the fatigue test while F_p ultimate bending load measured in quasi static test.

F_{max}/F_P (%)	95	90	80	70
$n_{Adhesive\ method}$	48	77	10,541	615,201
$n_{Powder\ metallurgy\ method}$	118	148	152,730	789,508

Figure 36 Fatigue lives of AFSs under fatigue tests [55]

The deflection curves with fatigue life are reported in figure 37. Similar variation patterns can be seen by the deflection curves at different load levels and the fatigue process is essentially divided into two stages: the stable stage and the transient breakage stage. About 90% of the entire fatigue process occurred during the stable stage. In this stable stage, the displacement changed gradually in accordance with the cyclic variation of the fatigue load, and the specimen remained undamaged and free of macroscopic cracks. However, the higher fatigue cycle number resulted in macroscopic cracks appearing, growing, and penetrating in the specimen, and thus resulting in final rupture. On comparison, it can be seen that (figure 37-a) has a longer stabilization stage than (figure 37-b), indicating that the powder metallurgy approach has longer fatigue life than adhesive method.

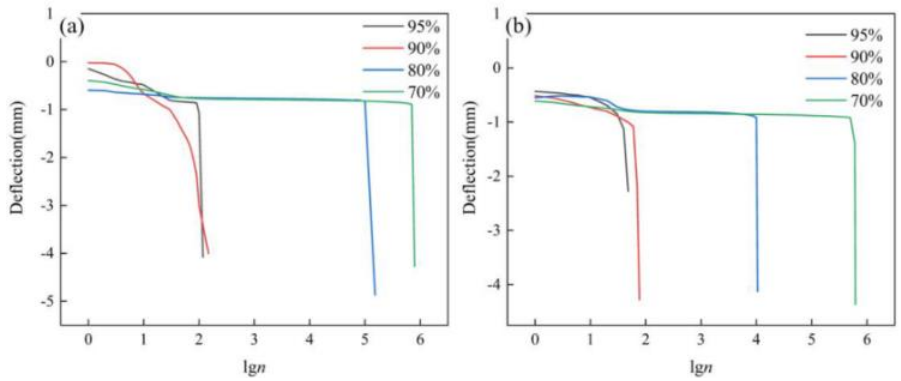

Figure 37 Deflection life curves at different load levels. a) Power metallurgy AFS b) adhesive bonded AFS [55]

The fatigue fracture modes of AFSs are displayed in figure 38. The dotted yellow lines indicate the resulting cracks. The fracture mechanism for powder metallurgy process (figure 38-a) is core shear with cracks developing at larger cells or close to the upper indenter. Fatigue failure

resulted from microscopic cracks expanded in 45° direction towards the panel when the load reached critical collapse threshold. On the other hand, core shear and interface debonding are the failure modes of adhesive technique (figure 38-b). Separation occurred between the core layer and panels when the crack reached the joining interface. The absence of debonding behavior in the powder metallurgy process may also indicate that it has stronger bonding interfaces than the adhesive method.

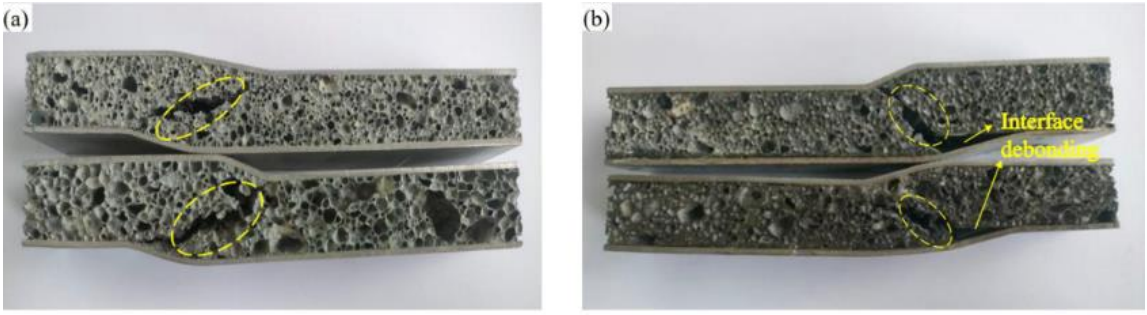

Figure 38 Fatigue failure modes of AFSs. a) powder metallurgy b) adhesive boding [55]

Chang Yan [56] analyzed the fatigue performance and damage mechanisms through SEM of adhesive bonded AFSs using aluminum foam as a core material and carbon fibers as face-sheet by employing a high frequency fatigue testing machine. The material used, the production method and the test conditions are presented in table 2 while the important test findings are summarized as follows.

Si	Fe	Cu	Mn	Mg	Cr	Zn	Ti	Othes	Al
≤ 0.12	0.15	2.2	0.04	2.3	0.06	5.7~6.7	0.05	0.15	Margin

Figure 39 Chemical composition of 7050 aluminum alloy [56]

Five groups of specimens were prepared and tested in this work. To analyze the effect of density of core material on the fatigue behavior, three groups of specimens using 3 plies of carbon fiber fabric face sheets were prepared with different densities of core. On the other hand, to investigate the influence of carbon fiber plies on the performance of AFSs, three groups of specimens with carbon fiber plies of 1, 3, and 5 were tested. 0.60 g/cm^3 was the foam core density in all of the three groups. The stiffness degradation criterion was used to define the ending of tests.

The S-N curves of AFSs with different core densities and 3 plies of carbon fiber face sheet are shown in figure 40. It is evident that increasing loading level resulted in decreased fatigue life irrespective of foam core density. When the loading level increased from 20% to 25% as shown in fig 41 with foam core density of 0.60 g/cm^3 and 3 plies carbon fiber as face-sheet material, the number of cycles decreased from 505382 to 194899. The number of cycles decreased continuously as the loading level increased further. The tested specimens from other groups also followed the same pattern. The present research shows that AFS is highly dependent on loading levels, which implies that when the loading level is slightly increased, the life of AFS may be drastically reduced. As a result, AFS can be utilized safely with low cyclic loadings. According to figures 40 and 42, the fatigue life of AFSs decreased with the increase of foam core density at the same loading level and with the increase of carbon fiber plies

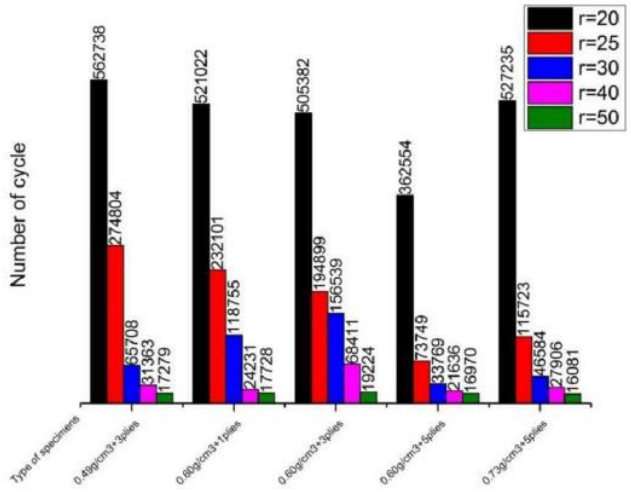

Figure 41 No. of cycles of different types of specimens [56]

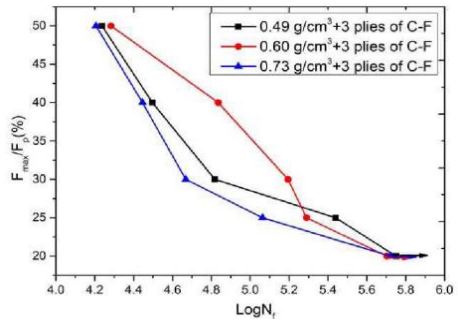

Figure 40 S-N curves of AFSs with different core densities [56]

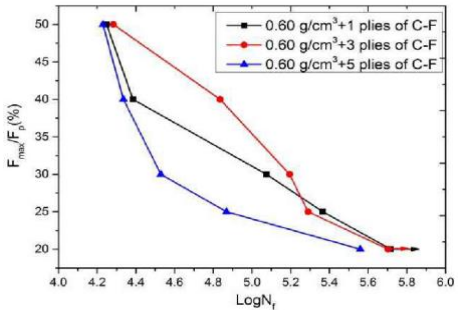

Figure 42 S-N curves of AFSs with different face sheet thicknesses [56]

Under cyclic loading conditions, the AFS structure failed through a foam core shear. The primary cause of aluminum foam core damage under fatigue was stress concentration at foam's cell ridge or cell wall. Some small defects and cracks can be seen at cell ridge and cell walls of some foams according to figure 43, which are sufficient to induce stress concentration and thus result in whole failure of the foam. The initiation of damage from the thinnest region of cell wall was considered another source of fatigue damage mechanism for aluminum foam as depicted in figure 44, where a fracture source is located in the center and clear fatigue fringes that extend in both directions along the arrows can be seen. The damage is propagating along the direction of arrow whereas the direction of fringes is perpendicular to that of arrow. The cell wall is often thinnest in the center, thus making it easy for the damage to start there. The primary cause of fatigue damage in the current study is that the crack proceeded along the cell wall rather than through the cell itself. The fatigue life would be improved by a thicker cell wall because this would make the crack initiation more challenging and allow for a longer crack propagation path.

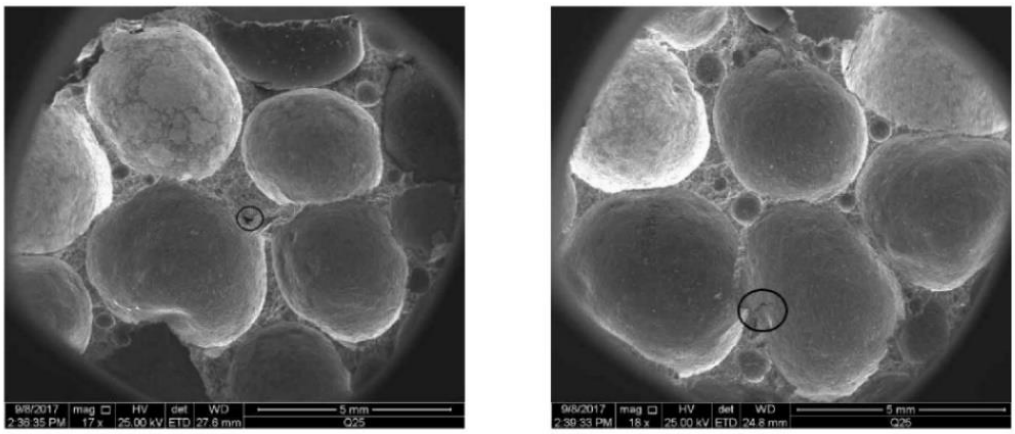

Figure 43 Aluminum foam morphology with small defects and cracks [56]

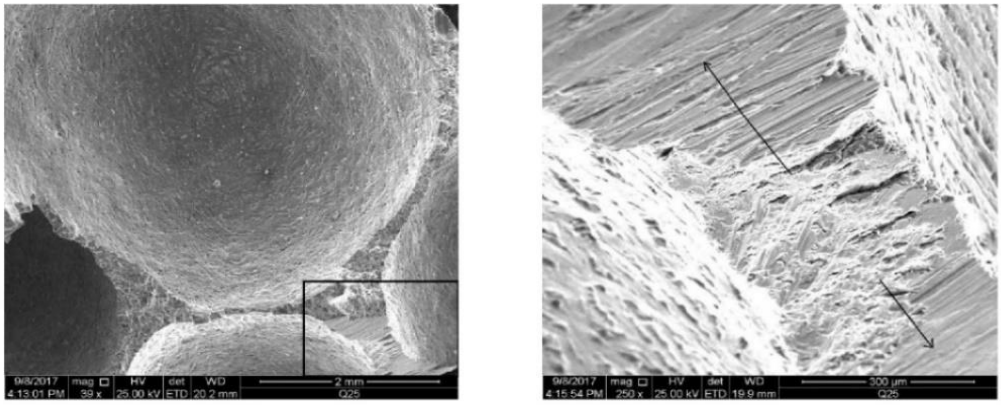

Figure 44 Crack initiation and propagation at cell wall. a) general view b) more detailed view of the marked area in (a) [56]

No.	Material used and joining technique	Production method	Test conditions	Reference
01	Aluminum alloy 5056 with a composition of (Al 94.8% + Mg4.5% + Fe 0.4% + Si 0.3%) was used as a face-sheet material whereas a closed cell pure aluminum foam (average density 0.4 g/cm^3, porosity 85%, 25 cm thick and 7 mm average cell size) was used as a core material. The face sheet and core material were cut in lengths of 300 mm, widths of 50 mm, thickness of 1 mm of face sheet and 25 mm of core material.	Two different joining techniques were used to make the AFSs for comparison purpose. One of them was liquid diffusion welding while the other was adhesive bonding. To fabricate AFS by liquid diffusion welding method, Zn10Al was used as a joining alloy. The joining surfaces were placed in a 450°C melting solder bath for 50s to induce joining alloy on joining surfaces. The heat press approach was employed to finally join the pre-coated surfaces aided with ultrasonic vibration for 1 min to achieve high joining strength. On the other hand, Aerial adhesive film was used to manufacture adhesive bonded AFS using a heat compress method at 80 °C for 5 min.	To validate the joining strength of two different kinds of AFSs, the peel strength test was carried out at WDW-100 universal testing machine. Fatigue tests were conducted at MTS-809 fatigue test machine with a span length of 200 mm, stress ratio of (R= -0.1) and 7 Hz as a cycle frequency. The lengths, widths, and thicknesses of AFSs for mechanical tests were 300 mm, 50 mm, and 27 mm respectively.	27

02	Pure aluminum foam with closed cells was used as a core material for AFS whereas aluminum alloy 5056 was utilized as a face sheet material. The thicknesses of core material and face sheet were of 25 mm and 1 mm respectively.	The core materials with distinct densities were prepared. 0.3 g/cm^3 and 0.4 g/cm^3 were considered as low-density samples while 0.6 g/cm^3 as high-density samples. Aerial glue coat was employed as a joining glue and the AFSs were made by hot press method at 90 °C for 10 min.	MTS-809 fatigue test machine was used to perform three-point bending fatigue tests on AFS using span length of 200 mm, stress ratio of R= -0.1 and 7 Hz as a cycle frequency. The length, width, and thickness of AFSs were 300 mm, 50 mm, and 27 mm respectively. The fatigue tests stopped if the samples had clearly fractured, or the strain was greater than 20%.	54
03	The AFSs prepared by powder metallurgy and adhesive bonding processes were considered for the research. The metal powders of Al, Si, Cu, Mg, and a blowing agent of TiH_2 were considered as materials for powder metallurgy process. For Adhesive bonded AFS, pure aluminum was used as a foam core material with a density of 0.73 g/cm^3 while 6061 aluminum alloy with a thickness of 0.8 mm was employed as a face sheet material.	For AFSs manufactured by powder metallurgy process, the mixed metal powders of Al, Si, Cu, Mg and TiH_2 as a blowing agent were put into a cavity, made of aluminum alloy 3003 with a thickness of 3 mm. To obtain foaming precursors, hot and cold rolling were performed with 330-400 °C hot rolling temperature range. After that the foaming process was carried out with a foaming temperature of 620 °C for 10-15 min. A uniform layer of graphite was deposited on the precursor's surface to quickly heat during the process. The required AFSs were obtained by wire cutter. The adhesive bonded AFS was fabricated using epoxy resin glue E-44 and hardener 650. After joining the panel	Three-point bending fatigue tests were conducted on AFSs with lengths, widths and thicknesses of 170 mm, 30 mm, and 24 mm respectively. The cycle frequency was 15 Hz with a load ratio of R= 0.1. Four load levels of 95%, 90%, 80% and 70% were set and maximum load of fatigue test machine was 20 KN. The tests ended when there were clear cracks and the upper panel's middle deflection value was 15% or greater of its thickness.	55

		was placed in a drying box for two hours at 80 °C and left there for 48 hours.		
04	Three kinds of aluminum foams having densities of 0.49 g/cm^3, 0.60 g/cm^3 and 0.73 g/cm^3 were used as core for AFSs. The core material was 7050 aluminum alloy with chemical composition listed in figure 39. The yield strengths of the foams were 4.17, 4.40 and 8.80 MPa respectively under quasi-static compression. The face sheet material was carbon fiber fabric named BR-CFC.	The aluminum foam was produced by melt foaming method (ALPORAS). The aluminum foams were sandwiched by 1,3 and 5 plies of carbon fiber fabric to investigate the effect of carbon fiber ply sequence on the fatigue behavior of AFS. To fabricate AFSs, E44 epoxy resin and 650 resin firming agents were used as adhesive	High frequency testing machine GPS-100 was used to carry out fatigue tests. Depending on the specimen being evaluated, the frequency of the machine adjusts automatically between 80 Hz and 250 Hz, with an average load relative error of ±0.5 %. The load ratio was R= 0.1. AFSs were 150 mm long, 30 mm wide, and varied in thickness according to the number of carbon fiber plies. The cyclic loading was a percentage of the ratio of peak load in fatigue test to the peak load in quasi static test. The loading levels were 20%, 25%, 30%, 40% and 50%.	56

Table 2 Fatigue behavior of AFSs under various investigations

3. Materials and Methods

In this research work, the focus is devoted to the compressive behavior of aluminum foam sandwiches under fatigue (dynamic) loading conditions. For this purpose, three samples of aluminum foam sandwiches were considered for analysis. The core material of the AFS was pure (closed-cell) aluminum foam which was produced by melt foaming approach (ALPORAS) with TiH_2 (Titanium Hydride) acting as a foaming agent. 6000-series aluminum alloy AA6016 (AlSi1.2Mg0.4) was considered to be the face-sheet material for AFSs. Among the 6000-series alloys in the database, this alloy has the highest ductility. The detailed chemical composition and mechanical properties of face sheet material AA6016 are listed in tables 1 and 2 respectively. Zn2Al was used as a joining alloy to bond the face-sheet and core materials through the brazing process [24]. In order to have a detailed examination of AFSs under fatigue loading conditions, the samples underwent through the following sequence of operations and analysis: three-point bending fatigue tests, optical microscopy analysis at low and high magnification followed by samples cutting, resin mounting and polishing, and scanning electron microscopy analysis with EDS (Energy-Dispersive X-ray Spectroscopy).

Al	Si	Mg	Fe	Mn	Zn	Cu	Ti	Cr	Residuals
96.4-98.8	1.0-1.5	0.25-0.6	0-0.5	0-0.2	0-0.2	0-0.2	0-0.15	0-0.1	0-0.15

Table 3 Chemical composition of AA6016. All values are percentage weight [57]

Elastic modulus (GPa)	Elongation at break (%)	Fatigue strength (MPa)	Poisson ratio	Shear modulus (GPa)	Shear strength (MPa)	UTS (MPa)	Yield tensile strength (MPa)
69	11-27	68-89	0.33	26	130-170	200-280	110-210

Table 4 Mechanical properties of AA6016 aluminum alloy [57]

3.1 Three-Point Bending Fatigue Test

Three-point bending fatigue tests were carried out on the brazed AFSs, using a fatigue test machine (ElectroForce 5500) and recorded the compressive deformation behavior of all the samples. The samples were tested with a loading force ranging between -10N and -120N (only compression-compression loading conditions). Pre-load of -5N was initially applied to have an improved contact with the specimen. The loading frequency was 10 Hz. Tests were conducted at room temperature Until a clear rupture, or a strain could be noticed in the samples, the experiments were stopped. The schematic of testing is shown in figure 41.

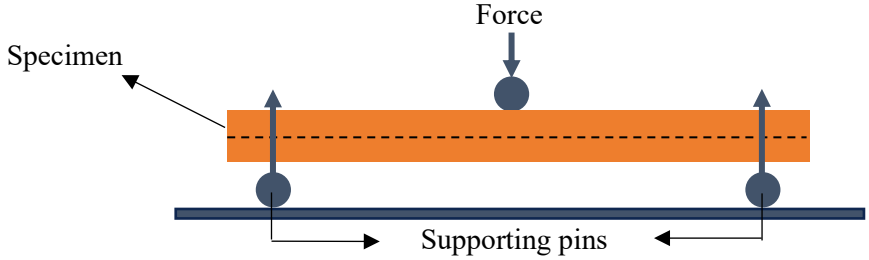

Figure 45 Schematic of AFSs for three-point bending fatigue testing

3.2 Optical Microscopy

Optical microscopy is a method that makes use of visible light to view and examine the specific characteristics of a material. It operates using the principles of light reflection, refraction, and absorption. A light source, often a lamp or a laser, illuminates the area by focusing and directing the light onto the sample. For the samples to have the optimum contrast and visibility, the illumination's intensity and angle can be changed. There are several different ways that light interacts with the sample, including transmission (depending on how transparent or translucent the sample is when part of the light is passed through it), reflection (the intensity and direction of the light reflected off the sample's surface rely on the reflective properties of the sample), and absorption (part of the light may be absorbed by sample depending on its composition). The objective lens takes light from the sample and focuses it onto the focal plane, providing a magnified image of the sample. Additional lenses or eyepieces can be employed to further magnify the image created by the objective lens which enables closer examination of the sample's characterization at higher magnification levels. The resultant images can be viewed directly through the eyepieces or projected onto a computer screen for additional analysis, measurement, or recording. The optical microscopy (Reichert-Jung M used in this research work is shown in figure 46. It is a reversed metallographic microscope and metallic samples are observed exploiting light reflection. Before conducting optimal microscopy analysis, the samples undergo some crucial operations such as samples cutting, resin mounting in fume cupboard and polishing, and finally washing. . Mirror polishing of samples is mandatory to have proper light reflection and focusing.

The cross-sections of the aluminum foam sandwiches after fatigue tests were observed by means of optical microscopy in order to evaluate eventual failure phenomena at the joined interface or in the foam structure.

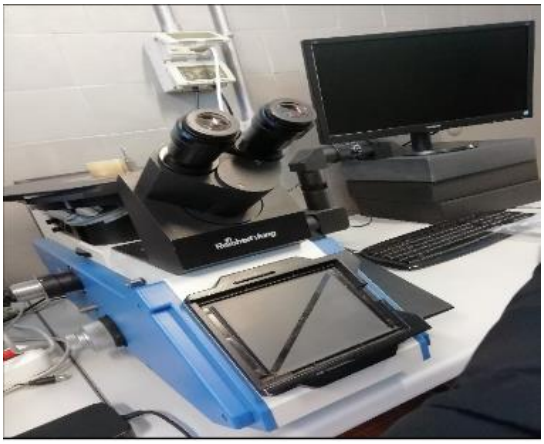

Figure 46 Optical microscopy used for the analysis

3.2.1 Samples Cutting

In order to evaluate the various types of failure in AFSs caused by fatigue loading conditions (compression-compression), the cutting operation was performed using a TR80 Evolution Remet cutting machine depicted in figure 47 to prepare the samples for optical and scanning electron microscopy analysis. The cutting machine was equipped with an abrasive blade (as a

cutting blade) and fluid flow (water) around the cutting zone during the cutting operation. Each AFS was cut into three subparts. The cutting procedure was straightforward because the foam core and the face-sheet materials were comprised of aluminum mainly. Several factors must be considered while executing cutting operation in order to ensure precision, effectiveness, and safety. Some of them are material and tool section, cutting speed and feed rate, fixturing and work holding, cooling and lubrication, chip removal from the cutting area, safety and quality control and inspection. The cut samples are shown below in figure 48.

Figure 47 Cutting machine

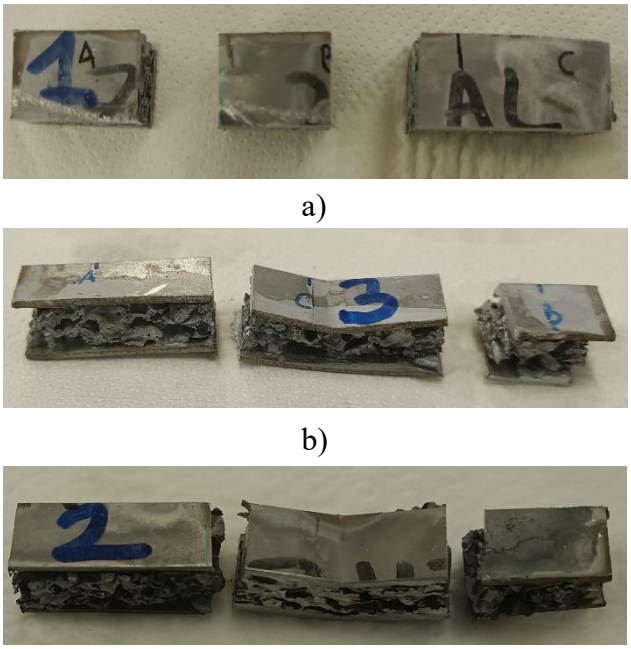

Figure 48 Cut samples of AFSs. a) sample 1 b) sample 3 c) sample 2

3.2.2 Resin Mounting

Prior to optical microscopy analysis, the samples are resin mounted to provide support and protection. Resin mounting makes sure that the sample is held firmly in place while preserving a smooth and level surface for precise measurements and focusing. It also preserves the sample during handling and microscopy by serving as a barrier against pollutants, scratches, and impacts. The sample should not be affected by the mounting material due to chemical reactions or mechanical forces. If the specimen is going to be electropolished or studied with a scanning electron microscopy, the mounting medium needs to be electrically conducting as well as stick to the specimen. Improved light transmission, simpler sample manipulation, and long-term sample preservation are all made possible by resin mounting.

The resin mounting operation was carried out in fume cupboard. Technovit 4071 was used as an epoxy resin. Both the epoxy resin and hardener were measured and mixed together according to instructions set by the manufacturer. The employed proportion was 2:1. After mixing both in a mixing container, the mixture was thoroughly stir using a stir stick for 3-5 minutes to ensure proper blending. Stirred gently in a circular motion, scrapping the bottom and edges of the container. This step is critical for good curing and the prevention of uncured areas in the resin. Following that the mixture was carefully poured into a mold along with the

sample and allowed to set and harden for 24 hours. The mold has to be free of any debris that can contaminate the sample. The resin mounted samples are shown below in figure 49.

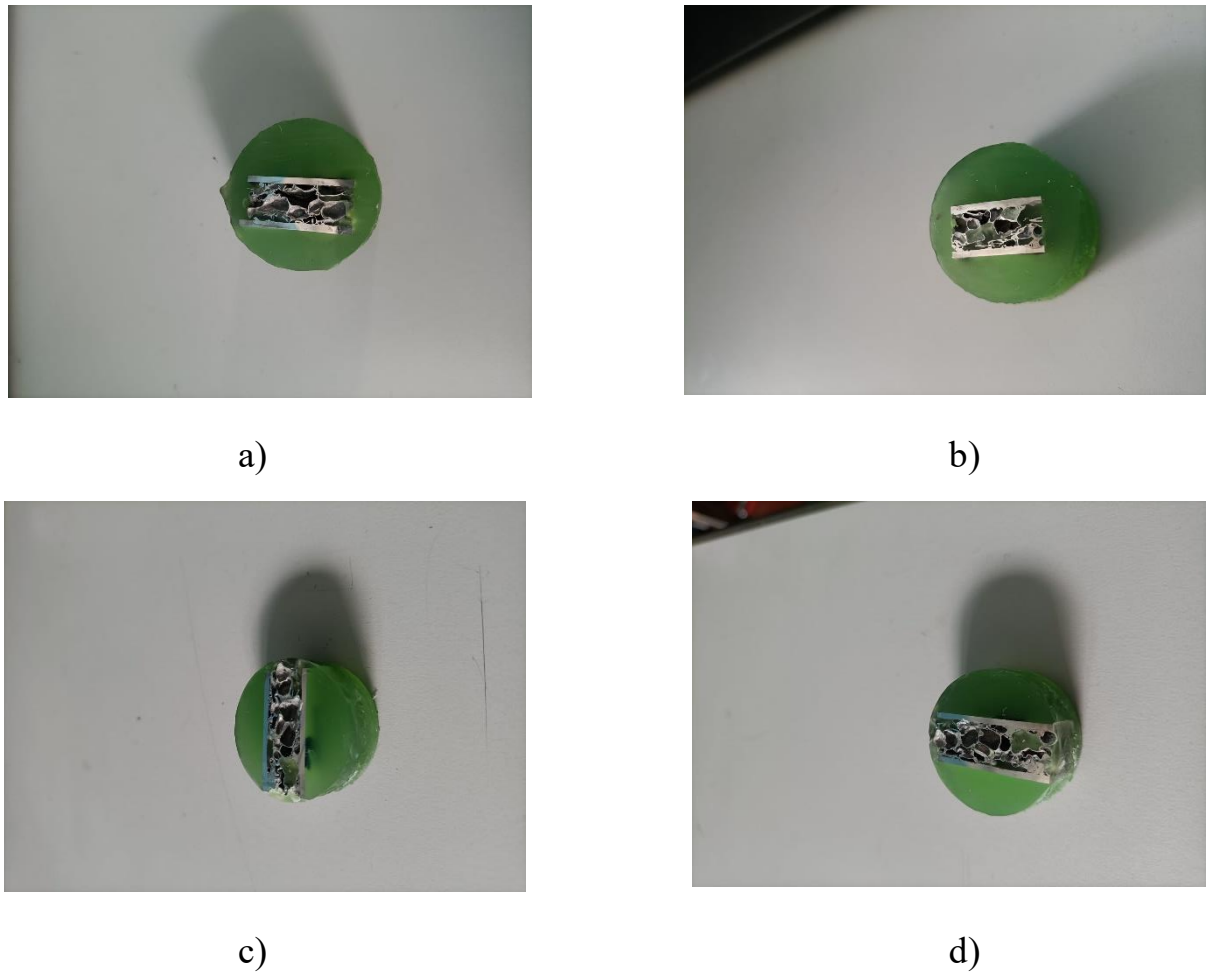

Figure 49 Resin mounted samples. a) sample 1-A b) sample 1-B c) sample 2 d) sample 3

3.3.3 Polishing of Resin Mounted Samples

Polishing is the process of carefully abrading the surface of a sample to eliminate defects, roughness, or irregularities that may interfere with microscopic analysis. By lessening light scattering and enhancing light transmission through the material, polishing improves the sample's visibility and clarity. The process started by firstly grinding the sample's surface on a polishing machine shown in figure 50 with abrasive papers (Silicon Carbide SiC) of different sizes. More coarse abrasive papers were used initially. The coarseness of the papers is indicated by a number. In order to eliminate the scratches from the previous coarser paper, finer papers (higher number) were used for each subsequent stage. This was more easily accomplished by orienting the specimen perpendicular to the prior scratches and then observing for these previously oriented scratches to be eliminated. Each grinding stage was carried out thoroughly with water to minimize sample heating and prevent contamination from coarser grit present on the specimen surface.

After the intermediate grinding, the specimens went through polishing (with SiC abrasive papers up to 4000 grit) and final polishing with diamond paste (0.05-0.01µm particle size) and/or alumina suspension (0.05 µm particle size) diluted in water without lubricant. The amount of water, alumina suspension, and disc speed were all established by trial and error. After polishing the specimens were cleaned with ethanol and dried to avoid staining.

Figure 50 Machine used for grinding and polishing resin mounted samples.

3.3 Scanning Electron Microscopy (SEM) with Energy Dispersive Spectroscopy (EDS)

Scanning Electron Microscope (SEM) presents itself as the most powerful and adaptable instrument for material characterization. In a way similar to that of light microscope which utilizes visible light for imaging, the SEM makes use of electrons for the same purpose. SEM used in this study is shown in figure 51 while the general structure of SEM is displayed in figure 52.

3.3.1 Working of Scanning Electron Microscopy (SEM)

The SEM's operation depends on the detection of electrons when they reflect back after striking a specimen's surface. An electron source is the key element of scanning electron microscope. Most of the scanning electron microscopes use heated tungsten filament as the source of electrons. In this case the heat provides the electrons with greater energy, causing them to be directed in a certain direction and creating a single concentrated electron beam. Between the electron source and the condenser, there is an anode whose main function is to deflect the electrons away and align them in a thin, single straight line. This is because of the opposite

charges of electrons and anode. The condenser is followed by a scan coil and an objective lens. The electron beam induced by the source travels through all these passages. The electrons in an electron beam strike the sample, reflect, and disperse randomly in all directions. This process, known as electron escape, enables the user to determine a correlation between the scattered and retained electrons. The detector which is further attached to a sensor picks up the signal which is created as a result of interactions between the electrons of electron beam and sample, and the electron escape. The sample is mostly made up of bumps and valleys. The electrons in larger amount often escape when they strike the sample's bump region, whereas relatively fewer electrons manage to reflect and escape when they strike the valleys. This variation in electron escape results in microscopic representation of the material.

3.3.2 Backscattered and Secondary Electrons, and EDS

Backscattered and secondary electrons are the two types of electrons utilized for imaging in SEM. After an elastic interaction between the electron beam and the sample, back scattered electrons, which are part of the initial electron beam, are reflected back. In contrast, secondary electrons come from the samples' atoms and form as a result of an inelastic interaction between the sample and the electron beam. The two types convey different Kind of information since secondary electrons originate from the surface regions whereas back scattered electrons emerge from the deeper sections of the sample. When it comes to atomic number, the back scattered electrons imaging is highly sensitive; the greater the atomic number, the brighter the material looks in the image. Secondary electron imaging can deliver more precise surface data.

Energy dispersive spectroscopy (EDS) is an analytical method that is incorporated into scanning electron microscopy (SEM) systems. It makes use of X-rays spectroscopy in order to evaluate the sample's elemental composition. The atoms inside the sample generate distinctive X-rays as a result of their interactions with the focused electron beam. These X-rays are detected and measured by EDS, which provides the details of the elements present inside the sample. The elemental maps of the sample can be generated by combining SEM imaging with EDS analysis. Though EDS determines the distribution and concentration of elements, SEM provides visual morphology and structure. Elemental mapping makes it possible to characterize phases, interfaces, and compositional changes by revealing the spatial arrangement of various elements inside the sample.

Figure 51 SEM used for the analysis

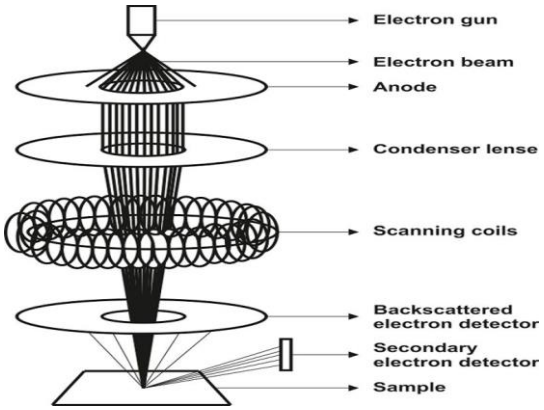

Figure 52 Structure of SEM [58]

4. Results and Discussion

In this chapter, the results and comments are addressed section by section. First, the fatigue tests conducted on AFSs are reported along with graphs of force vs displacement, and number of cycles vs maximum and minimum displacements experienced by samples. Following that, optical microscopy at high and low magnifications, and scanning electron microscopy are explained.

4.1 Fatigue Test Results

The fatigue tests were carried out on three samples of aluminum foam sandwiches according to the conditions outlined in section materials and methods (3.1). Sample 1 was subjected to 4.5 million loading cycles, while samples 2 and 3 underwent 2.7 million and 149.557 thousand loading cycles, respectively. Sample 1 did not display any evident fracture modes as a result of fatigue loading, with the exception of a little deformation at the sandwich's edges measured that may have been brought on by higher porosity there, as seen in figure 54. On the other hand, sample 2 and sample 3 exhibited failure modes such as debonding behavior or delamination and crushing of aluminum foams as reported in figures 55 and 53 respectively. The thicknesses of all the samples were measured after the testing, not before.

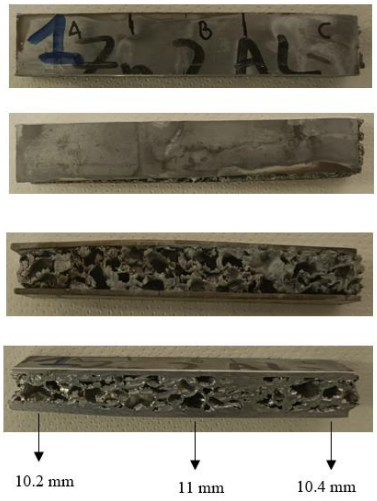

Figure 54 Sample 1 with 4.5 million loading cycles and slight deformation at edges

Figure 55 Failure morphology of Sample 2 after 2.7 million loading cycles.

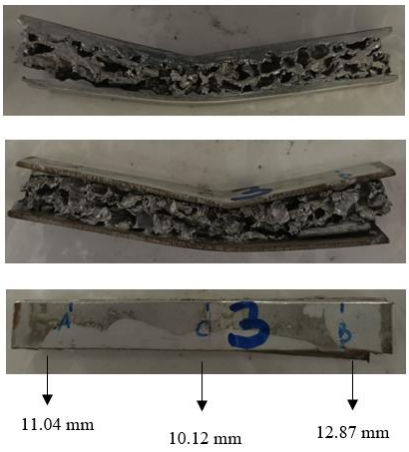

Figure 53 Failure morphology of sample 3 after 149.557 thousand loading cycles

4.2 Force vs Displacement Graph

The force vs displacement graphs for sample 1, 2 and 3 are depicted in figures 56, 57 and 58 respectively. The graphs are created by plotting values from some of the loading cycles for each sample. The longest fatigue life was shown by sample 1, whereas sample 3 had the shortest fatigue life. As shown in figure 56, sample 1 exhibited a narrow hysteresis loop (resulting from

loading cycles) that indicates a smaller difference between the loading and unloading paths, suggesting a relatively small energy loss and a higher degree of elastic behavior for early loading cycles. However, the plastic behavior can be seen with increased loading cycles, and after the test, we discovered a small deformation (shown in figure 54) at the edges of sample 1. Sample 2 also depicted similar trends as shown in figure 57. The hysteresis cycles for samples 2 show a sort of "knee" which seems to start from cycle '5po' and becomes more evident at higher cycles (e.g., from '8190 P') and can be associated to the progression of failure. The damage of the sample develops by progressive failure of joining points. However, sample 3 as shown in figure 58 exhibits a wide hysteresis loop even from the early loading cycles and the area enclosed by the loop continuously increases with increasing number of loading cycles, indicating a larger difference between loading, and unloading paths, high energy dissipation and greater degree of plastic or irreversible deformation, thus revealing a distinct behavior from sample 1 as sample 3 is characterized by failure at a low number of cycles.

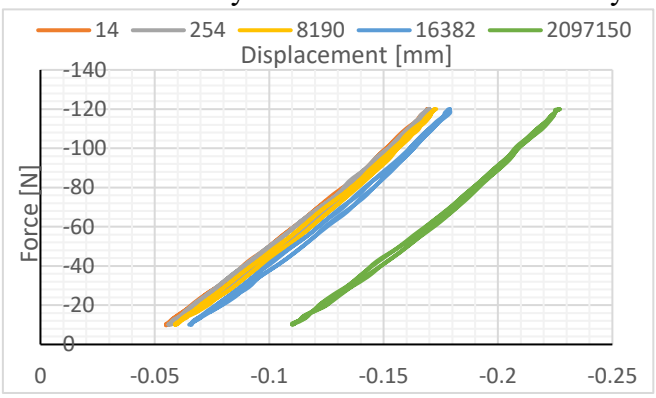

Figure 56 Force vs displacement graph of sample 1

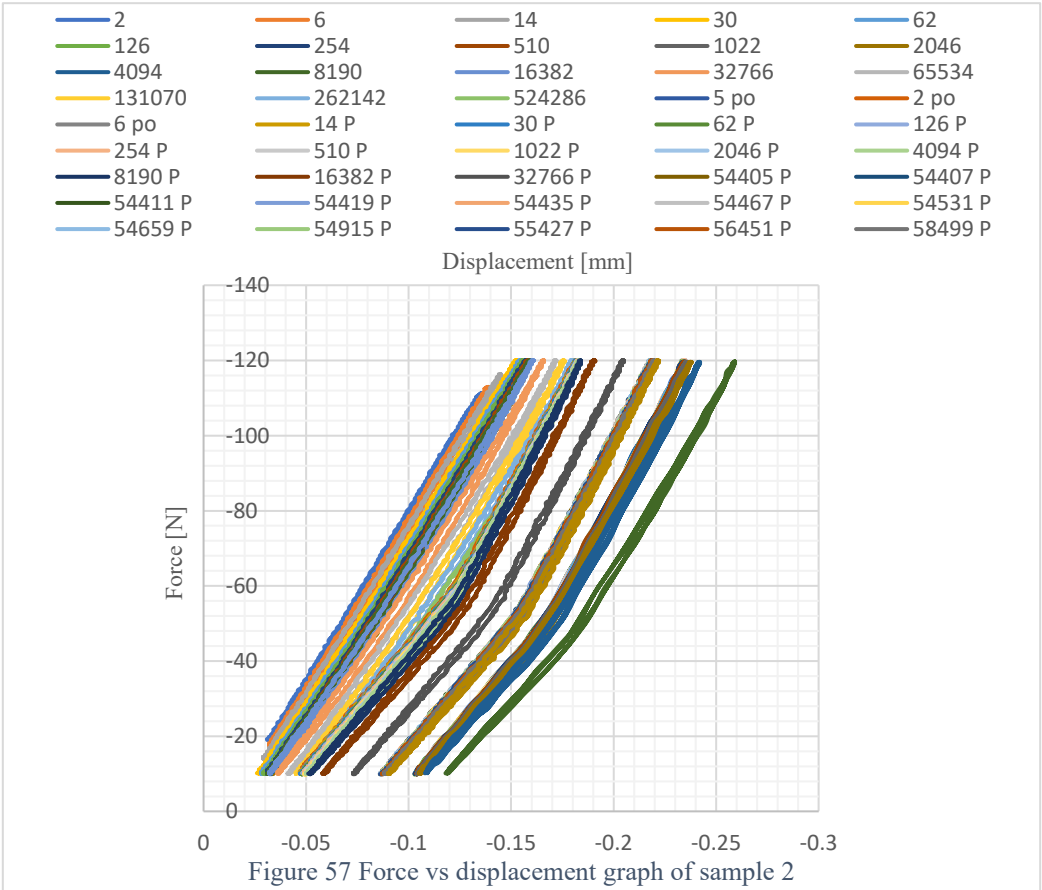

Figure 57 Force vs displacement graph of sample 2

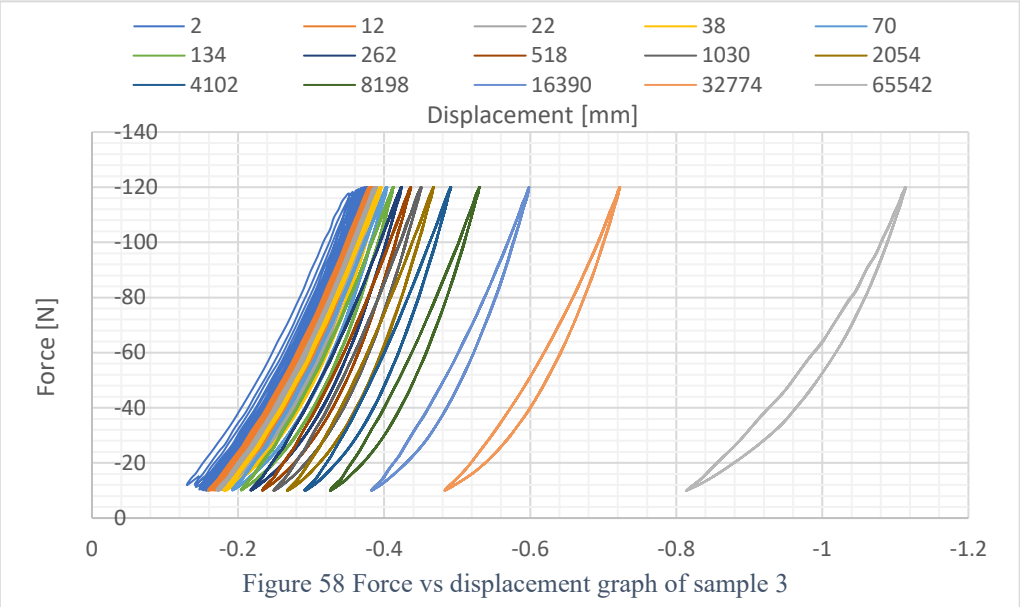

Figure 58 Force vs displacement graph of sample 3

4.3 Max. and Min. Displacement vs Number of cycles

The deflection curves of sample 1, 2 and 3 are shown in figures 59, 60 and 61. The minimum displacement decreases significantly during the initial loading cycles for Sample 1 (figure 59), and after 0.1 million loading cycles, the deflection curve enters a stable stage. The plastic deformation and fracture initiation cause the initial abrupt rise in the minimum displacement, while damage stabilization and material's adaptability to cyclic loading are responsible for the stability that follows. During the test of sample 2, there was an interruption due to an electric current stoppage. This phenomenon is depicted on the graph as a shift of the curve in figure 60 at around 52000 loading cycles, which is not an actual variation in deformation. As illustrated in figure 61, we can see a consistent decrease in the minimum displacement for sample 3 with increased loading cycles, suggesting a progressive fatigue failure. The slope gets steeper after 32 thousand loading cycles for sample 3. The initiation and growth of cracks inside the material cause this behavior to take place. As cracks expand, they weaken the material, resulting in a lower load-carrying capacity and higher stress concentrations. As a result, the material's capacity to deform elastically declines, which causes the minimum displacement to decrease.

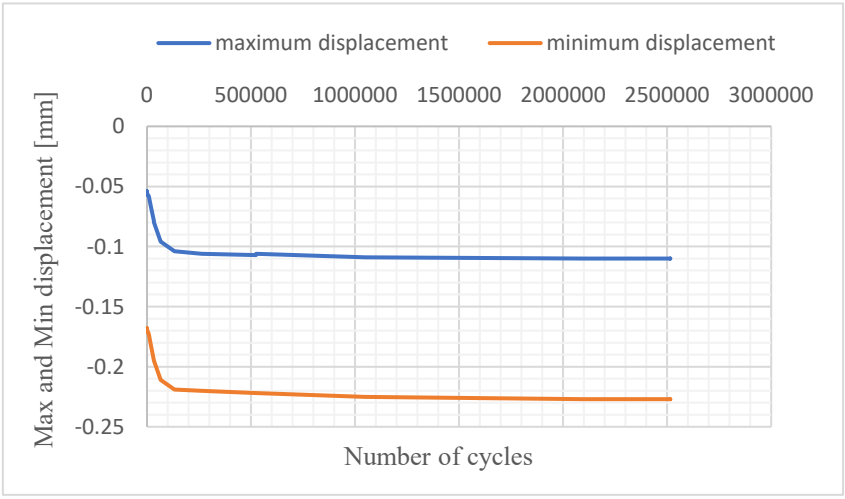

Figure 59 No. of cycles vs max and min displacement for sample 1

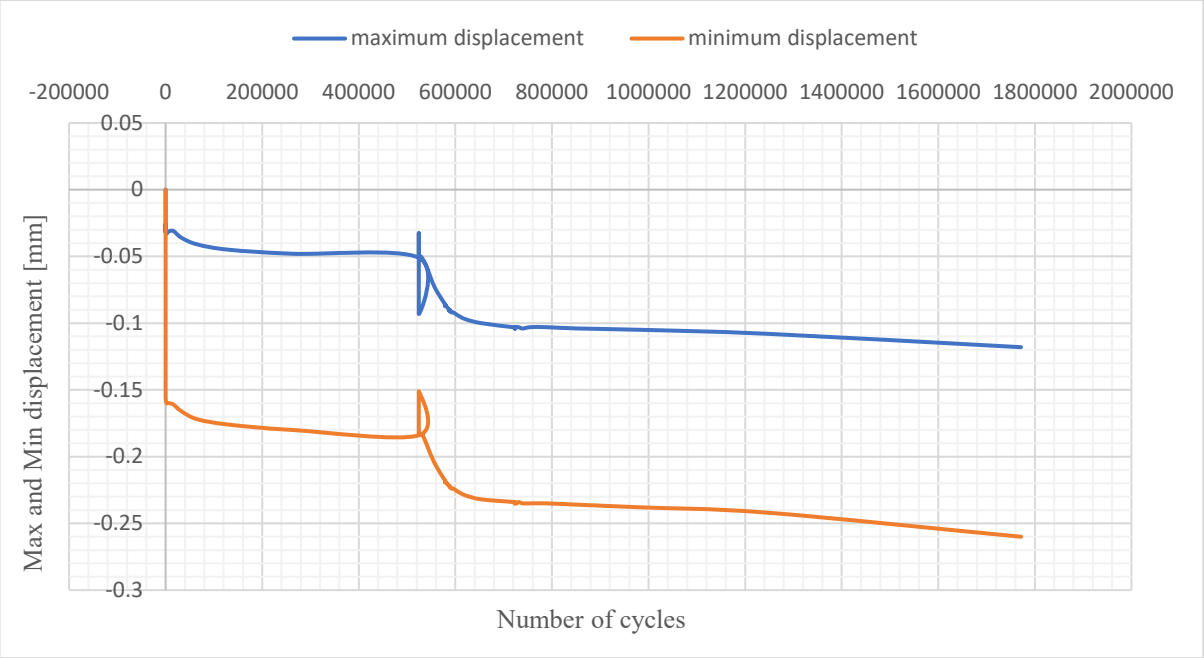

Figure 60 No. of cycles vs max and min displacement for sample 2

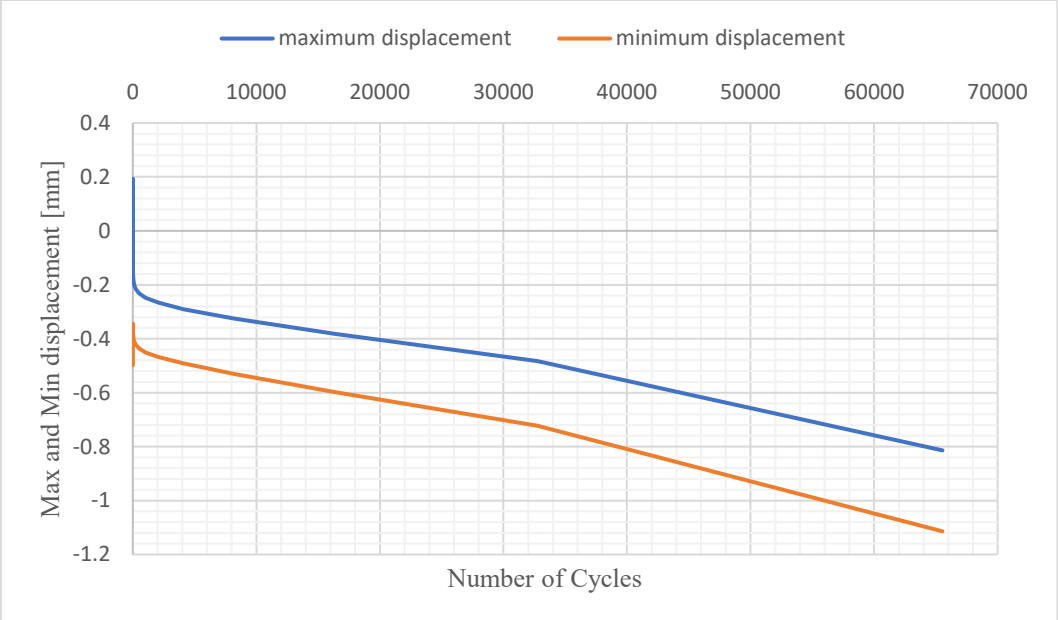

Figure 61 No. of cycles vs max and min displacement for sample 3

4.4 Optical Microscopy Analysis

All the samples of AFSs were analyzed at different magnifications (10x, 20x and 50x) in order to understand the behavior of materials at different loading conditions, structural analysis, defects identification due to fatigue loading and surface characterization. The optical microscopy of each sample is categorized into two groups i.e., aluminum plates (face-sheet material) and aluminum foam itself. The analysis of optical microscopy for samples 1, 2 and 3 is reported as follows.

4.4.1 Sample 1-A (Aluminum plates)

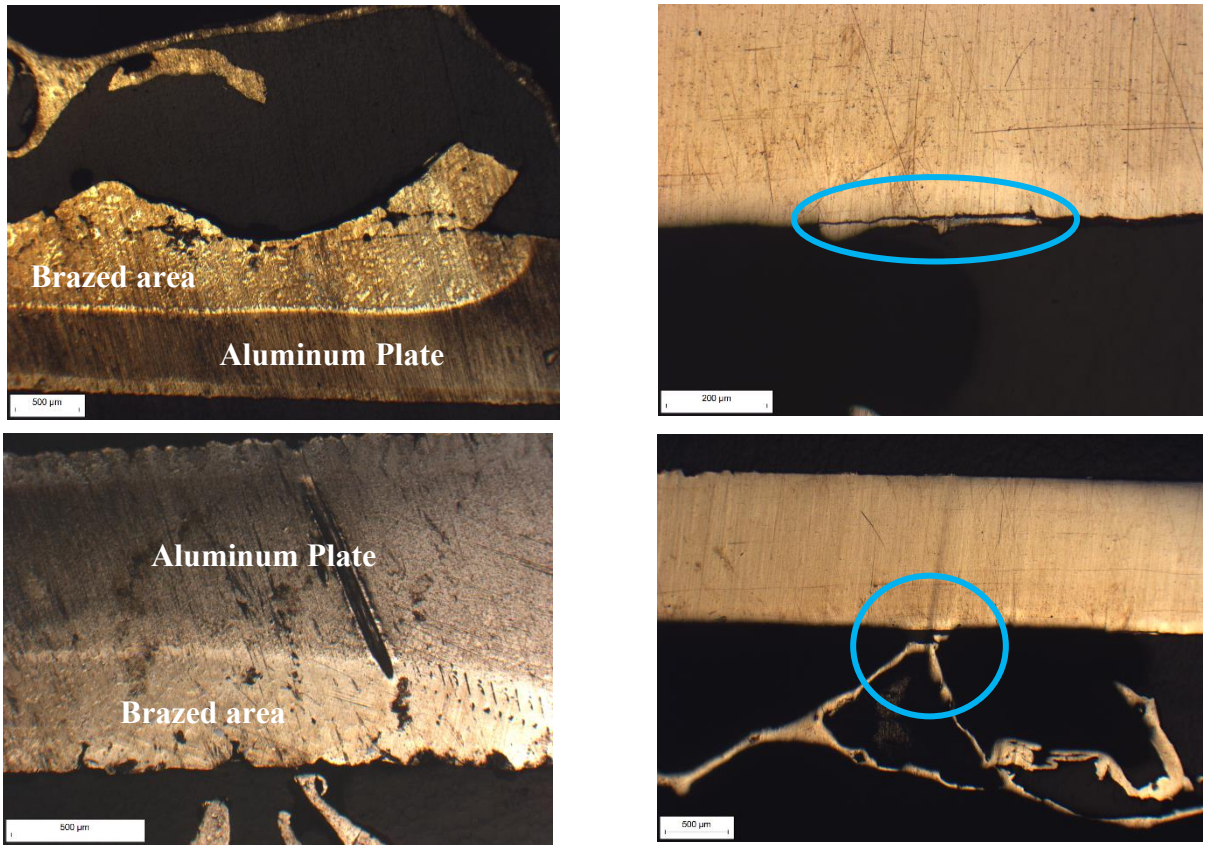

Figure 62 Optical microscopy analysis of aluminum plates of sample 1-A at magnifications of 10x, 20x, and 50x

4.4.2 Sample 1-A (Aluminum foam)

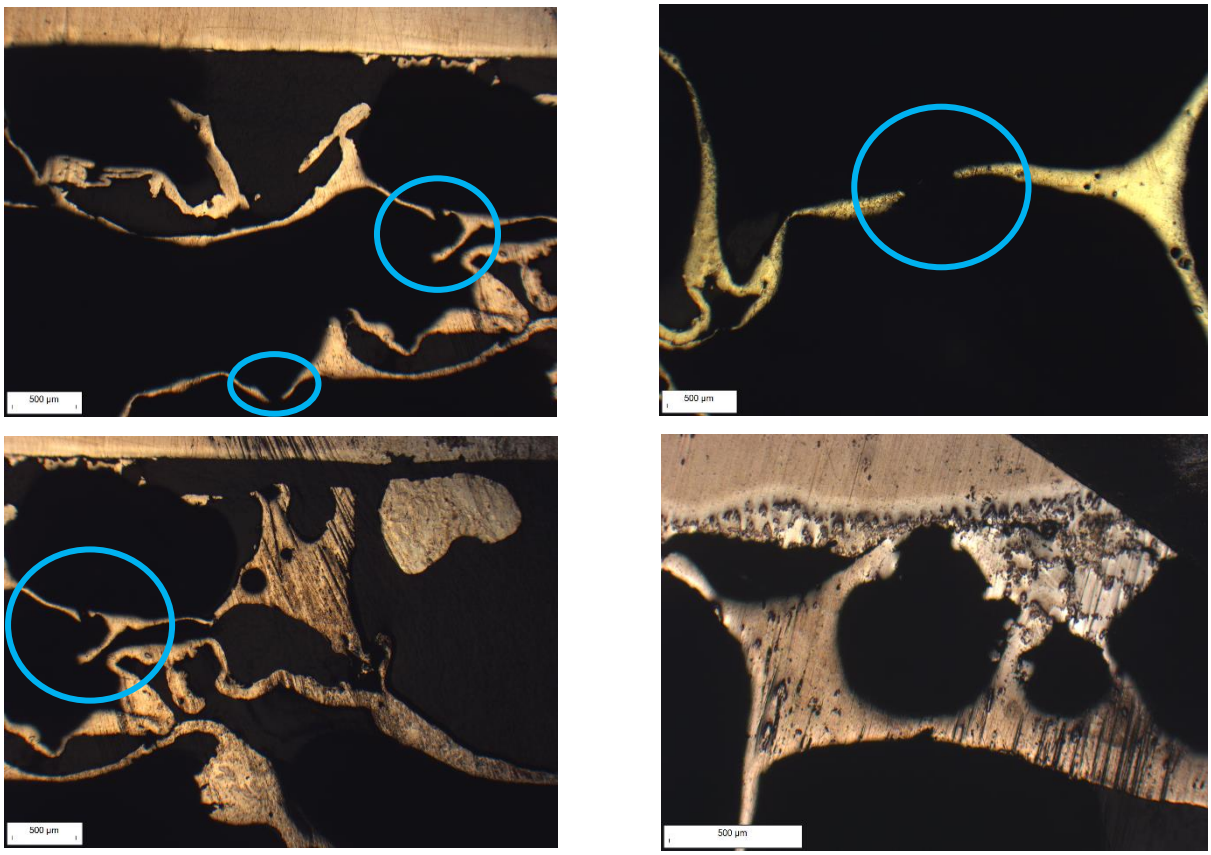

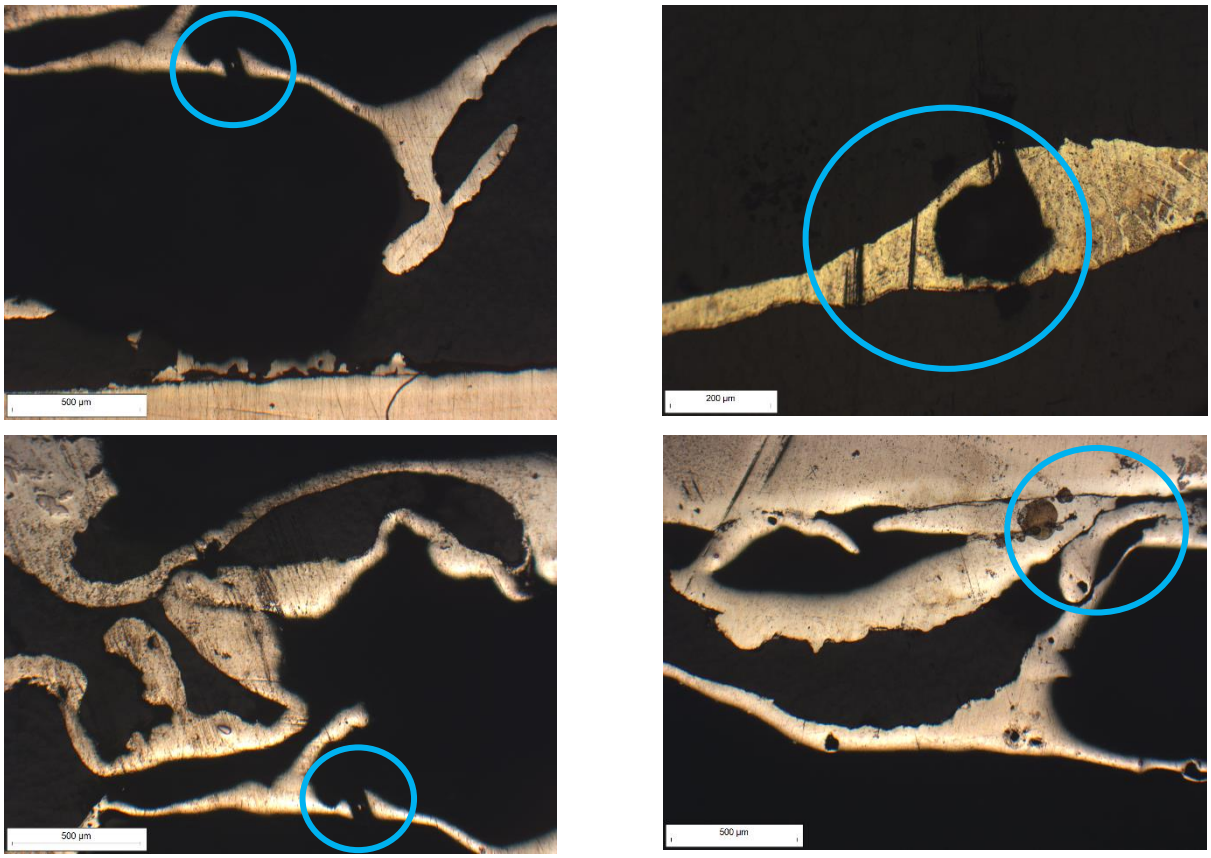

Figure 63 Optical microscopy analysis of aluminum foam of sample 1-A at magnifications of 10x, 20x, and 50x.

4.4.3 Sample 1-B (Aluminum plates)

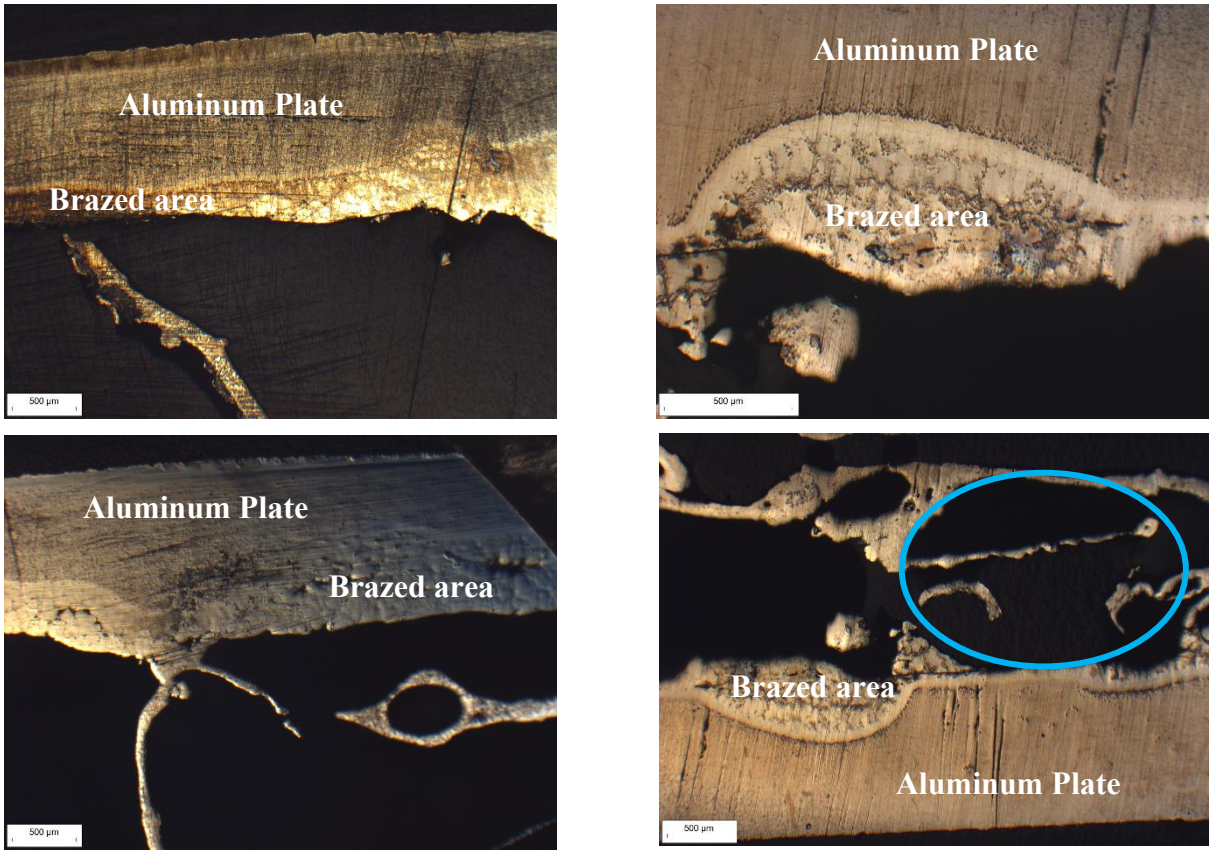

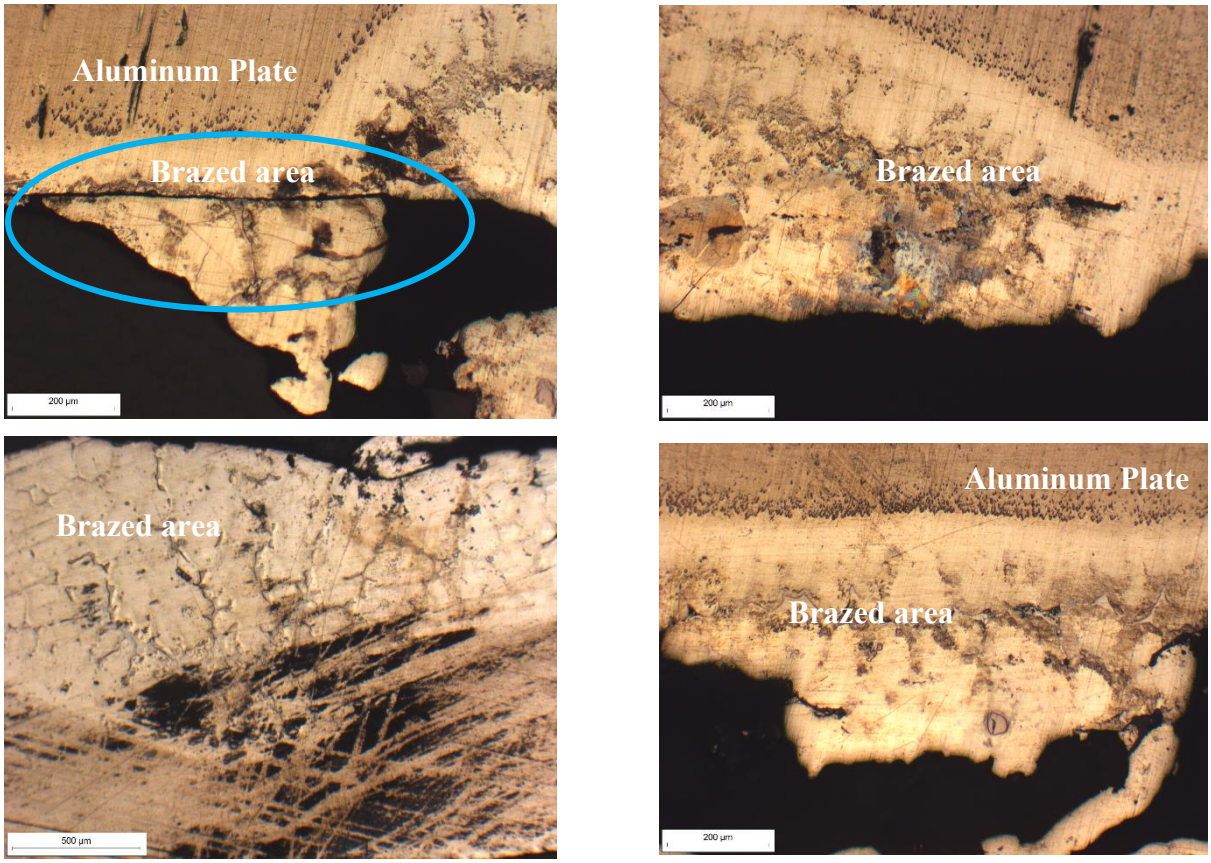

Figure 64 Optical microscopy analysis of aluminum plates of sample 1-B at magnifications of 10x, 20x, and 50x

4.4.4 Sample 1-B (Aluminum foam)

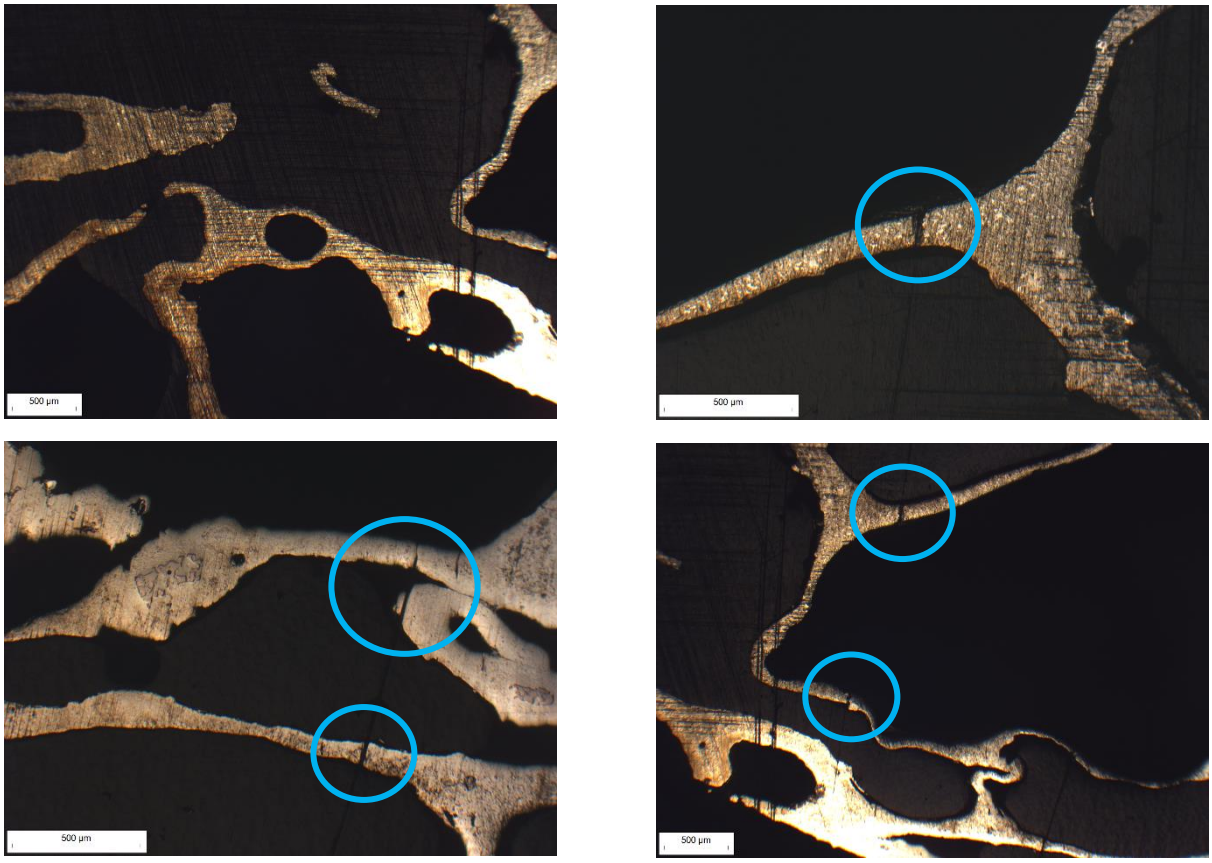

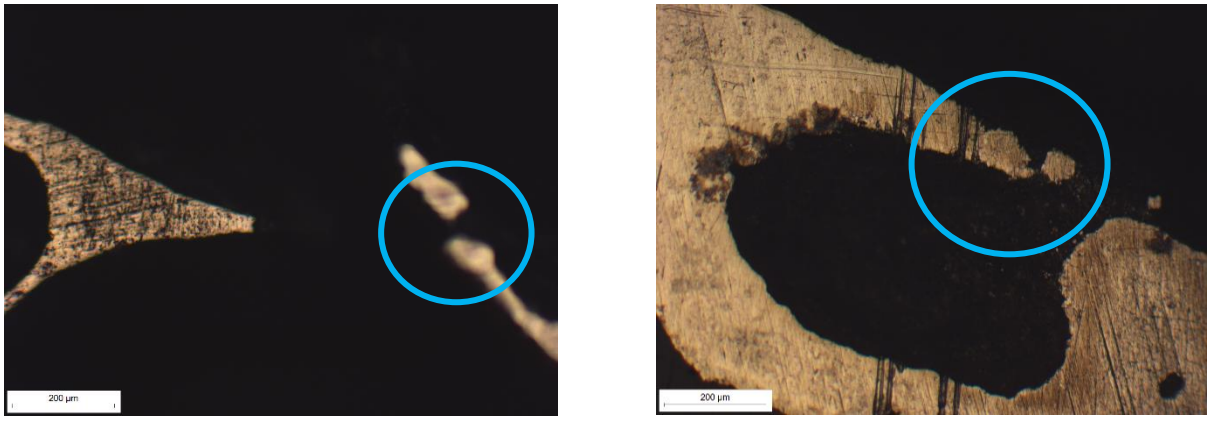

Figure 65 Optical microscopy analysis of aluminum foam of sample 1-B at magnifications of 10x, 20x, and 50x

4.4.5 Sample 2 (Aluminum plates)

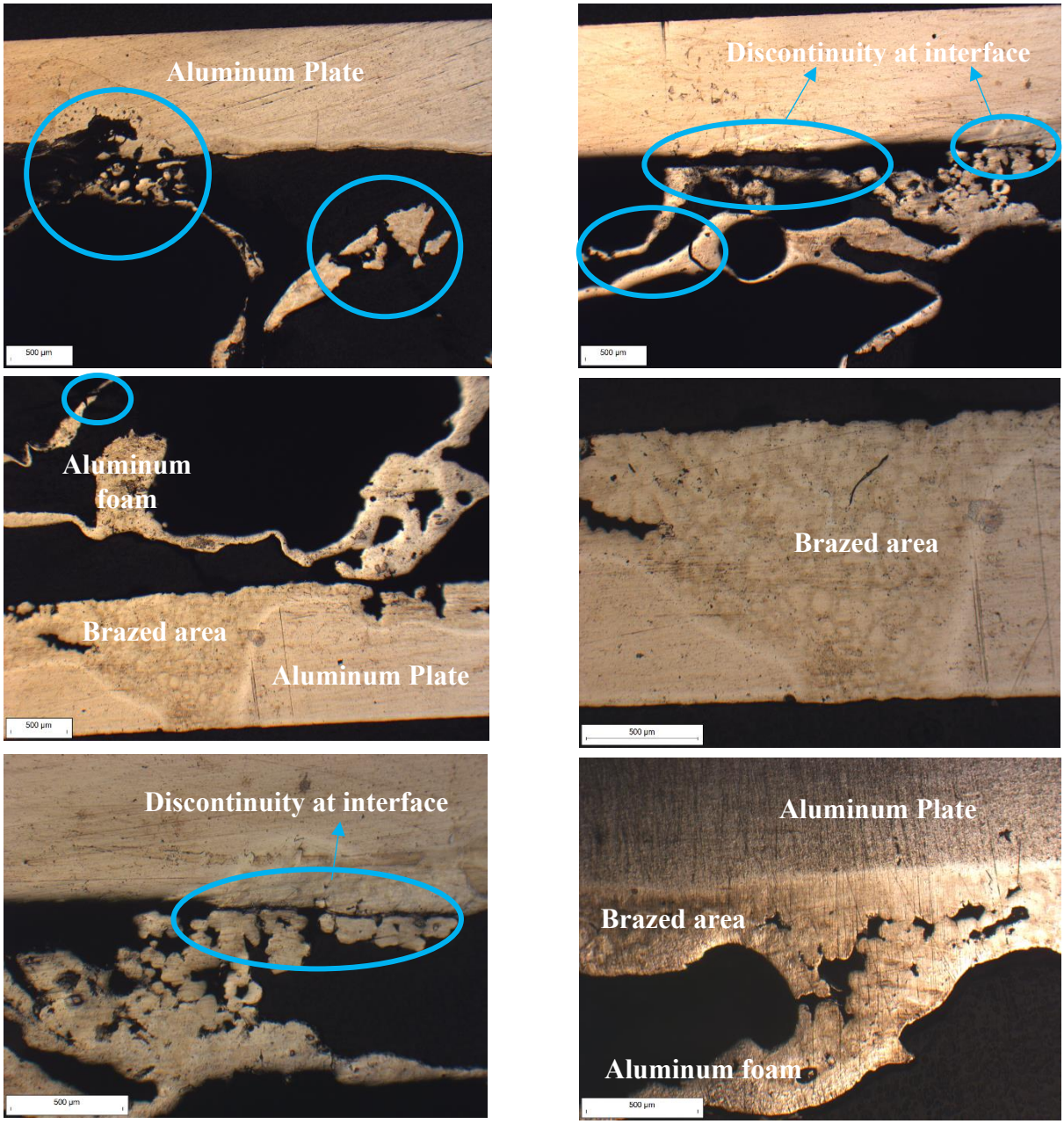

Figure 66 Optical microscopy analysis of aluminum plates of sample 2 at magnifications of 10x, 20x, and 50x.

4.4.6 Sample 2 (Aluminum foam)

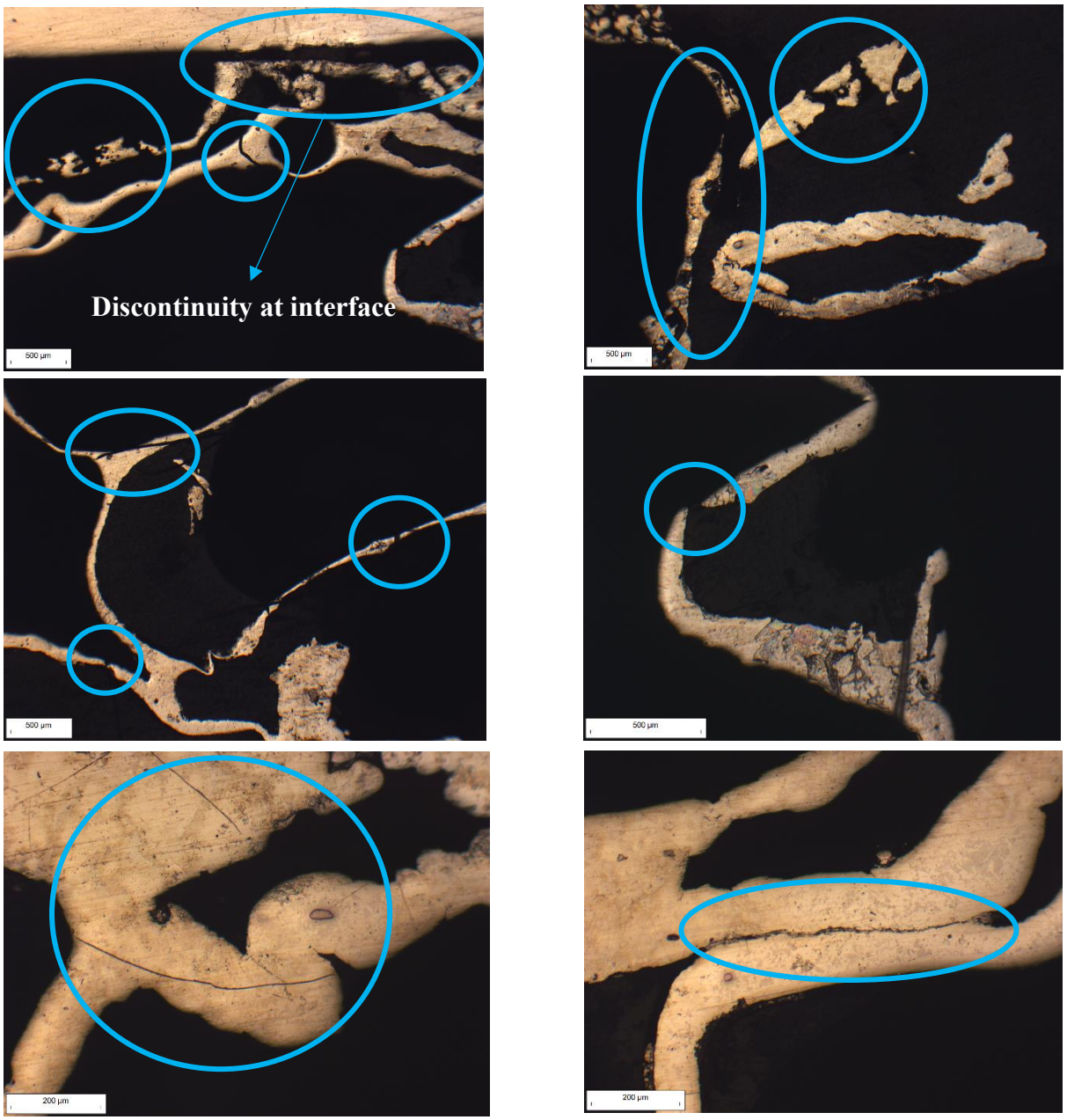

Figure 67 Optical microscopy analysis of aluminum foam of sample 2 at magnifications of 10x, 20x, and 50x

4.4.7 Sample 3 (Aluminum plates)

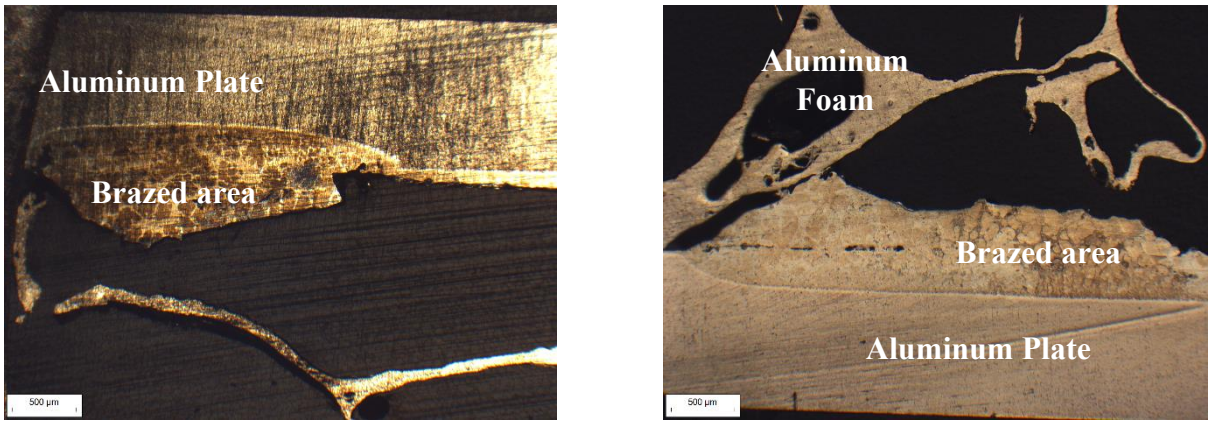

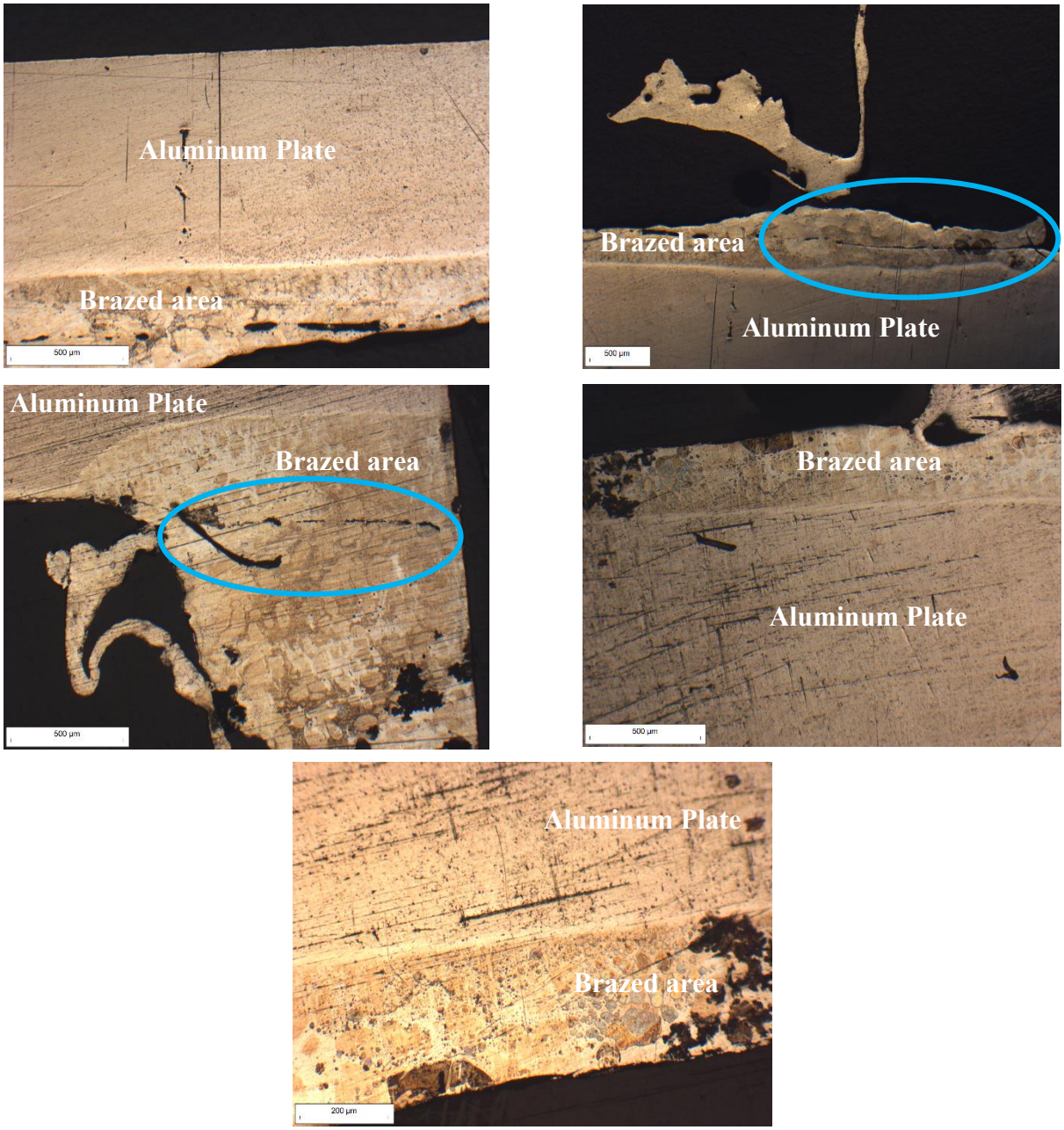

Figure 68 Optical microscopy analysis of aluminum plates of sample 3 at magnifications of 10x, 20x, and 50x

4.4.8 Sample 3 (Aluminum foam)

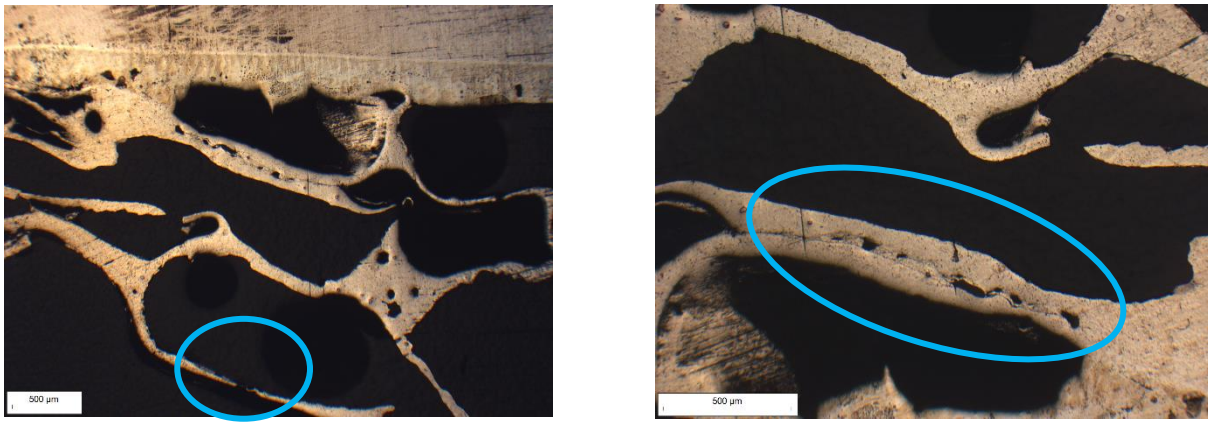

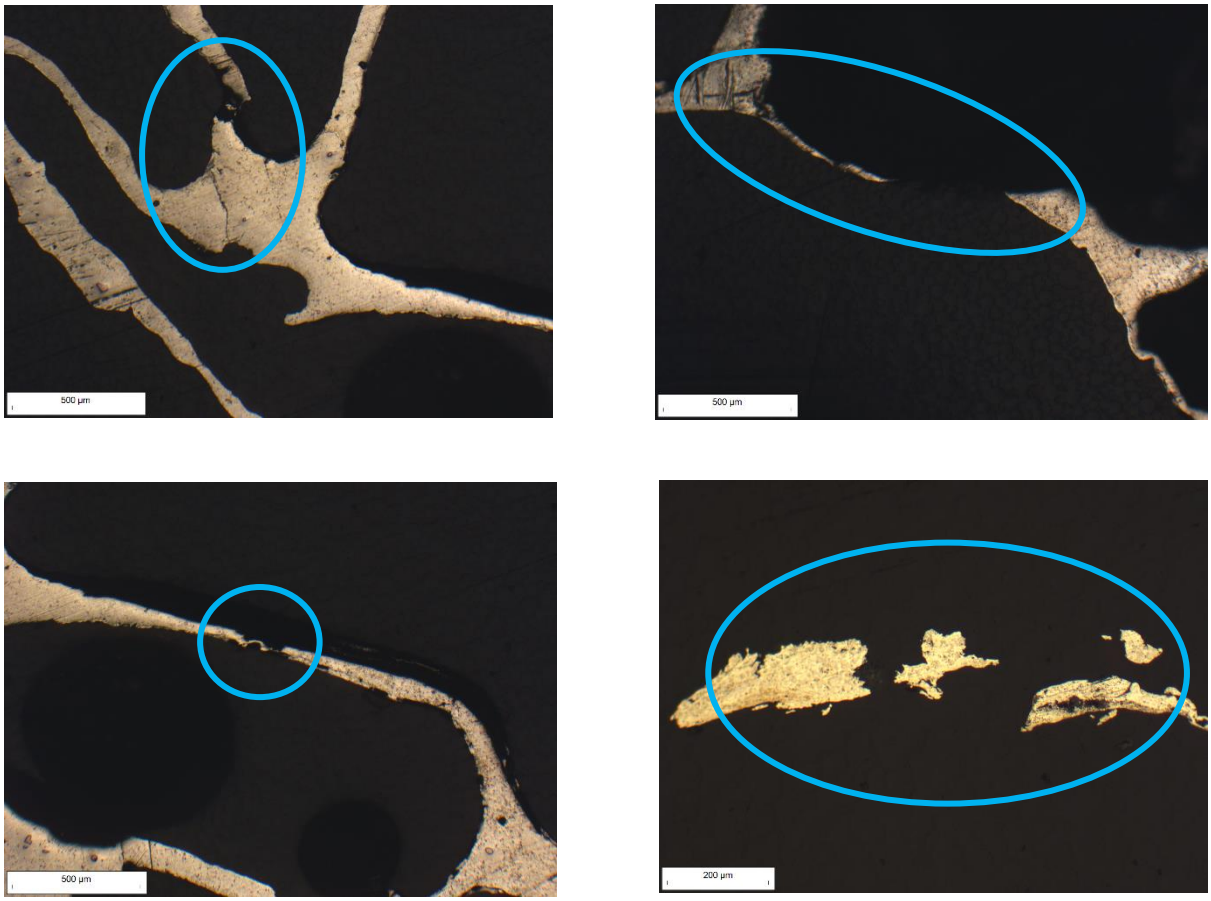

Figure 69 Optical microscopy analysis of aluminum foam of sample 3 at magnifications of 10x, 20x, and 50x.

Optical microscopy (of all the samples) evidenced that the joining interface presents several continuous regions and some gaps that may be attributed to the foam inhomogeneities as well as to some foam production process issues or the gaps (discontinuity) may occur due to the fatigue loading conditions. This is true for all the samples. Certain failures (highlighted in blue circles) can also be seen in the correspondence of foam cell walls; however, it is difficult to identify a definite pattern in the observed samples using this approach.

4.5 Optical Microscopy Analysis at Low Magnification

Optical microscopy at low magnification (6x) is also carried out on all the samples since it provides a wide field of view for observing the overall structure of the samples and detecting any defects or deviations in the foam and sandwich layers. Moreover, the reduced magnification makes it possible to quickly analyze large areas of the sample, allowing for surface characterization, and the identification of any surface irregularities that may negatively affect the material performance. Wild M420 is an optical microscopy with low magnification utilized in the study. The analysis for each sample is reported as follows.

Sample 1 (Plates exposed to tensile load during the test)

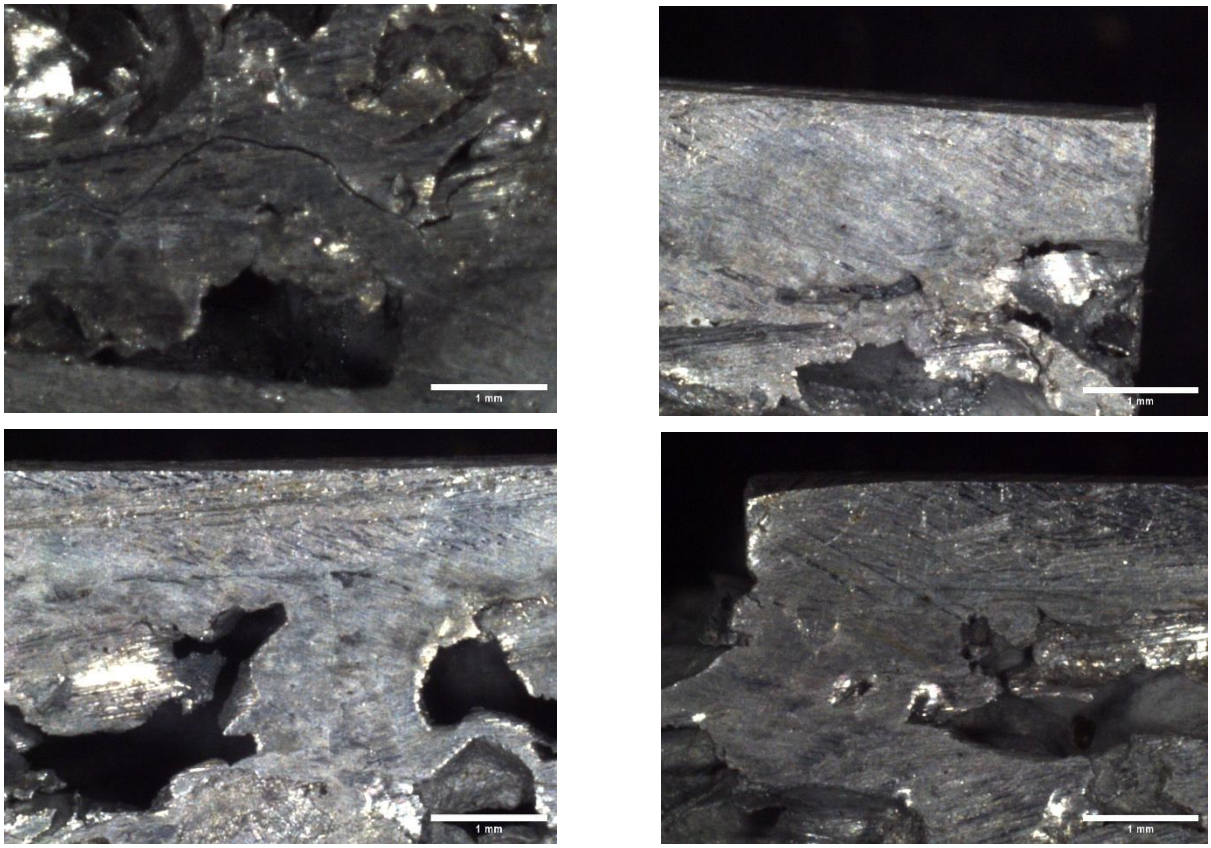

Figure 70 Low magnification optical microscopy at 6x of sample 1 with plates exposed to tensile loading.

Sample 1 (Plates exposed to compressive load during the test)

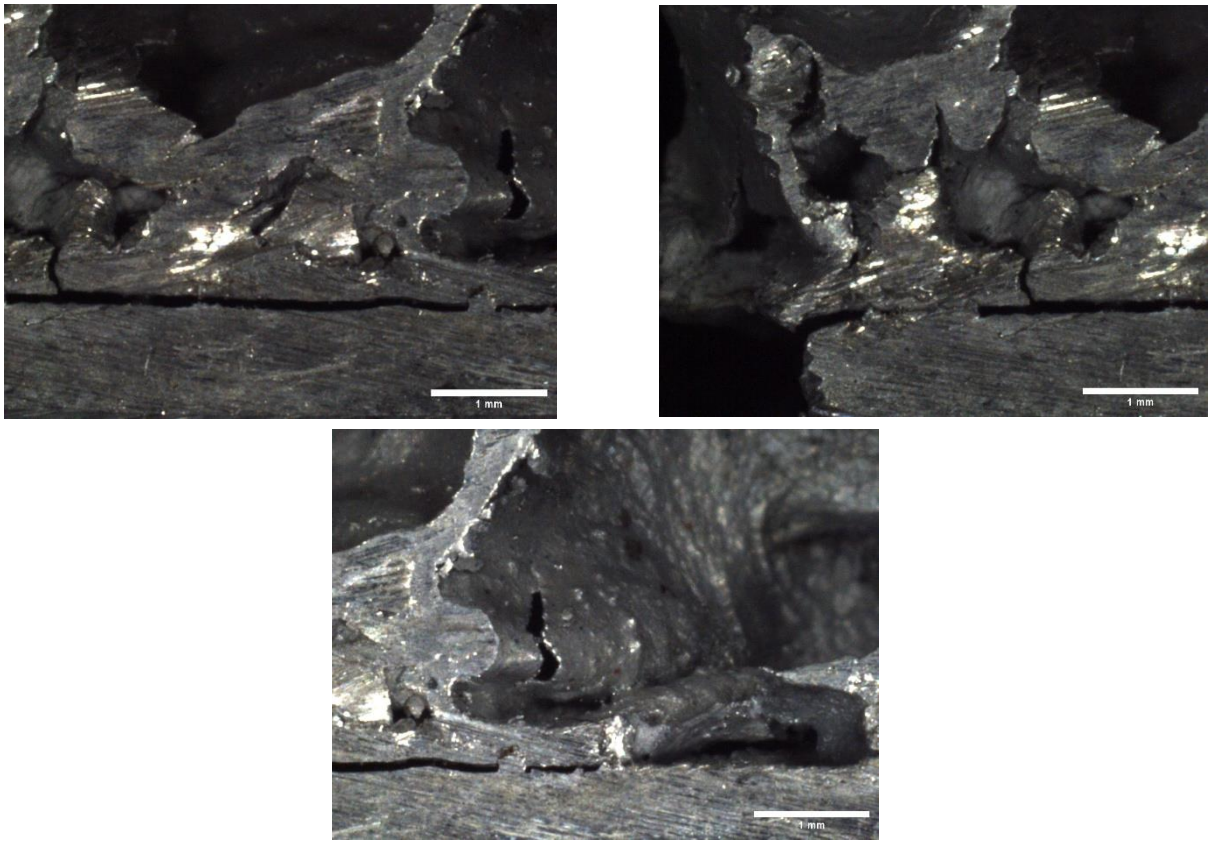

Figure 71 Low magnification optical microscopy at 6x of sample 1 with plates exposed to compressive loading.

Sample 2 (Plates exposed to tensile load during the test)

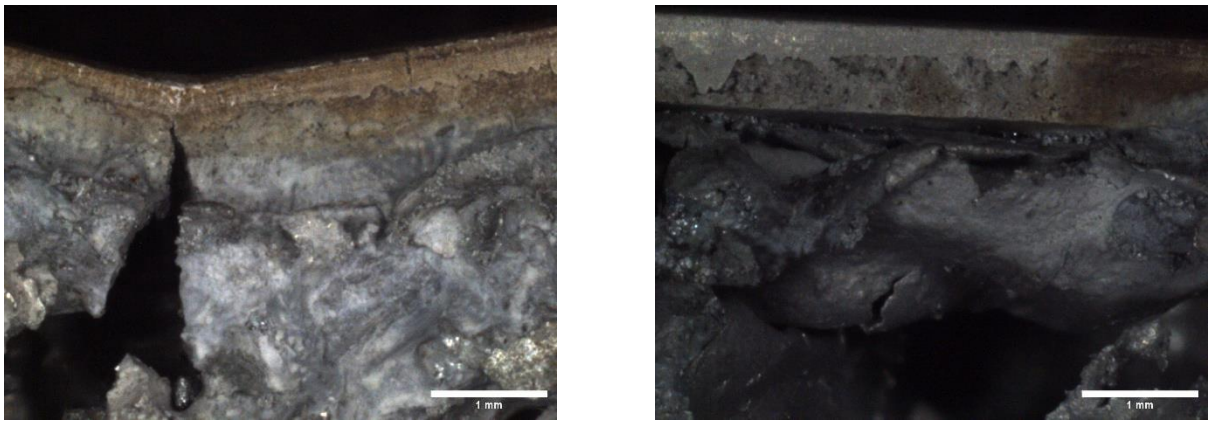

Figure 72 Low magnification optical microscopy at 6x of sample 2 with plates exposed to tensile loading

Sample 2 (Plates exposed to compressive load during the test)

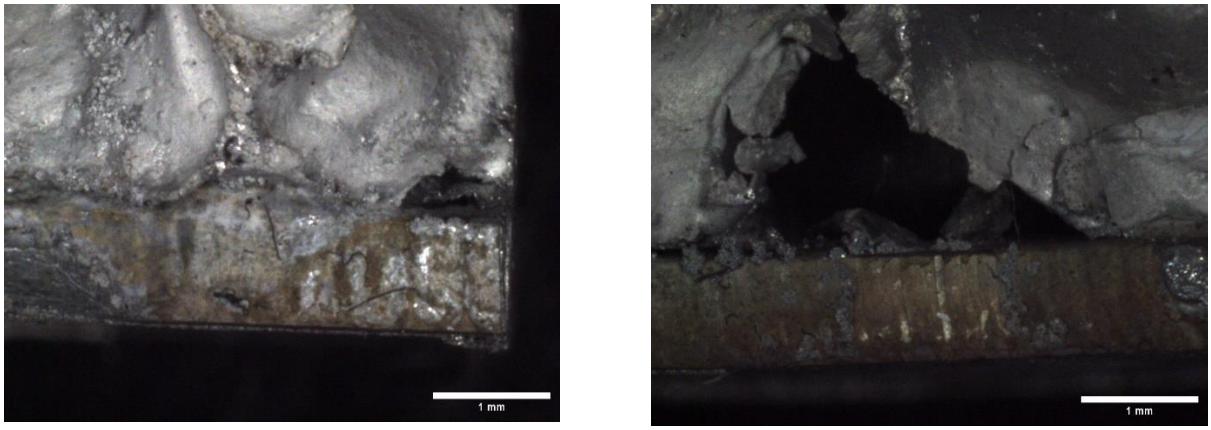

Figure 73 Low magnification optical microscopy at 6x of sample 2 with plates exposed to compressive loading.

Sample 3 (Plates exposed to tensile load during the test)

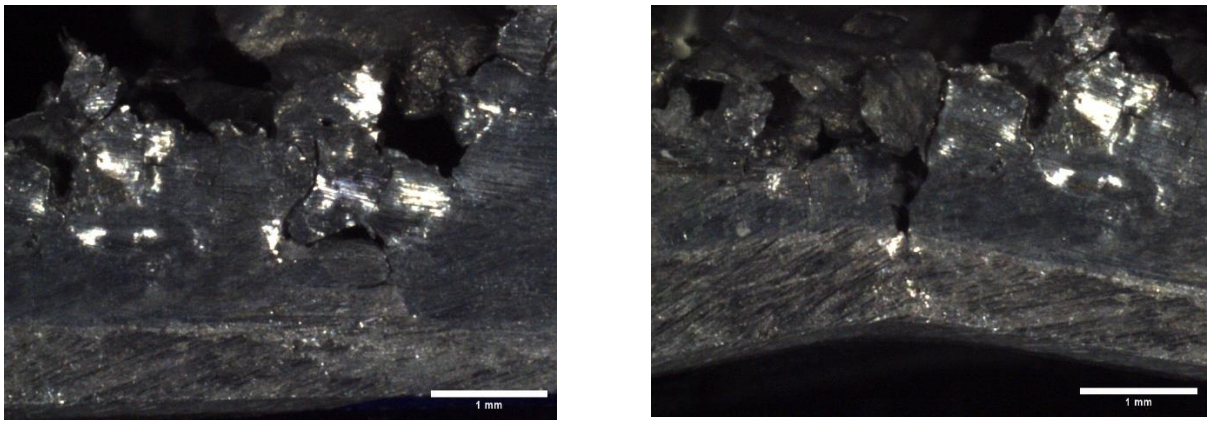

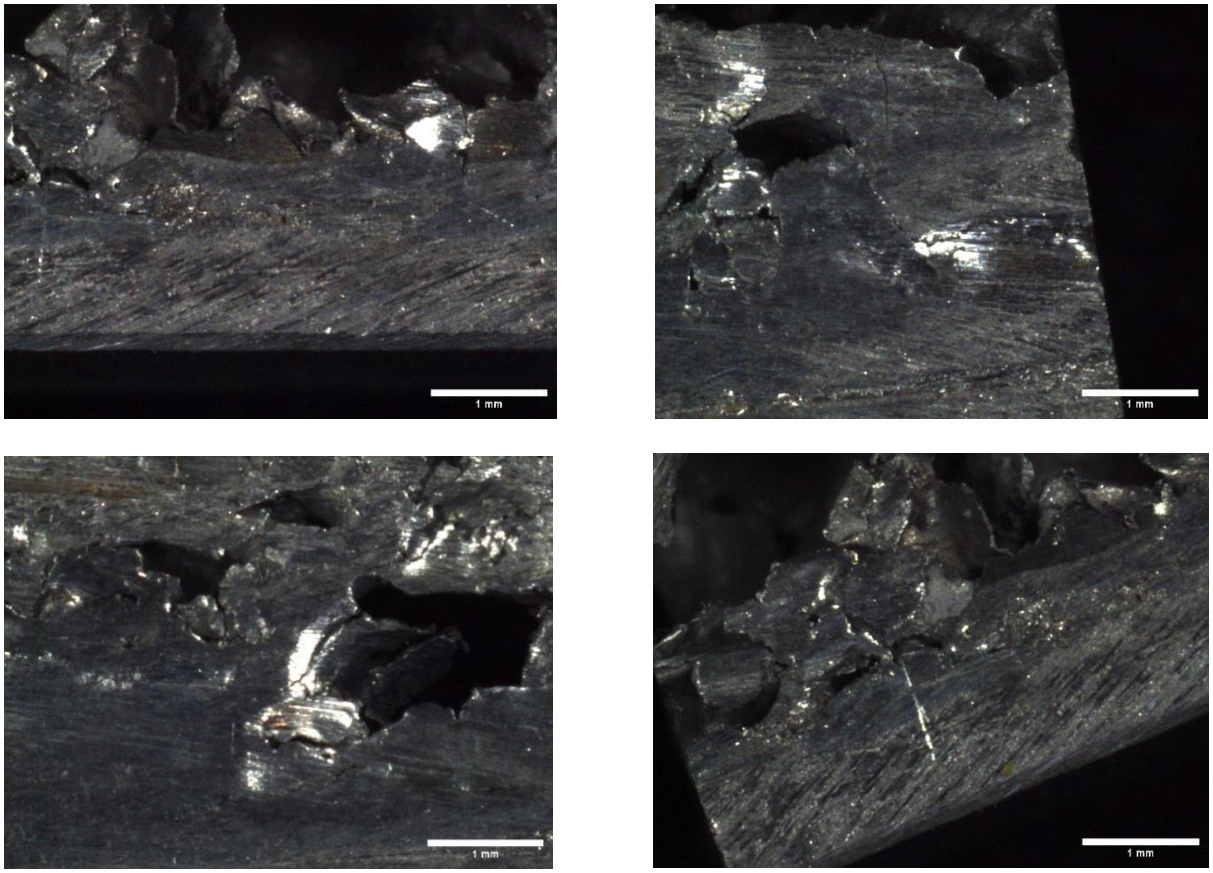

Figure 74 Low magnification optical microscopy at 6x of sample 3 with plates exposed to tensile loading.

Sample 3 (Plates exposed to compressive load during the test)

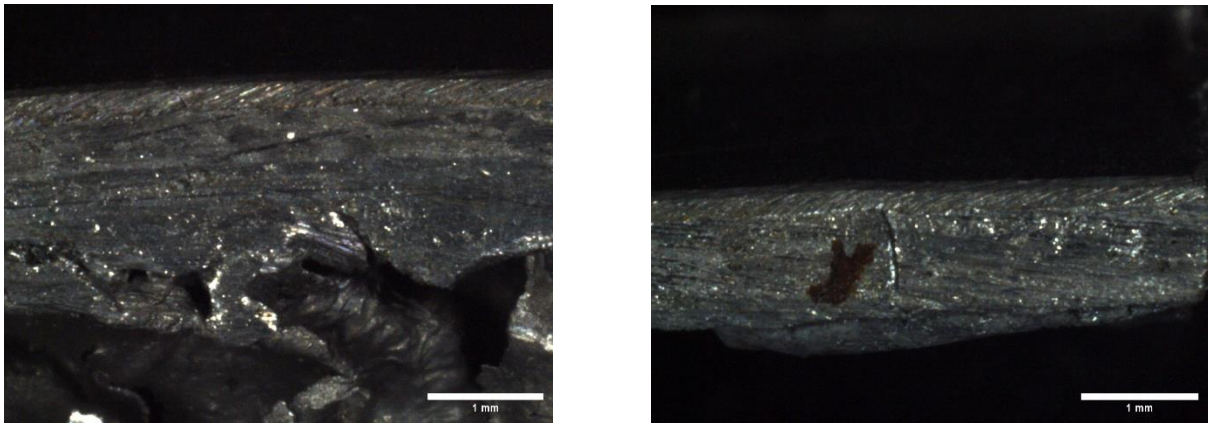

Figure 75 Low magnification optical microscopy at 6x of sample 2 with plates exposed to compressive loading

After observing all of these images at low magnification, it is feasible to state that sample 1 is exhibiting a few cracks on the foam side close to the joining region (probably involved in the brazing area) and on the foam walls. This result agrees with the absence of global failure of this sample after 4.5 million loading cycles, but also with certain damage to it after this loading condition. However, samples 2 and 3 show the formation of important cracks corresponding to the point of higher stress that develop through the foam and propagate towards the aluminum plate while passing through the joining region.

4.6 Scanning Electron Microscopy (SEM) with Energy Dispersive X-ray Spectroscopy (EDS) Analysis

The SEM-EDS analysis for material characterization and elemental identification was devoted to aluminum plate failure during fatigue test, aluminum foam itself and the aluminum plate failed during cutting operation. The failed aluminum plate during operation, failed aluminum plate during cutting and aluminum foam are shown in figure 76.

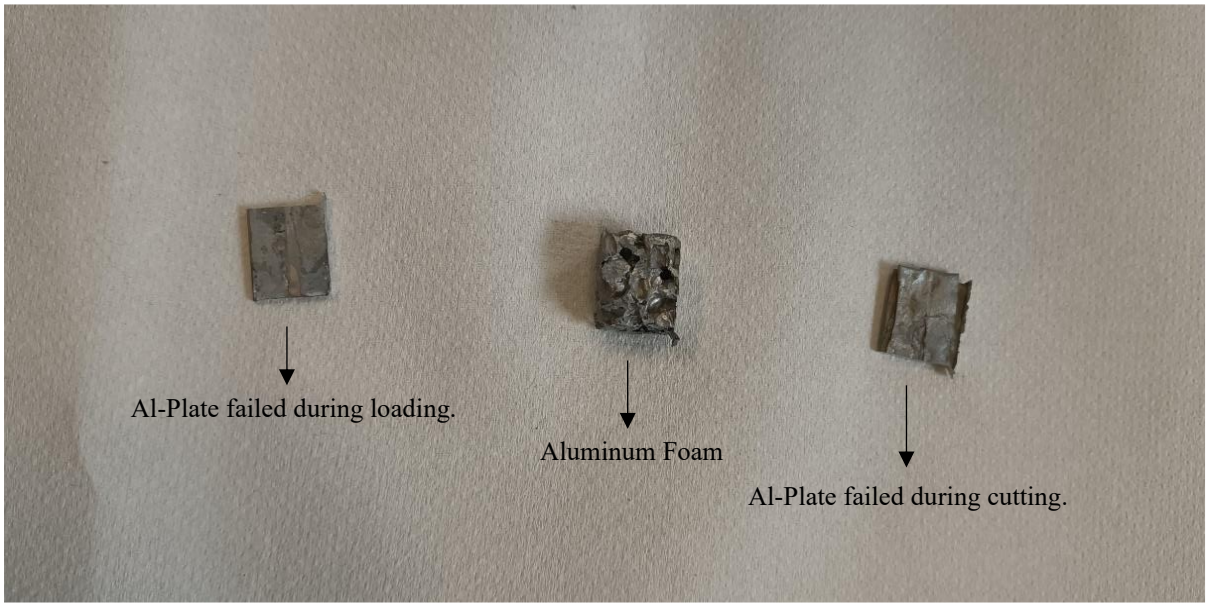

Figure 76 Samples underwent SEM-EDS analysis.

4.6.1 Aluminum Plate Failure During Fatigue Loading

View 000

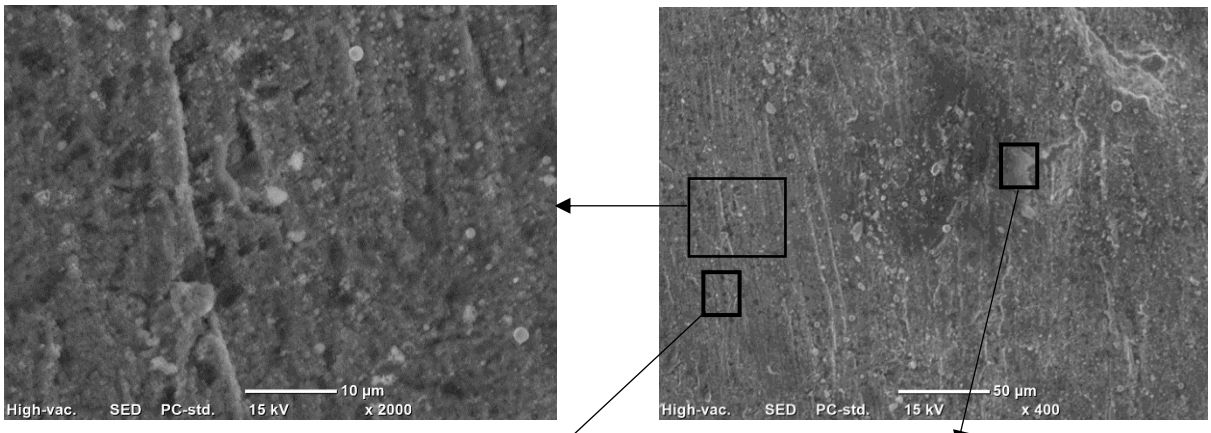

Element	(keV)	Mass%
O K*	0.525	12.36
F K*	0.677	12.36
Mg K*	1.253	3.06
Al K	1.486	21.98
Si K*	1.739	0.43
Zn K*	8.630	41.95
Cs L*	4.285	7.86
Total		100.00

Element	(keV)	Mass%
O K	0.525	12.28
F K	0.677	25.10
Mg K	1.253	11.05
Al K	1.486	16.26
Si K	1.739	0.50
Zn K	8.630	25.45
Cs L	4.285	9.36
Total		100.00

Figure 77 SEM-EDS analysis at view 000

View 001

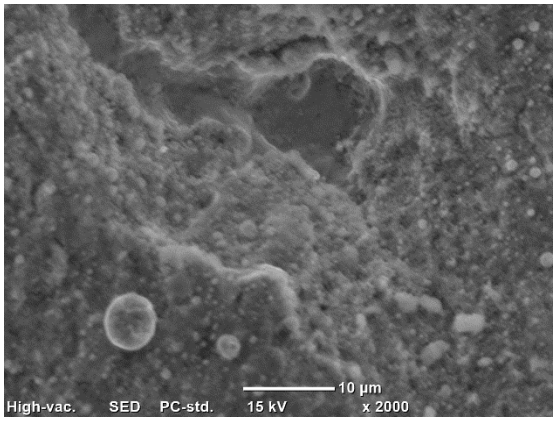

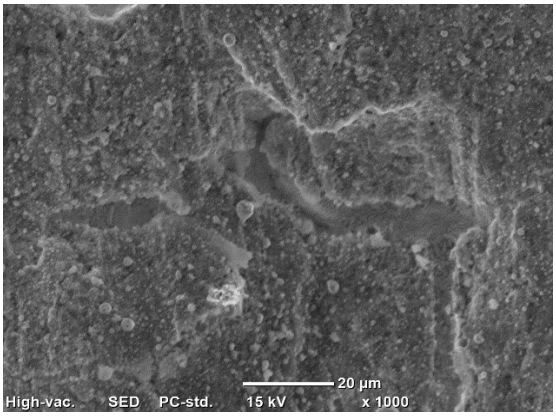

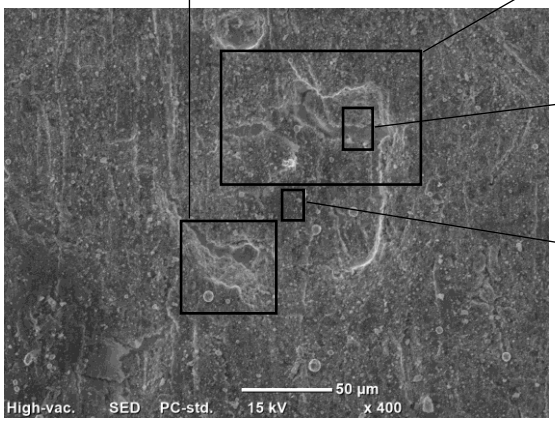

Element	(keV)	Mass%
O K	0.525	14.47
F K	0.677	15.58
Mg K	1.253	6.01
Al K	1.486	18.43
Si K	1.739	0.33
Zn K	8.630	30.23
Cs L	4.285	14.95
Total		100.00

Element	(keV)	Mass%
O K	0.525	14.75
F K	0.677	21.87
Mg K	1.253	8.85
Al K	1.486	15.35
Si K	1.739	0.39
Zn K	8.630	29.44
Cs L	4.285	9.35
Total		100.00

Figure 78 SEM-EDS analysis at view 001

View 002

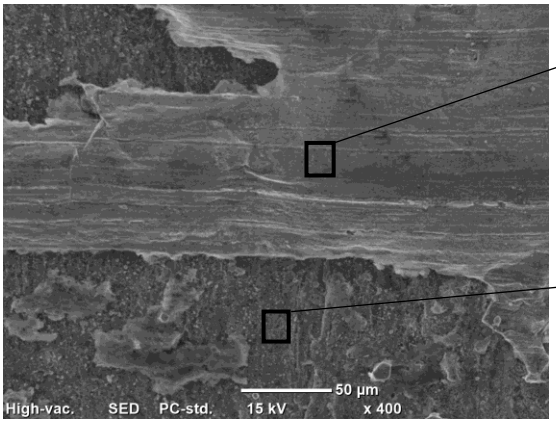

Element	(keV)	Mass%
O K	0.525	11.96
F K		ND
Mg K	1.253	0.56
Al K	1.486	10.42
Si K	1.739	0.19
Zn K	8.630	72.01
Cs L	4.285	4.86
Total		100.00

Element	(keV)	Mass%
O K	0.525	14.36
F K	0.677	11.28
Mg K	1.253	4.65
Al K	1.486	17.76
Si K	1.739	0.29
Zn K	8.630	43.63
Cs L	4.285	8.03
Total		100.00

Figure 79 SEM-EDS analysis at view 002

View 003

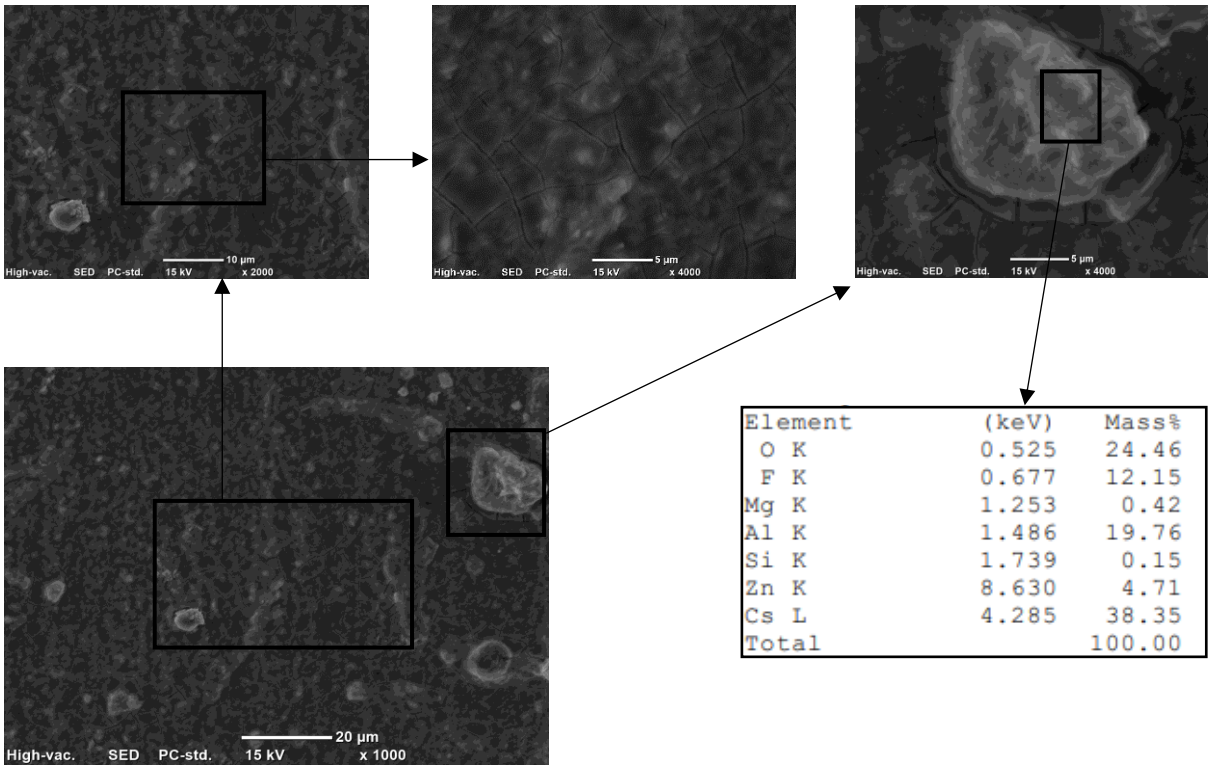

Element	(keV)	Mass%
O K	0.525	24.46
F K	0.677	12.15
Mg K	1.253	0.42
Al K	1.486	19.76
Si K	1.739	0.15
Zn K	8.630	4.71
Cs L	4.285	38.35
Total		100.00

Figure 80 SEM-EDS analysis at view 003

View 004

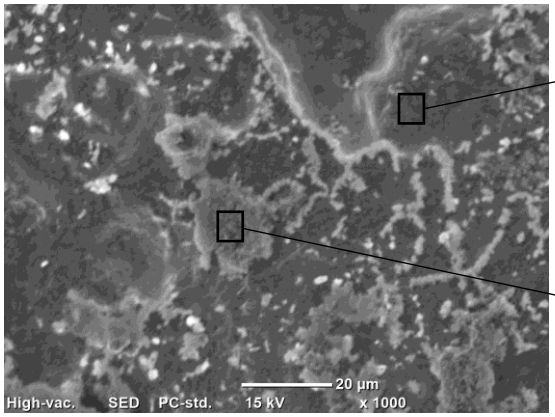

Element	(keV)	Mass%
O K	0.525	2.52
F K	0.677	2.28
Mg K	1.253	1.43
Al K	1.486	19.27
Si K	1.739	1.71
Zn K	8.630	72.79
Cs L		ND
Total		100.00

Element	(keV)	Mass%
O K	0.525	6.57
F K	0.677	7.90
Mg K	1.253	3.26
Al K	1.486	12.39
Si K	1.739	0.94
Zn K	8.630	55.76
Cs L	4.285	13.18
Total		100.00

Figure 81 SEM-EDS analysis at view 004

View 005

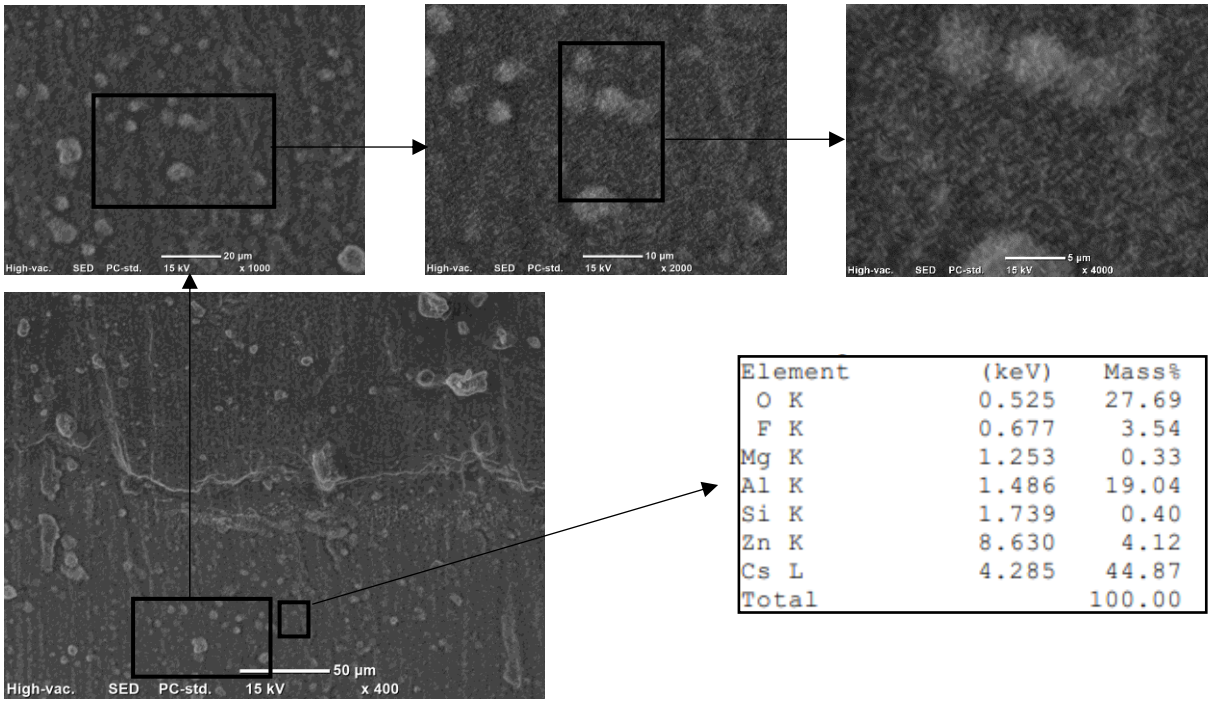

Element	(keV)	Mass%
O K	0.525	27.69
F K	0.677	3.54
Mg K	1.253	0.33
Al K	1.486	19.04
Si K	1.739	0.40
Zn K	8.630	4.12
Cs L	4.285	44.87
Total		100.00

Figure 82 SEM-EDS analysis at view 005

Through SEM-EDS analysis of aluminum plate failed during loading, we can observe that in most of the regions, the major contribution is coming from Zinc (being reactive with aluminum), followed by aluminum. However, there are some zones having high percentage of Cesium (Ce) and Fluorine (F) as shown in figures 77-82. These elements are the constituents of the deoxidizing agent (cesium fluoroaluminate flux) used in brazing operation. The flux not only reacts but remains there even after the brazing operation.

4.6.2 Aluminum Plate Failure During Cutting Operation

View 001

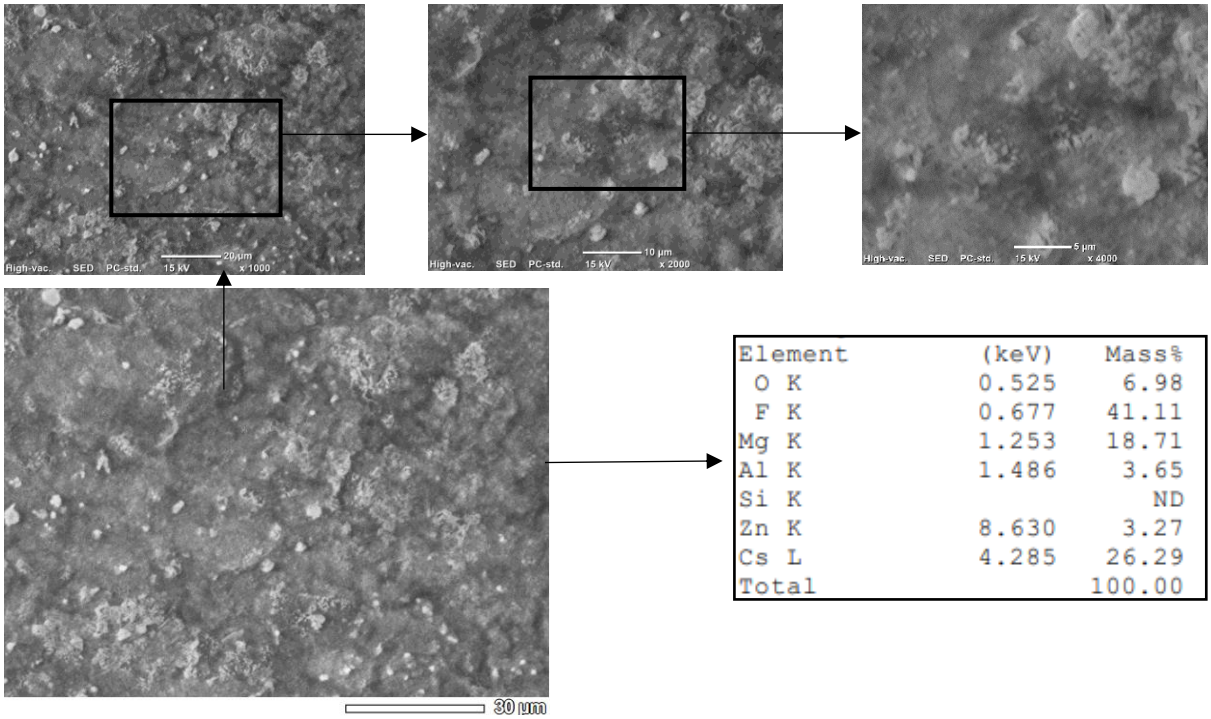

Element	(keV)	Mass%
O K	0.525	6.98
F K	0.677	41.11
Mg K	1.253	18.71
Al K	1.486	3.65
Si K		ND
Zn K	8.630	3.27
Cs L	4.285	26.29
Total		100.00

Figure 83 SEM-EDS analysis at view 001

View 002

Element	(keV)	Mass%
O K	0.525	21.14
F K	0.677	0.50
Mg K	1.253	1.21
Al K	1.486	15.22
Si K	1.739	9.47
Zn K	8.630	47.84
Cs L	4.285	4.62
Total		100.00

Element	(keV)	Mass%
O K	0.525	13.32
F K	0.677	7.84
Mg K	1.253	3.28
Al K	1.486	22.90
Si K	1.739	3.14
Zn K	8.630	42.13
Cs L	4.285	7.40
Total		100.00

Element	(keV)	Mass%
O K	0.525	15.01
F K	0.677	0.21
Mg K	1.253	3.26
Al K	1.486	16.07
Si K	1.739	0.36
Zn K	8.630	62.02
Cs L	4.285	3.07
Total		100.00

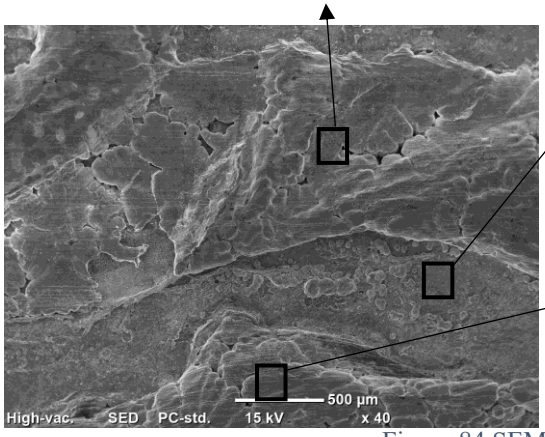

Figure 84 SEM-EDS analysis at view 002

Similar findings to those we observed for aluminum plate failure during fatigue operation may be noticed for aluminum plate failure during cutting operation. Higher influence of flux can bee seen in view 001. The flux reacts with the oxide layer present on the aluminum surface (i.e,. Al_2O_3) and helps dissolving brazing alloy. The flux oxidizes during the brazing process, and as the Zn becomes liquid, it further reacts with aluminum plate and dissolves certain amount of Al too. Zn solidification may result in the dendritic morphology seen in view 002.

4.6.3 Aluminum Foam Failed Side

View 000

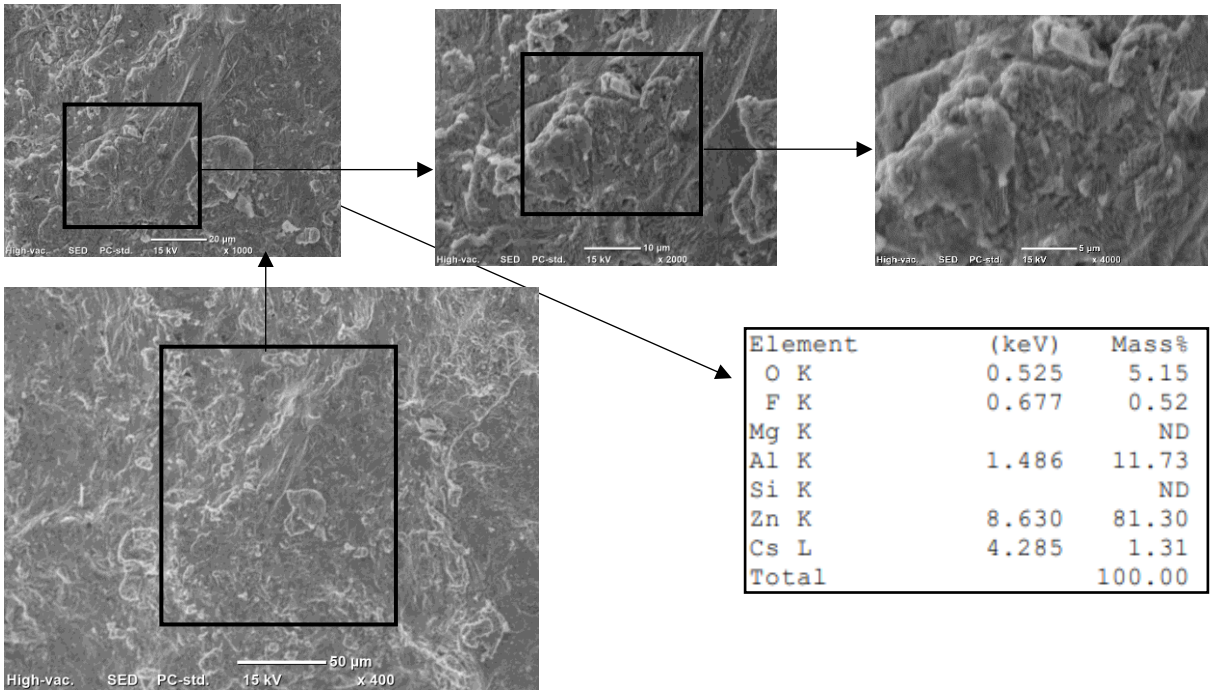

Element	(keV)	Mass%
O K	0.525	5.15
F K	0.677	0.52
Mg K		ND
Al K	1.486	11.73
Si K		ND
Zn K	8.630	81.30
Cs L	4.285	1.31
Total		100.00

Figure 85 SEM-EDS analysis at view 000

View 001

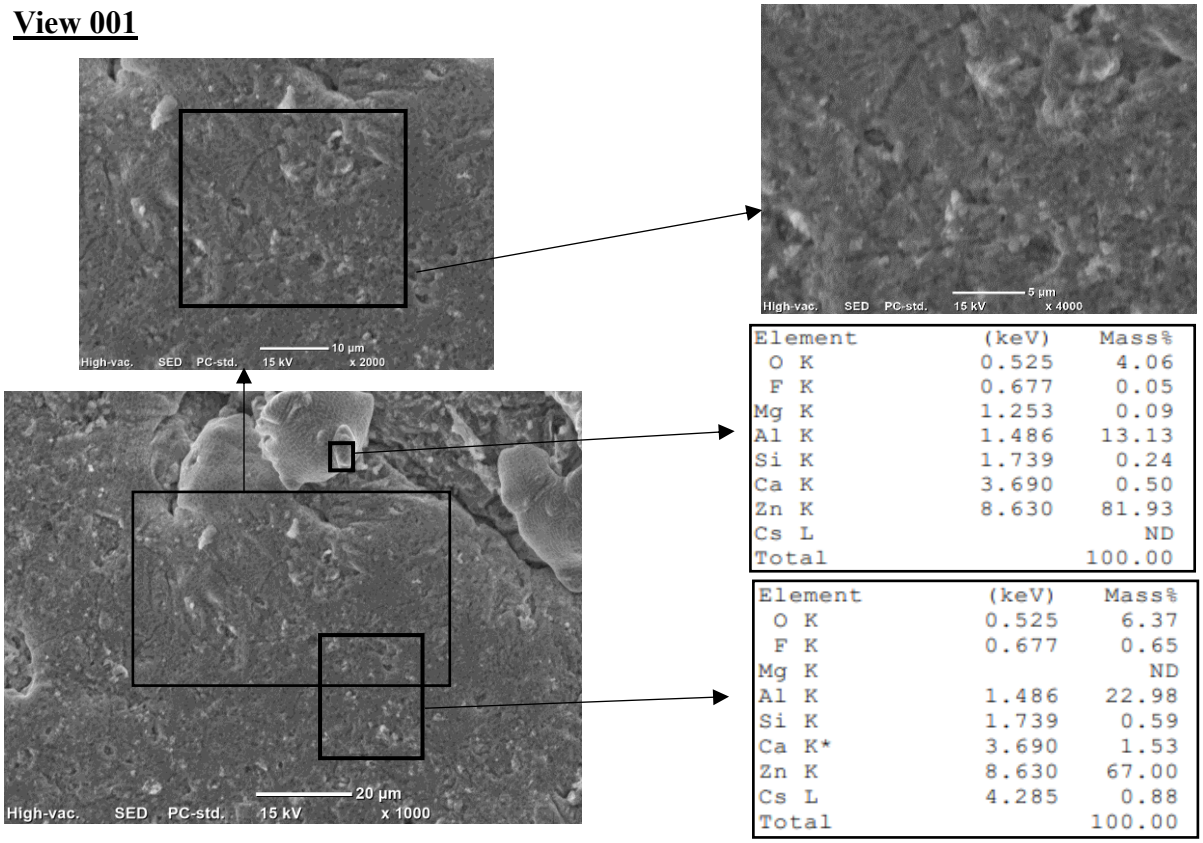

Element	(keV)	Mass%
O K	0.525	4.06
F K	0.677	0.05
Mg K	1.253	0.09
Al K	1.486	13.13
Si K	1.739	0.24
Ca K	3.690	0.50
Zn K	8.630	81.93
Cs L		ND
Total		100.00

Element	(keV)	Mass%
O K	0.525	6.37
F K	0.677	0.65
Mg K		ND
Al K	1.486	22.98
Si K	1.739	0.59
Ca K*	3.690	1.53
Zn K	8.630	67.00
Cs L	4.285	0.88
Total		100.00

Figure 86 SEM-EDS analysis at view 001

4.6.4 SEM-EDS of Sample 1-B to Analyze Discontinuity in the Joining Interface.

View 000

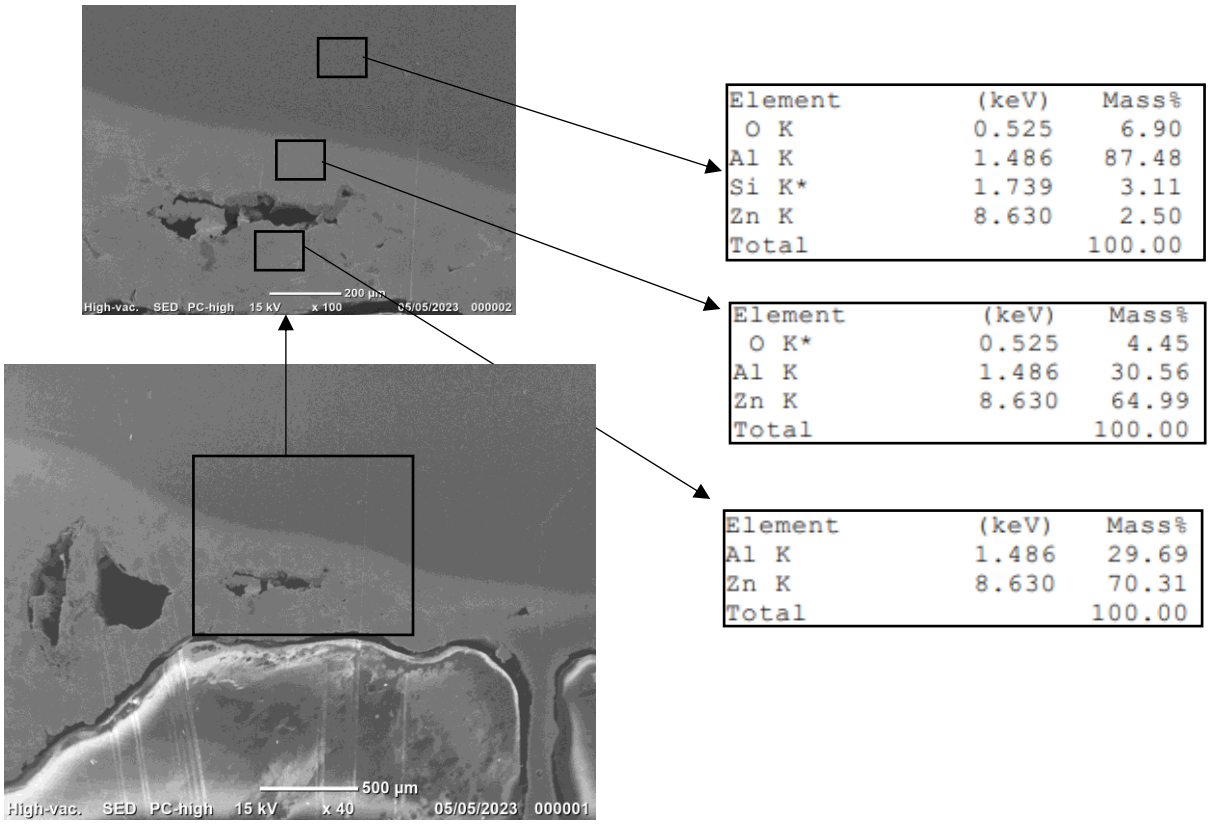

Element	(keV)	Mass%
O K	0.525	6.90
Al K	1.486	87.48
Si K*	1.739	3.11
Zn K	8.630	2.50
Total		100.00

Element	(keV)	Mass%
O K*	0.525	4.45
Al K	1.486	30.56
Zn K	8.630	64.99
Total		100.00

Element	(keV)	Mass%
Al K	1.486	29.69
Zn K	8.630	70.31
Total		100.00

Figure 87 SEM-EDS analysis of sample 1-B at view 000

View 001

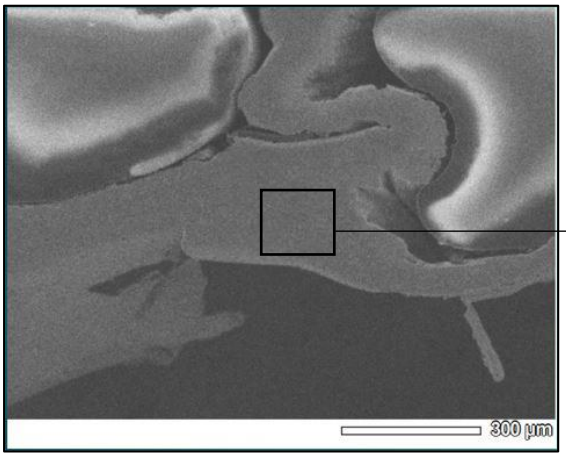

Element	(keV)	Mass%
O K*	0.525	4.27
Al K	1.486	86.09
Si K	1.739	9.64
Total		100.00

Figure 88 SEM-EDS analysis of sample 1-B at view 001

View 002

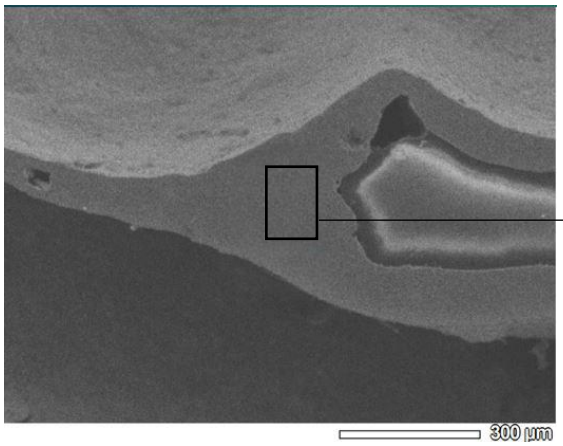

Element	(keV)	Mass%
O K*	0.525	4.31
Al K	1.486	89.06
Ca K*	3.690	2.69
Ti K*	4.508	3.95
Total		100.00

Figure 89 SEM-EDS analysis of sample 1-B at view 002

View 003

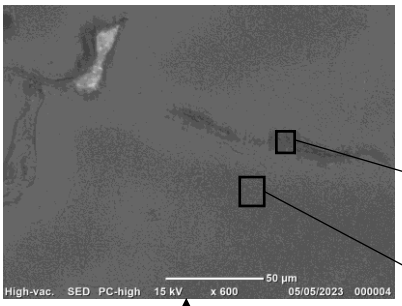

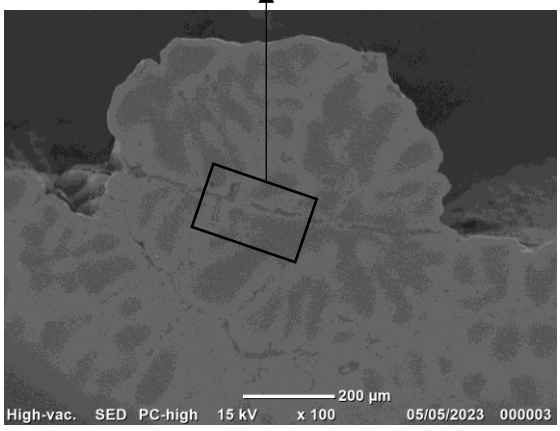

Element	(keV)	Mass%
O K	0.525	23.88
F K*	0.677	10.58
Mg K*	1.253	3.74
Al K	1.486	14.74
Si K	1.739	23.58
Zn K*	8.630	16.39
Cs L*	4.285	7.09
Total		100.00

Element	(keV)	Mass%
O K	0.525	2.03
F K		ND
Mg K	1.253	0.40
Al K	1.486	48.33
Si K	1.739	0.95
Zn K	8.630	48.29
Cs L		ND
Total		100.00

Figure 90 SEM-EDS analysis of sample 1-B at view 003

View 004

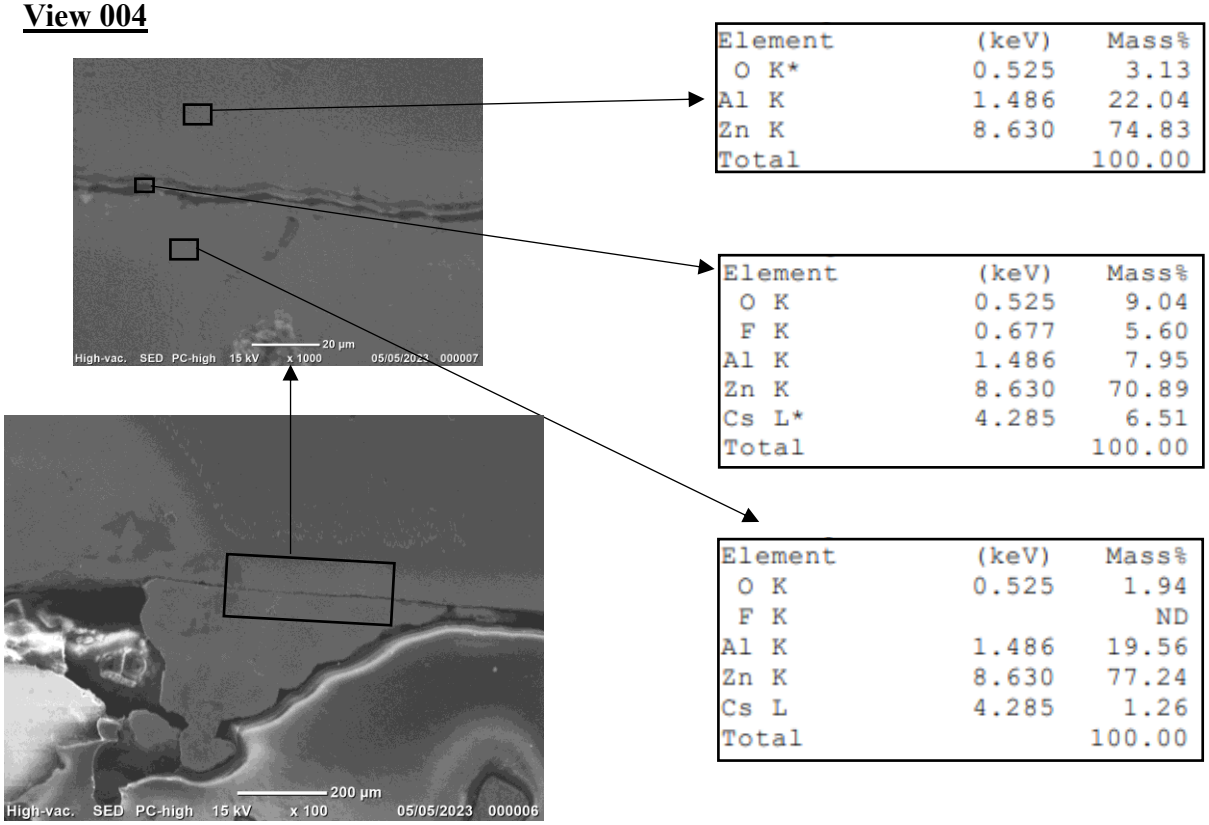

Figure 91 SEM-EDS analysis of sample 1-B at view 004

SEM images of the failed (discontinuous) joint are demonstrating not only the detachment of joining but also the reactivity of the zinc employed as a brazing alloy with both the aluminum plate and the foam. There is also evidence of flux residuals. However, no fracture morphologies have been found on these surfaces. Similarly, SEM-EDS analysis of the joint's cross-section is revealing the existence of reaction regions (dendritic structures at the interface that demonstrate the development of the liquid phase during the brazing process) with the production of zinc and aluminum phases. In addition, we can observe that the discontinuous zone illustrated in figures 90 and 91 contains both cesium (Cs) and fluorine (F). Some cesium fluoroaluminate flux residuals can be found on the fracture surfaces, as mentioned in section 4.3.1. The presence of these compounds in the joint's discontinuities may indicate that a significant quantity of the flux in a certain area of the joint may have an adverse effect on the joint's mechanical properties.

Aluminum foam's cell wall surface and the cell wall's cross-section have very distinct chemical compositions as depicted in figures 88 and 89. On the cell wall's surface, Silicon (Si) is present, while the cross-section contains calcium (Ca) and titanium (Ti). The silicon content might be a result of the silicon-containing aluminum alloy used to make foam. The presence of calcium contributes to the thickening of the melt and causes the formation of calcium oxide (CaO) on the external surface and in the cross-section. The titanium is a result of the TiH_2 employed as a foaming agent during the foam manufacturing process.

4.6.5 SEM of Aluminum Foam (3 different views to verify the chemical composition)

View 001

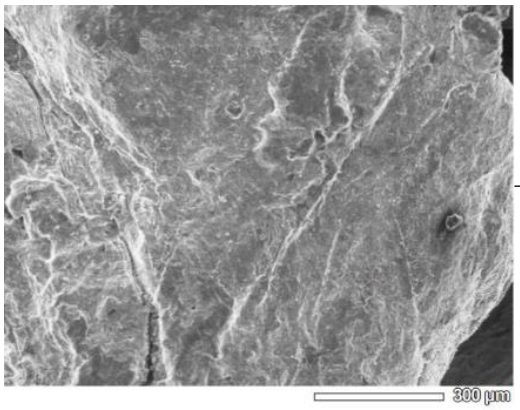

Element	(keV)	Mass%
O K	0.525	13.71
Al K	1.486	80.57
Ca K	3.690	5.72
Total		100.00

View 002

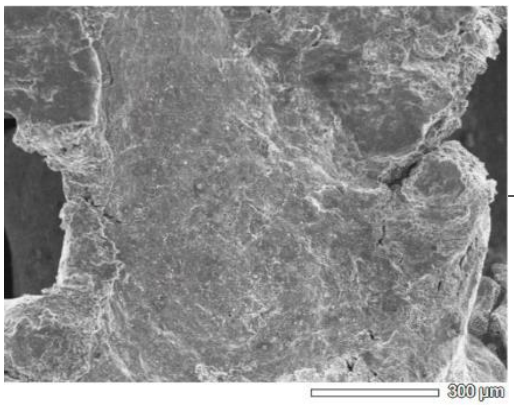

Element	(keV)	Mass%
O K	0.525	10.73
Al K	1.486	82.14
Ca K	3.690	7.13
Total		100.00

View 003

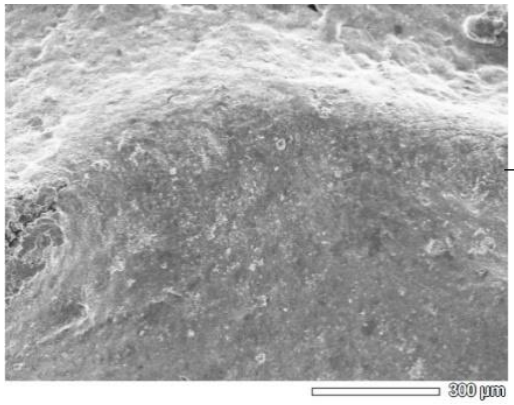

Element	(keV)	Mass%
O K	0.525	13.45
Al K	1.486	79.87
Ca K	3.690	6.68
Total		100.00

Figure 92 SEM-EDS analysis of aluminum foam at different zones

More or less, we can see the same chemical composition in all of the above views of aluminum foam taken at different zones. The major contribution is of aluminum while Ca is used as a melt thickening agent. The presence of oxygen can be due to factors such as the generation of thin oxide film on aluminum, processing conditions such as temperature and atmosphere that encourage oxidation and inadequate removal of oxygen during production.

4.7 Conclusion

The purpose of this study was to look into the behavior of aluminum foam sandwiches (AFSs) fabricated by brazing under fatigue (compression-compression) loading conditions. This was accomplished by applying controlled fatigue loading (three-point bending) to aluminum foam sandwiches (AFSs). Understanding the material's response at various fatigue levels, as well as the associated failure mechanisms, was critical. The experimental investigation revealed important results, such as strong fatigue resistance (up to 4.5 million loading cycles without failure) for some samples and high data variability owing to the foam and joint inhomogeneities. In some cases, delamination (debonding behavior), failure of foam cell walls, and cracks in the aluminum foam, as well as the existence of a clear discontinuity in the interface region at certain places, were observed.

The use of the foam production technique, in which a foaming agent is applied to the molten metal to produce a gas, causes an inherent problem defined by the random formation of porosity. As a result, this randomness also extends to the contact points formed in joints, posing a challenge.

One noticeable finding is that cesium (Ce) and fluorine (F), characteristic elements of the deoxidizing agent employed in brazing, were found in the discontinuous zone. This discovery implies the possibility of a correlation between the existence of these elements and the formation of the noticed interface discontinuity. However, more thorough investigation is required to fully understand the underlying mechanism and importance of this relationship. Understanding the involvement of cesium and fluorine in the creation of interface discontinuities will help us understand how these elements influence the way the chemicals interact and the structure of aluminum foam sandwiches.

The sensitivity of materials to damage and deformation is demonstrated by the appearance of delamination, definite failure of foam cell walls, and cracks in the aluminum foam samples under compression-compression fatigue loading conditions. These observed findings show that the aluminum foam sandwiches (AFSs) gradually deteriorate and become weaker when they are subjected to cyclic loading. The accumulation of damage over several loading cycles may result in delamination and fracture of foam cell walls. Under cyclic loadings, cracks may develop as a result of stress concentration (where we have maximum bending moment) or defects within the foam material and propagate to the aluminum plates while passing through the bonding interface.

Delamination, some failure of foam cell walls, aluminum foam cracking, and discontinuity at the joining interface are all indications that the structural integrity of aluminum foam sandwiches has to be taken into account during design and engineering phases. The overall durability and reliability of materials may be compromised by these events, potentially resulting in poor structural performance, loss of energy absorption capability, and a reduction in load bearing capacity.

References

[1] “M.F. Ashby, A.G. Evans, N.A. Fleck, L.J. Gibson, J.W. Hutchinson, and H.N.G. Wadley. Metal Foams: A Design Guide, 2000.”

[2] “Lefebvre, L-P., John Banhart, and David C. Dunand. ‘Porous metals and metallic foams: current status and recent developments.’ Advanced engineering materials 10.9 (2008): 775-787.”

[3] “M.F. Ashby, A.G. Evans, N.A. Fleck, L.J. Gibson, J.W. Hutchinson, H.N.G. Wadley: Metal Foams: A Design Guide, electric book, Butterworth-Heinemann, ISBN: 978008 0511467.”

[4] “Zimar, A. M. Z., et al. "Non-linear behaviour of open-cell metal foam under tensile loading." 2016 Moratuwa Engineering Research Conference (MERCon). IEEE, 2016.”

[5] “García-Moreno, F. Commercial Applications of Metal Foams: Their Properties and Production. Materials 2016, 9, 85. https://doi.org/10.3390/ma9020085.”

[6] “Mahajan, Sunil M., and Ganesh A. Jadhav. "Aluminum foaming for lighter structure." Int. J. Comput. Eng. Res 5.01 (2015): 70-74.”

[7] “Banhart, John. "Manufacture, characterisation and application of cellular metals and metal foams." Progress in materials science 46.6 (2001): 559-632.”

[8] “Qingxian, Hao, Qiu Sawei, and Hu Yuebo. "Development on preparation technology of aluminum foam sandwich panels." Rare Metal Materials and Engineering 44.3 (2015): 548-552.”

[9] “Baumeister, J. "German Patent 40 18 360 1990." US Patent 5 (1996): 1992.”

[10] “Baumeister, J., J. Banhart, and M. Weber. "Verfahren zur Herstellung eines metallischen Verbundwerkstoffs [Process for manufacturing metallic composite materials]." German Patent 44.26 (1994): 627.”

[11] “Hommel, Patrick, Daniel Roth, and Hansgeorg Binz. "Derivation of motivators for the use of aluminum foam sandwich and advantageous applications." Proceedings of the Design Society 1 (2021): 933-942.”

[12] “Zhang, Junshan, Yukun An, and Haoyuan Ma. "Research progress in the preparation of aluminum foam composite structures." Metals 12.12 (2022): 2047.”

[13] “Banhart, J. (2018). Production of Metal Foams: Handbook of Comprehensive Composite Materials II.”

[14] “Seeliger, H. W. "AFS-Weiterentwicklung erreicht Serienreife: Aluminiumschaum frisch vom Band." Aluminium Kurier News 03 (2011): 16.”

[15] “Hommel, P., D. Roth, and H. Binz. "Deficits in the application of aluminum foam sandwich: An industrial perspective." Proceedings of the design society: DESIGN conference. Vol. 1. Cambridge University Press, 2020.”

[16] “Yao, Cheng, et al. "Fabrication and fatigue behavior of aluminum foam sandwich panel via liquid diffusion welding method." Metals 9.5 (2019): 582.”

[17] “Chung, H. J., et al. "Plasma treatment using nitrogen gas to improve bonding strength of adhesively bonded aluminum foam/aluminum composite." Journal of alloys and compounds 459.1-2 (2008): 196-202.”

[18] “Baştürk, Suat Bahar, and Metin Tanoğlu. "Development and mechanical behavior of FML/aluminium foam sandwiches." Applied Composite Materials 20 (2013): 789-802.”

[19] “Li, Zhibin, et al. "Deformation and failure mechanisms of sandwich beams under three-point bending at elevated temperatures." Composite structures 111 (2014): 285-290.”

[20] “Hackert, Alexander, et al. "Composite sandwich with aluminum foam core and adhesive bonded carbon fiber reinforced thermoplastic cover layer." Key Engineering Materials 744 (2017): 277-281.”

[21] “Li, Yuxiang, Chao Chen, and Ruixiang Yi. "Recent development of ultrasonic brazing." The International Journal of Advanced Manufacturing Technology 114 (2021): 27-62.”

[22] “Song, Y. F., et al. "Fabrication, microstructure and shear properties of Al foam sandwich." Materials and Manufacturing Processes 31.8 (2016): 1046-1051.”

[23] “Huang, Yongxian, et al. "Fluxless soldering with surface abrasion for joining metal foams." Materials Science and Engineering: A 552 (2012): 283-287.”

[24] “Ubertalli, Graziano, Monica Ferraris, and Muhammad Kashif Bangash. "Joining of AL-6016 to Al-foam using Zn-based joining materials." Composites Part A: Applied Science and Manufacturing 96 (2017): 122-128.”

[25] “Tensi, H. M., and M. Wittmann. "Influence of surface preparation on the diffusion welding of high strength aluminium alloys." Diffusion Bonding 2 (1991): 101-110.”

[26] “Kitazono, K., et al. "Solid-state diffusion bonding of closed-cell aluminum foams." Materials Science and Engineering: A 327.2 (2002): 128-132.”

[27] “Yao, Cheng, et al. "Fabrication and fatigue behavior of aluminum foam sandwich panel via liquid diffusion welding method." Metals 9.5 (2019): 582.”

[28] “Pang, Qiu, Zhengjian Wu, and Zhili Hu. "The influence of process parameters on the preparation of closed-cell aluminum foam by friction stir processing." The International Journal of Advanced Manufacturing Technology 120.3-4 (2022): 2489-2501.”

[29] “ Peng, Pai, et al. "High-performance aluminium foam sandwich prepared through friction stir welding." Materials Letters 236 (2019): 295-298.”

[30] “Hangai, Yoshihiko, et al. "Fabrication of aluminum foam/dense steel composite by friction stir welding." Metallurgical and Materials Transactions A 41 (2010): 2184-2186.”

[31] “Charit, Indrajit, and Rajiv S. Mishra. "Effect of friction stir processed microstructure on tensile properties of an Al-Zn-Mg-Sc alloy upon subsequent aging heat treatment." Journal of Materials Science & Technology 34.1 (2018): 214-218.”

[32] “Su, Xixi, et al. "Study on aluminum foam sandwich welding by friction stir welding technology." Materials Letters 304 (2021): 130605.”

[33] “Swensen, A. "Aluminum continues unprecedented growth in automotive applications." Light Metal Age 20 (2020).”

[34] “Automotive Life-Cycle Assessment Model. Jun 16, 2015. [(accessed on 2 August 202 1)]. European Aluminium. (Update December 2018) Available online: https://www.eu ropean-aluminium.eu/resource-hub/automotive-lca-model.”

[35] “Sakurai, Takeo. "The latest trends in aluminum alloy sheets for automotive body panels." Kobelco technology review 28 (2008): 22-28.”

[36] “Ota, Yosuke, Tetsuya Masuda, and Shinpei Kimura. "Technical trends in aluminum alloy sheets for automotive body panels." Kobelco Technol. Rev 38 (2020): 16-20.”

[37] “Hirsch, Jürgen. "Recent development in aluminium for automotive applications." Transactions of Nonferrous Metals Society of China 24.7 (2014): 1995-2002.”

[38] “Long, R. S., E. Boettcher, and D. Crawford. "Current and future uses of aluminum in the automotive industry." Jom 69.12 (2017): 2635-2639.”

[39] “Banhart, John, and H-W. Seeliger. "Aluminium foam sandwich panels: manufacture, metallurgy and applications." Advanced Engineering Materials 10.9 (2008): 793-802.”

[40] “H. M. Helwig, F. García-Moreno, J. Banhart, Journal of Materials Science 2011, 46, 5 227.”

[41] “García-Moreno, Francisco. "Commercial applications of metal foams: Their properties and production." Materials 9.2 (2016): 85.”

[42] “ Kriszt, B., and H. P. Degischer. "Handbook of cellular metals: Production, processing, applications." Weinheim: Wiley-VCH (2002): 2002.”

[43] “Bray, Don E., and Roderick K. Stanley. Nondestructive evaluation: a tool in design, manufacturing and service. CRC press, 1996.”

[44] “Banhart, John, M. Ashby, and N. Fleck. "Metal foams and porous metal structures." Conference on Metal Foams and Porous Metal Structures. Vol. 14. 1999.”

[45] “Weber M. Thesis. Universityof Clausthal, MIT Press–Verlag, Bremen, 1997.”

[46] “Ehlers W, Mu¨llerscho¨n H, Klar O. Metal foams and porous metal structures. In: Banhart J, Ashby MF, Fleck NA, editors. Int. Conf., Bremen, Germany, 14–16 June. Bremen: MIT Press–Verlag, 1999. p. 255.”

[47] “Deshpande VS, Fleck NA. Metal foams and porous metal structures. In: Banhart J, AshbyMF, Fleck NA, editors. Int. Conf., Bremen, Germany, 14–16 June. Bremen: MIT Press–Verlag, 1999. p. 247.”

[48] “Yu CJ, Claar TD, Hall IW, Frantz RE, Hasson DF. Metal foams and porous metal structures. In: Banhart J, AshbyMF, Fleck NA, editors. Int. Conf., Bremen, Germany, 14–16 June. Bremen: MIT Press–Verlag, 1999. p. 347.”

[49] “Olurin OB, Fleck NA, AshbyMF. Metal foams and porous metal structures. In: Banhart J, Ashby MF, Fleck NA.”

[50] “Huiming, Zhang, et al. "Compressive properties of aluminum foams by gas injection method." China Foundry 9.3 (2012).”

[51] “Yan, Chang, Xu Ding Song, and Shuo Feng. "Aluminum foam sandwich with different face-sheet materials under three-point bending." Applied Mechanics and Materials 872 (2017): 25-29.”

[52] “Zu, Guoyin, et al. "Static three-point bending behavior of aluminum foam sandwich." Journal of alloys and compounds 540 (2012): 275-278.”

[53] “Zu, Guo-yin, et al. "Three-point bending behavior of aluminum foam sandwich with steel panel." Transactions of Nonferrous Metals Society of China 23.9 (2013): 2491-2495.”

[54] “Yao, Cheng, Zhengfei Hu, and Fan Mo. "Three-Point Bending Fatigue Behavior of Aluminum Foam Sandwich Panels with Different Density Core Material." Metals 11.10 (2021): 1542.”

[55] “Liu, Sitian, et al. "Fatigue of an Aluminum Foam Sandwich Formed by Powder Metallurgy." Materials 16.3 (2023): 1226.”

[56] “Yan, Chang, Jian Wang, and Xuding Song. "Fatigue behavior and damage mechanism of aluminum foam sandwich with carbon-fiber face-sheets." Journal of Mechanical Science and Technology 34 (2020): 1119-1127.”

[57] “https://www.makeitfrom.com/material-properties/6016-AlSi1.2Mg0.4-A96016-Aluminum.”

[58] “https://studiousguy.com/scanning-electron-microscope-working-principle/.’’